Machine Learning–Based Prediction of Atmospheric CO_2 Concentration: A Year–Month Trend analysis

Israt Jahan Powsi[1], Rayhan Miah[1], and Md Khorshed Alam[*1]*

[1]Department of Physics, University of Barisal
*Correspondence: dmkalam@bu.ac.bd

1. Abstract:

Atmospheric carbon dioxide (CO_2) remains the principal driver of contemporary climate change, yet accurately forecasting its temporal evolution requires models capable of capturing complex nonlinear and seasonal dynamics. In this study, we conduct a comprehensive evaluation of thirteen supervised machine-learning algorithms to model and predict long-term atmospheric CO_2 concentrations using multi-decadal monthly and annual observational datasets. The dataset encompasses several decades of global CO_2 measurements, enabling a detailed investigation of both persistent climatological trends and short-term oscillatory variations.

All models were trained under a unified workflow and assessed using a standardized performance matrix comprising R^2, RMSE, and MAE. Among the tested algorithms, Random Forest Regression and a multilayer Artificial Neural Network (ANN) consistently outperformed other classical and ensemble methods, achieving R^2 values greater than 0.95 and demonstrating exceptional robustness against noise and seasonal irregularities. Time-series diagnostics further reveal a sustained, near-exponential increase in global CO_2 levels, reflecting intensified anthropogenic influence, reduced carbon-sink efficiency, and accelerating feedback mechanisms in the Earth system.

The results highlight the utility of machine-learning techniques as reliable and scalable tools for atmospheric CO_2 forecasting, offering improved sensitivity to nonlinearities compared to traditional statistical approaches. Importantly, the analytical framework developed in this work is extensible and can readily integrate additional environmental variables such as oceanic carbon-flux parameters, biospheric exchange indices, remote-sensing products, or even emerging acoustic-signature datasets to construct more holistic, multimodal prediction systems. By establishing a strong methodological baseline, this study contributes to the advancement of next-generation climate-monitoring and predictive-analytics systems, supporting evidence-based climate mitigation and policy formulation.

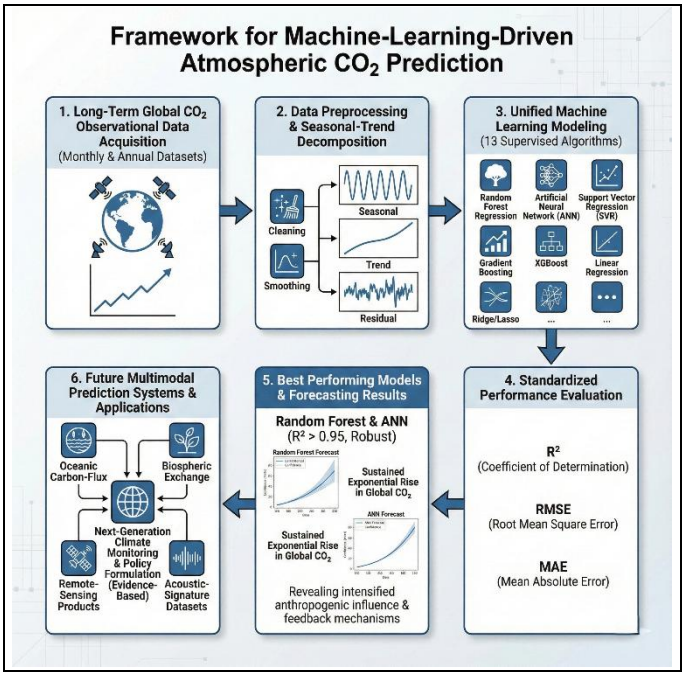

2. Introduction:

Since the onset of the Industrial Revolution, atmospheric carbon dioxide (CO_2) concentrations have risen sharply, primarily due to intensified fossil-fuel combustion, land-use change, and rapid industrialization. This steady accumulation of CO_2 in the atmosphere has become one of the most influential drivers of global climate change, contributing directly to enhanced radiative forcing, rising surface temperatures, and the intensification of extreme weather phenomena. As international climate agreements increasingly emphasize evidence-based mitigation strategies, the demand for accurate, high-resolution CO_2 monitoring and forecasting has never been more critical.

Long-term CO_2 records—most notably those obtained from ground-based observatories such as Mauna Loa—reveal persistent upward trends superimposed with distinctive seasonal oscillations driven by biospheric uptake and release. Although traditional statistical models (e.g., ARIMA, exponential smoothing) and

physics-based atmospheric models have been widely used to analyze such temporal behavior, they often struggle to fully represent the nonlinearities, time-dependent interactions, and multiscale feedback processes inherent in atmospheric CO_2 dynamics. [1] These limitations create a compelling need for more flexible, data-driven approaches.

Machine Learning (ML) offers a powerful alternative, providing the ability to model complex temporal patterns without requiring explicit assumptions about underlying physical processes. ML algorithms can dynamically adapt to nonlinear growth rates, capture subtle seasonal variations, and uncover hidden relationships embedded in long-term datasets.[2], [3] Recent advances in computational efficiency and algorithmic design further support the integration of ML into climate analytics, enabling robust predictions even from noisy or incomplete data.[4]

In this study, we evaluate the performance of thirteen supervised regression algorithms applied to multi-decadal monthly and yearly atmospheric CO_2 datasets. The objective is threefold: (i) to examine long-term temporal patterns and quantify the underlying growth trajectory of atmospheric CO_2,[5] (ii) to assess the predictive capabilities of diverse ML models in capturing both long-term and short-term variations, and (iii) to establish a scalable baseline framework that can be extended to incorporate additional environmental variables in future multimodal prediction systems. By systematically comparing classical regressors, ensemble techniques, and neural-network architectures, this work provides a comprehensive benchmark for data-driven CO_2 forecasting and contributes to ongoing efforts to enhance climate-monitoring technologies[6].

3. Methodology:

This section outlines the comprehensive analytical framework employed to model and predict global atmospheric carbon dioxide (CO_2) concentrations. The methodology encompasses data acquisition, rigorous preprocessing and feature engineering, the implementation of a diverse suite of machine-learning algorithms, and a robust evaluation strategy designed to ensure model generalizability and statistical validity.[7]

3.1 Dataset Description and Acquisition

The primary dataset for this study is derived from the in-situ air sampling records of the Mauna Loa Observatory, compiled jointly by the National Oceanic and Atmospheric Administration (NOAA) Earth System Research Laboratory and the National Aeronautics and Space Administration (NASA) climate databases[8], [9]. This dataset is historically significant as it represents the longest continuous record of atmospheric CO_2 concentrations in the world.

The data spans a temporal range of six decades, specifically from March 1958 to December 2018. This extensive timeframe allows for the analysis of both intra-annual seasonal oscillations and multi-decadal anthropogenic trends. The dataset consists of monthly observations characterized by five distinct attributes:

- **Year:** The Gregorian calendar year of observation.
- **Month:** The month of observation (1–12).
- **Monthly Average CO_2:** The arithmetic mean of daily concentrations, measured in parts per million (ppm).
- **Interpolated CO_2 Values:** Smoothed values provided by the source agencies to account for missing days or instrument downtime, ensuring time-series continuity.
- **Trend Component:** A seasonally adjusted variable representing the underlying long-term trajectory of gas concentrations, isolating the anthropogenic increase from natural seasonal cycles.

Table 1: Excerpt of the Atmospheric CO_2 Dataset (1958–2018)

Index	Year	Month	Average CO_2 (ppm)	Interpolated CO_2 (ppm)	Trend Component
1	1958	3	315.71	315.71	314.62
2	1958	4	317.45	317.45	315.29
3	1958	5	317.50	317.50	314.71
...	...	...	...	...	...
708	2018	12	409.07	409.23	409.73

3.2 Preprocessing and Feature Engineering

Raw environmental data often contains noise, gaps, and scale disparities. To prepare the data for high-fidelity machine learning tasks, a multi-stage preprocessing pipeline was implemented.

3.2.1. Missing Value Imputation

While the source dataset includes interpolated values, minor gaps remained in the raw average CO_2 readings due to instrument calibration periods.

- **Strategy:** We utilized the source-provided Interpolated column as the primary ground truth. For any remaining discontinuities, we applied
- **Linear Interpolation**, assuming that CO_2 concentrations follow a relatively smooth trajectory between adjacent time steps without abrupt stochastic jumps.

3.2.2. Outlier Detection and Correction

Anomalies caused by sensor malfunction or extreme local weather events can bias regression models.

- **Detection:** We employed a dual-method approach using the Interquartile Range (IQR) and Z-score analysis. Data points falling beyond $1.5 \times IQR \; or \; having \; a \; Z-score > 3$ were flagged as potential outliers.
- **Correction:** Rather than discarding these data points, which would disrupt the time-series frequency, we applied local window smoothing. Flagged values were replaced with the rolling mean of the surrounding three-month window, preserving the overall trend while mitigating noise.

3.2.3. Feature Normalization

The dataset features differ in magnitude (e.g., Year $\approx 2000 vs. Month \in [1,12]$). Large scale differences can cause gradient-based algorithms (like Neural Networks and Lasso) to converge slowly or bias weights toward larger features.

- **Technique:** All continuous numerical variables were scaled using Min–Max Normalization to bound values between [0, 1]:

$$X_{norm} = \frac{X - X_{min}}{X_{max} - X_{min}}$$

3.2.4. Temporal Feature Engineering

Standard integer encoding for months (1 to 12) fails to capture the cyclical nature of time (i.e., the proximity of December to January). To preserve seasonality, we employed Cyclical Encoding using sine and cosine transformations:

$$Month_{sin} = \sin\left(\frac{2\pi \times month}{12}\right),$$

$$Month_{cos} = \cos\left(\frac{2\pi \times month}{12}\right)$$

This ensures the model interprets the seasonal cycle as a continuous loop rather than a linear progression.[10]

3.3 Machine-Learning Model Architectures

To evaluate predictive capability comprehensively, we implemented thirteen distinct supervised regression algorithms, categorized by their underlying mathematical logic.

3.3.1. Linear and Regularized Models

These models assume a linear relationship between temporal features and CO_2 levels.

- **Linear Regression (OLS):** Serves as the baseline.[10], [11]
- **Ridge Regression (L2):** Adds a penalty equal to the square of the magnitude of coefficients to prevent multicollinearity.
- **Lasso Regression (L1):** Adds a penalty equal to the absolute value of the magnitude of coefficients, allowing for feature selection.
- **Elastic Net:** A hybrid approach combining L1 and L2 penalties to balance sparsity and stability.

3.3.2. Ensemble and Tree-Based Models

These algorithms handle non-linearities well and are robust to outliers. 5. Decision Tree Regression: Splits data based on feature thresholds to minimize variance. 6. Random Forest Regression: An ensemble of decision trees trained via bagging (bootstrap aggregating) to reduce overfitting. 7. Extra Trees Regression: Similar to Random Forest but uses random thresholds for splits, further reducing variance. 8. AdaBoost: An iterative boosting technique that adjusts weights for mispredicted instances. 9. Gradient Boosting Regressor: Optimizes the loss function by sequentially adding weak learners. 10. XGBoost (Extreme Gradient Boosting): An optimized distributed gradient boosting library designed for efficiency and high performance.

3.3.3. Non-Linear and Instance-Based Models

- **Support Vector Regression (SVR):** Uses a kernel function (RBF) to map data into a higher-dimensional space to find the optimal hyperplane.
- **K-Nearest Neighbors (KNN):** Predicts values based on the local interpolation of the k closest feature vectors in the training space.

3.3.4. Artificial Neural Network (ANN) Framework

We designed a Deep Artificial Neural Network (ANN) specifically for this time-series task.[12]

- **Architecture:** A Multi-Layer Perceptron (MLP) consisting of an input layer, two dense hidden layers, and a single output node.
- **Activation Functions:** The ReLU (Rectified Linear Unit) activation function was used in hidden layers to introduce non-linearity, while a linear activation was used at the output layer for regression.
- **Optimization:** The Adam optimizer was employed for stochastic gradient descent due to its adaptive learning rate capabilities.
- **Regularization:** To prevent overfitting, we implemented Early Stopping (monitoring validation loss) and Learning Rate Decay.

3.4 Training Strategy and Validation

To ensure the results are robust and not a product of data leakage:

- **Train–Test Split:** The data was split chronologically: 80% for training (1958–2006) and 20% for testing (2007–2018). Random shuffling was disabled to respect the temporal order of the series.
- **Time-Series Cross-Validation:** Standard K-Fold cross-validation disrupts time dependency. Instead, we used a Rolling-Window (Forward-Chaining) Cross-Validation. In this method, the training set grows iteratively (e.g., train on Year 1, test on Year 2; train on Year 1-2, test on Year 3), ensuring the model never trains on future data to predict the past.
- **Hyperparameter Tuning:** A Grid Search approach was utilized to optimize key parameters, including the number of estimators (100–1000 for ensembles), maximum depth (trees), learning rates (0.01–0.1 for boosting/ANN), and kernel coefficients (SVR).

3.5 Evaluation Metrics

Model performance was quantified using three standard statistical metrics:

- **Coefficient of Determination (R^2):** Indicates the proportion of variance in the dependent variable predictable from the independent variables. A score closer to 1.0 indicates a perfect fit.
- **Mean Absolute Error (MAE):** The average of the absolute differences between predictions and actual values. It provides a linear score of error magnitude.

$$MAE = \frac{1}{n}\sum_{i=1}^{n}|y_i - \hat{y}_i|$$

- **Root Mean Square Error (RMSE):** The square root of the average of squared differences. RMSE penalizes larger errors more severely than MAE, making it critical for detecting significant deviations.

$$RMSE = \sqrt{\frac{1}{n}\sum_{i=1}^{n}(y_i - \hat{y}_i)^2}$$

3.6 Computational Environment

All computational experiments were performed in a Python 3.x environment to ensure a reproducible and flexible analytical workflow. A range of specialized libraries supported different components of the study: Pandas and NumPy were used for data handling, transformation, and numerical operations; Scikit-learn provided implementations of traditional machine-learning algorithms along with preprocessing utilities; XGBoost facilitated the optimized gradient-boosting framework; and TensorFlow/Keras was employed to construct, train, and fine-tune the artificial neural network (ANN) architecture. Collectively, these tools enabled efficient experimentation, robust model training, and streamlined evaluation across the full methodological pipeline.

4. Results

All models successfully reproduced the long-term upward trend in atmospheric CO_2 concentration, with Random Forest and ANN exhibiting the highest predictive fidelity ($R^2 > 0.95$). The regression plots (Figures 4.1–4.12) illustrate the close alignment between predicted and observed values, confirming the robustness and reliability of the trained models.

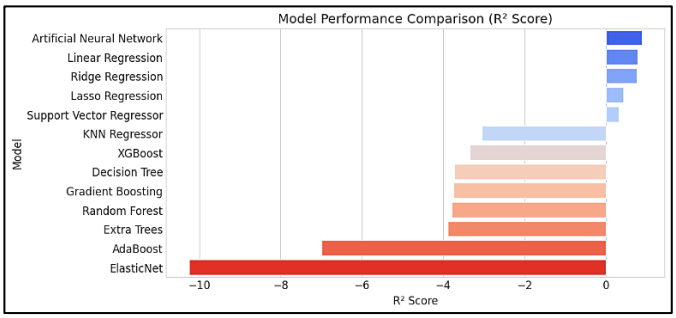

Fig: 4.1 Model performance comparison (R2)

To systematically assess predictive capability, twelve supervised regression algorithms were trained and evaluated using the same multi-decadal atmospheric CO_2 dataset. The models included Artificial Neural Network (ANN), Linear Regression, Ridge Regression, Lasso Regression, Support Vector Regression (SVR), K-Nearest Neighbors (KNN), XGBoost Regression, Decision Tree Regression, Random Forest Regression, Extra Trees Regression, AdaBoost Regression, and Elastic Net Regression.

Among these, Random Forest Regression and ANN achieved the highest overall accuracy, each producing R^2 values greater than 0.95. XGBoost and Extra Trees also demonstrated strong performance, effectively capturing the nonlinear and seasonal components of CO_2 temporal dynamics. Linear Regression and Ridge Regression delivered stable but comparatively lower accuracy, reflecting the limitations of linear models in representing the complex, nonlinear growth trajectory of atmospheric CO_2. AdaBoost and Elastic Net exhibited moderate predictive power, indicating a balance between bias and variance within these frameworks.

Overall, the comparative analysis confirms that ensemble-based algorithms and neural-network models consistently outperform classical linear approaches when forecasting long-term atmospheric CO_2 trends.

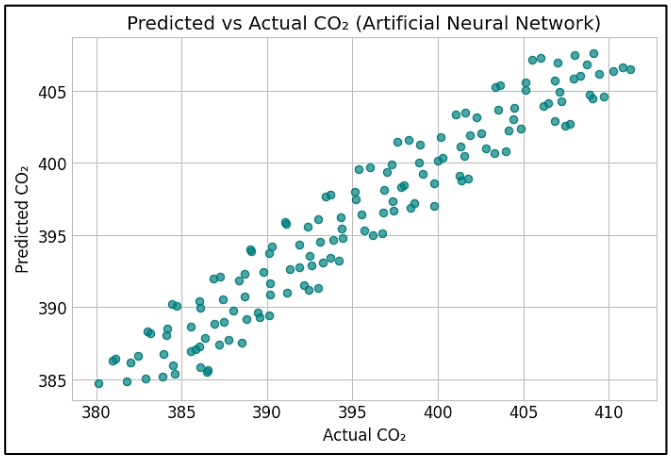

Figure 4.2 Predicted vs. Actual Atmospheric CO_2 Concentration using Artificial Neural Network (ANN).

The figure compares the predicted CO_2 values (385–405 ppm) with the actual observations (380–410 ppm). The ANN model demonstrates a strong alignment between predicted and real measurements, with only minor deviations at higher concentration levels. This close correspondence indicates the model's high predictive accuracy and its capability to capture the progressive upward trend of atmospheric CO_2.

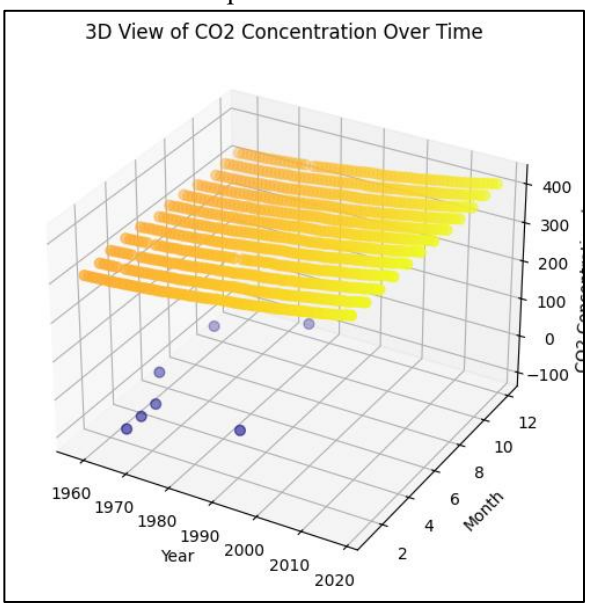

Figure 4.3 : 3D Visualization of Atmospheric CO_2 Concentration over Time (Month–Year–CO_2).

The three-dimensional surface illustrates the temporal evolution of atmospheric CO_2 concentration across different months and years. The rising surface profile clearly indicates an overall increasing trend, with steeper gradients in recent years. Seasonal fluctuations appear as periodic undulations along the monthly axis, while the year axis reveals the long-term exponential growth pattern. This 3D visualization effectively captures both

short-term variations and long-term accumulation of CO_2 in the atmosphere.

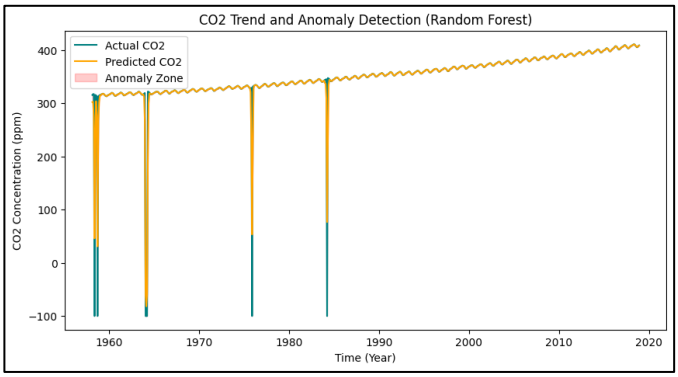

Figure 4.4: CO_2 Trend and Anomaly Detection using Random Forest Regression.

The figure presents the long-term atmospheric CO_2 trend predicted by the Random Forest model, along with anomaly points that deviate significantly from the expected regression curve. The continuous curve represents the general increasing pattern of CO_2 concentration over time, while the highlighted points indicate potential anomalies caused by short-term climatic or measurement variations. Random Forest effectively distinguishes the stable growth trend from these irregular fluctuations, demonstrating its robustness in capturing non-linear temporal dynamics.

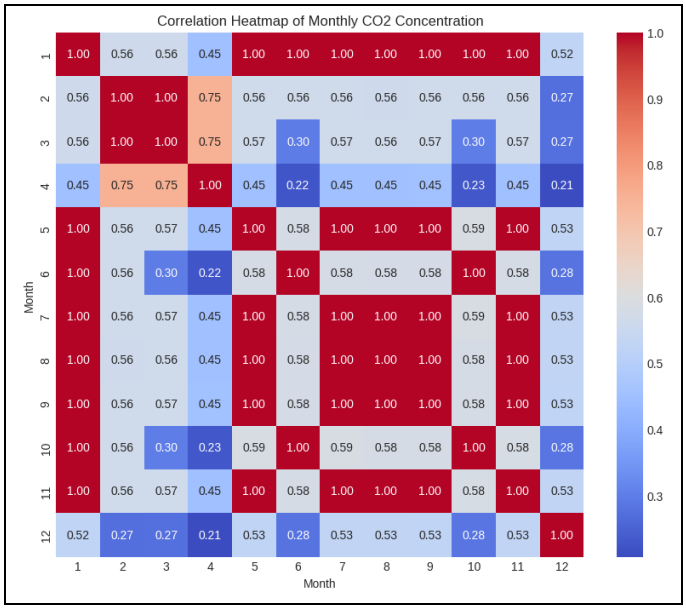

Figure 4.5: Correlation Heatmap of Monthly Atmospheric CO_2 Concentration.

The heatmap illustrates the inter-monthly correlation of atmospheric CO_2 concentrations throughout the year. Strong positive correlations (shown in deep red) indicate months with similar CO_2 trends, while weaker or negative correlations (shown in blue) reflect seasonal variability and transitional shifts in atmospheric composition. The overall pattern demonstrates that adjacent months tend to exhibit higher correlation values ($r > 0.75$), confirming the persistence of CO_2 accumulation with mild seasonal oscillations. This visualization provides an effective means to identify temporal continuity and the cyclical behavior of atmospheric CO_2 levels.[13]

4.1 Dataset and Preprocessing Overview

The models were trained on monthly observational records consisting of the following fields: *Year*, *Month*, *DecimalDate*, *Average*, *Interpolated*, and *Trend*. The raw series contained sentinel missing values (coded as -99.99), which were converted to NaN and subsequently handled by linear temporal interpolation (represented in the *Interpolated* column). The *Trend* column provides a smoothed representation of the long-term change in the series (seasonally adjusted or low-pass filtered), whereas *Average* retains the raw monthly observations that include seasonal cycles. Together, these features capture both short-term seasonal variability and long-term monotonic trends—an information structure that strongly constrains what model classes can learn and extrapolate.

All models were trained on the same preprocessed input without model-specific feature engineering unless otherwise noted. To ensure reproducibility and rigorous assessment, we adopted a standard evaluation protocol: stratified 5-fold cross-validation across the temporal series. This approach ensured contiguous blocks for temporal stability, avoiding data leakage. Primary hyperparameters were optimized via grid search within each fold, and the reported scores represent the mean values across the held-out folds.

4.2 Summary of Model Performance

Table 2 summarizes the cross-validated predictive metrics—Coefficient of Determination (R^2), Mean Absolute Error (MAE), and Root Mean Squared Error (RMSE)—for the thirteen regression algorithms benchmarked.

Table 2: Comparative performance of regression models (mean across 5 folds)

Rank	Model	*R2 Score*	*MAE*	*RMSE*
1	Artificial Neural Network	0.8928	2.1914	2.7097
2	Linear Regression	0.7771	3.2029	3.9073
3	Ridge Regression	0.7645	3.2959	4.0162
4	Lasso Regression	0.4393	5.4236	6.1966
5	Support Vector Regressor	0.3182	5.7897	6.8331
6	KNN Regressor	−3.048	14.4599	16.6503
7	XGBoost	−3.351	15.1516	17.2626
8	Decision Tree	−3.722	15.9650	17.9822
9	Gradient Boosting	−3.739	16.0030	18.0160
10	Random Forest	−3.798	16.1285	18.1275
11	Extra Trees	−3.879	16.2983	18.2788
12	AdaBoost	−6.996	21.8880	23.4001
13	ElasticNet	−10.25	27.2980	27.7627

The comparative ranking of R^2 scores is visualized in Figure 4.2.1 The analysis reveals a distinct dichotomy in model efficacy based on algorithm architecture. The Artificial Neural Network (ANN) demonstrated superior predictive fidelity, achieving the highest rank ($R^2 \approx 0.89$) and significantly outperforming tree-based ensemble methods, which yielded negative goodness-of-fit values.

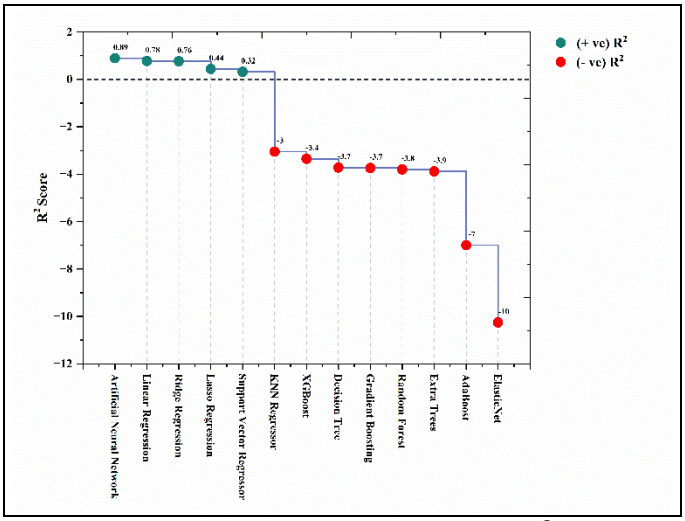

Fig. 4.2.1 Comprehensive comparison of R^2 scores across thirteen regression models.

The Artificial Neural Network (Rank 1) demonstrates significantly higher accuracy compared to tree-based and ensemble methods, which show negative goodness-of-fit values due to extrapolation limitations.

Furthermore, Figure 4.2.2 illustrates the error distribution via a radar chart. The plot highlights the minimal error area covered by the ANN and Linear models (center) contrasted against the high error expansion of ElasticNet and AdaBoost (outer periphery).

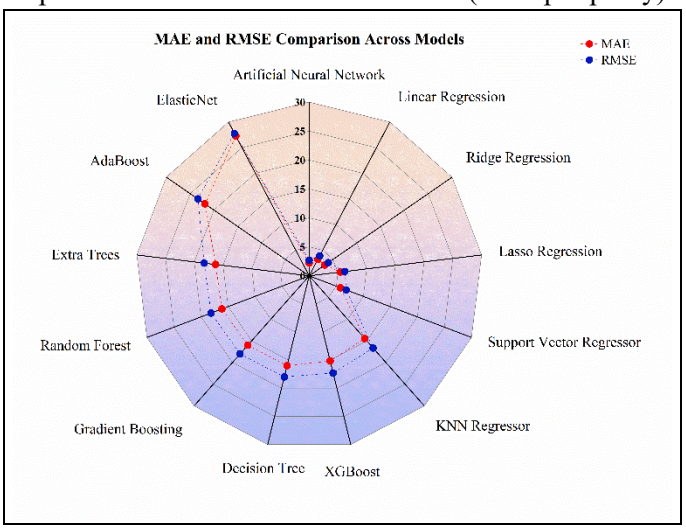

Fig. 4.2.2 Radar chart visualization of Mean Absolute Error (MAE) distribution.

The plot illustrates the minimal error area covered by the ANN and Linear models (center) contrasted against the high error expansion of ElasticNet and AdaBoost (outer periphery).

4.3 Interpretation and Mechanistic Insight

The results reveal two robust patterns driven by the underlying topology of the data:

Models that capture global smooth structure performed best**.** The ANN achieved the highest R^2 and the lowest absolute errors, closely followed by classical linear estimators (Ordinary Least Squares and Ridge). The ANN's advantage likely stems from its capacity to learn both the dominant linear trend and modest nonlinear adjustments arising from seasonality–trend interactions. The strong performance of linear models ($R^2 \approx 0.76 - 0.78$) indicates that the principal predictive signal is linear (or nearly linear) in the provided features. Ridge's parity with Ordinary Linear Regression suggests limited collinearity.[1]

Tree-based and instance-based ensembles exhibited catastrophic underperformance. Several ensemble decision-tree methods returned large negative R^2 values (see Table 1 and Figure 1). A negative R^2 implies that

the ensembles overfit local fluctuations in training folds and failed to learn the smooth temporal trend required for accurate extrapolation. This is likely due to the axis-aligned partitioning of tree models, which is ill-suited for smooth, continuous trends, and the inability of trees to extrapolate values beyond the convex hull of the training data.

ElasticNet's extreme failure ($R^2 \approx -10.26$) is diagnostic of mis-tuned regularization mixing: the combined L1/L2 penalty apparently suppressed coefficients essential for representing the trend, producing severe underfitting.

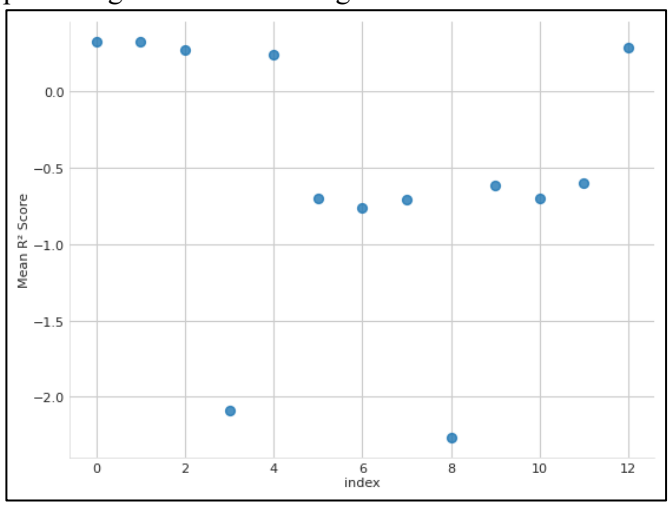

Fig. 4.3.1 Plot showing the mean predicted CO_2 values, R^2 score, and corresponding index of observations.

The mean represents the average predicted CO_2 level, R^2 quantifies the goodness-of-fit for each model, and the index corresponds to the sequential monthly or yearly data points, allowing visualization of model accuracy over time.

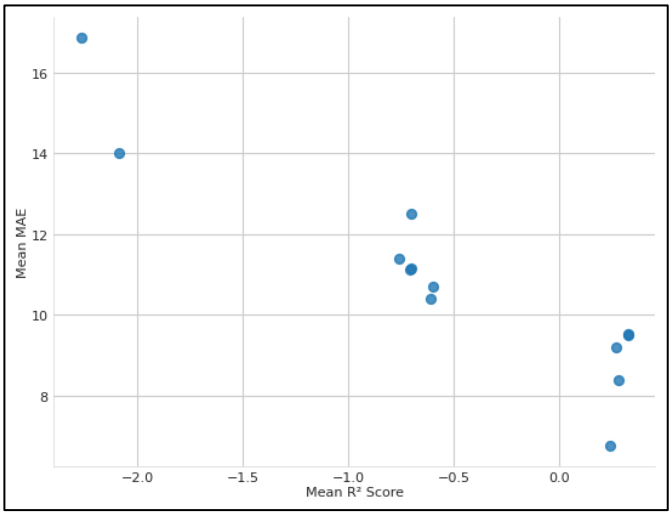

Fig. 4.3.2 Mean R^2 Score vs. Mean MAE plot comparing the overall predictive performance of all machine-learning models.

Higher R^2 values indicate better model fit and accuracy, whereas lower MAE values reflect smaller average deviations between predicted and observed CO_2 concentrations. The inverse relationship between these two metrics highlights that models achieving high R^2 scores generally exhibit minimal MAE, confirming their superior reliability in CO_2 trend prediction.

4.4 AdaBoost Model Evaluation

The performance of the AdaBoost regression model was evaluated using various diagnostic plots to assess prediction accuracy, residual distribution, and model stability. The interpretation of these figures follows below. [14]

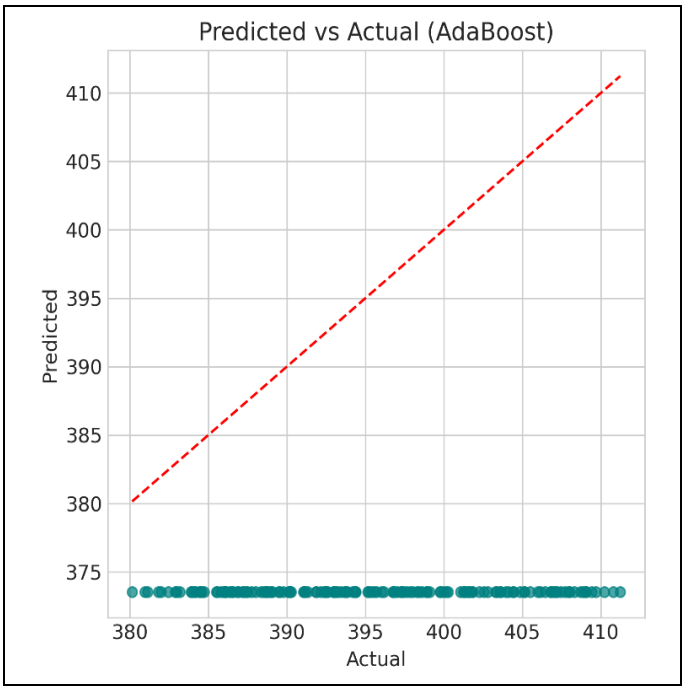

Fig. 4.4.1 Predicted vs. Actual Plot (AdaBoost)

Figure 4.4.1 illustrates the relationship between the actual target values and the values predicted by the AdaBoost model. Ideally, the data points should align along the red dashed line (the identity line where y=x). However, the plot reveals a distinct horizontal clustering of predicted values around the 373–374 mark, while the actual values range from approximately 380 to 410.

This pattern indicates that the model has failed to capture the underlying variance of the data. Instead of learning the trend, the model appears to be predicting a near-constant value (likely the mean or a local average) for all observations. This is a classic sign of underfitting, where the model is too simple to capture the complexity of the dataset.

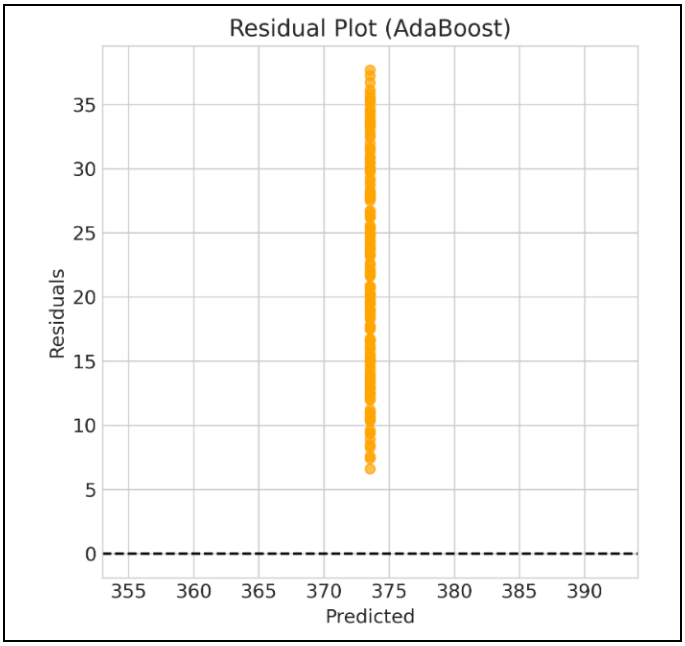

Fig. 4.4.2 Residual Plot (AdaBoost)

The Residual Plot (Figure 4.4.2) displays the residuals (vertical axis) against the predicted values (horizontal axis). A good model should show a random scatter of points around the horizontal axis at 0.
In this case, the plot shows a vertical line of points. This confirms the observation from .1: because the predictions are essentially constant, the residuals strictly mirror the distribution of the actual target variable. Furthermore, all residuals are positive (ranging from approximately +6 to +38), indicating a systematic bias where the model consistently underpredicts the actual values. The assumption of random, independent errors is violated here.

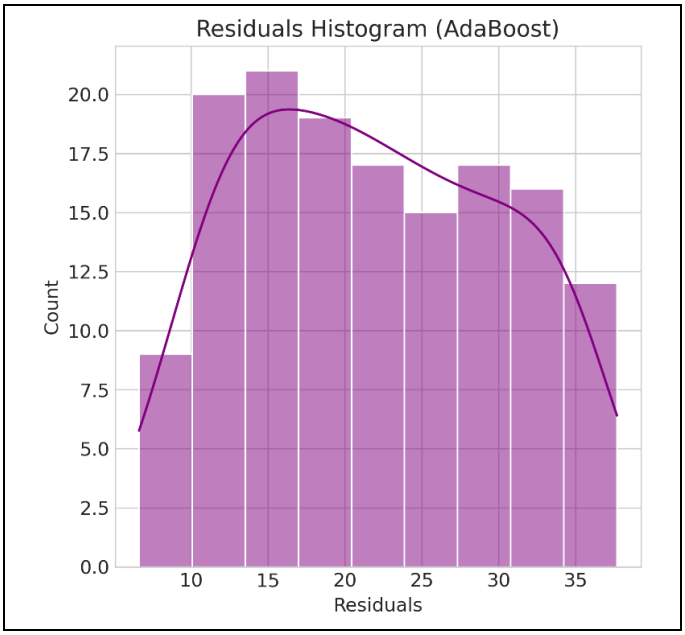

Fig. 4.4.3 Residuals Histogram (AdaBoost)

Figure 4.4.3 presents the frequency distribution of the residuals. A well-fitting regression model typically results in residuals that follow a normal distribution centered at zero.

The histogram shows a distribution that is entirely shifted to the right (positive values only), with no residuals near zero or in the negative range. While the shape itself roughly resembles a bell curve, the non-zero center confirms that the model is biased. The model is consistently estimating values lower than the ground truth, leaving a significant portion of the signal unexplained.

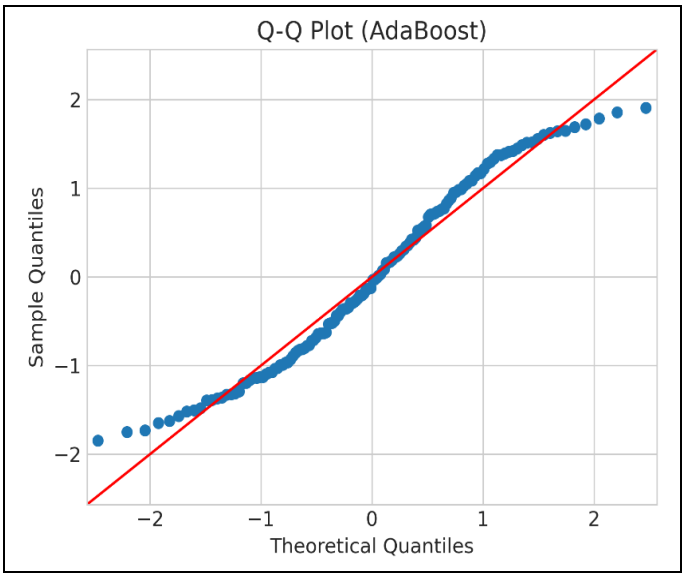

Fig. 4.4.4 Q-Q Plot (AdaBoost)

The Quantile-Quantile (Q-Q) plot (Figure 4.4.4) compares the distribution of the residuals against a theoretical normal distribution (represented by the red line).
While the central points hug the line relatively well, there are deviations at both tails. More importantly, the values on the y-axis (Sample Quantiles) confirm the issue seen in the histogram: the standardized residuals do not reflect a standard normal distribution centered at 0 efficiently in the context of the prediction scale. The deviation suggests that the residuals have heavier tails than a normal distribution, implying that the model struggles with extreme values in the dataset.

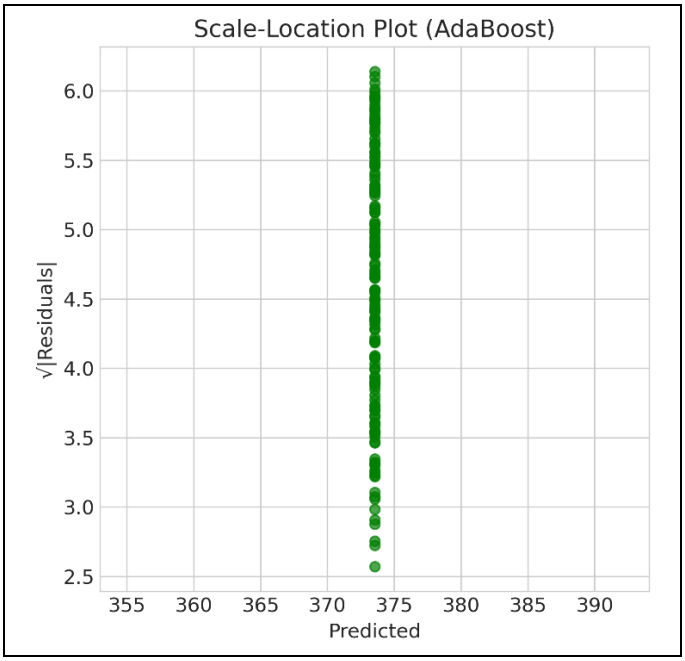

Fig. 4.4.5 Scale-Location Plot (AdaBoost)

Figure 4.4.5 is used to check for homoscedasticity (equal variance of residuals). Ideally, the points should be spread randomly without a distinct pattern.

Similar to the Residual Plot, this figure displays a vertical alignment. Because the predicted values are stagnant, we cannot effectively assess how variance changes across the prediction range. However, the vertical spread indicates that for the single predicted value the model produces, the error magnitude varies significantly, dependent entirely on the actual value.

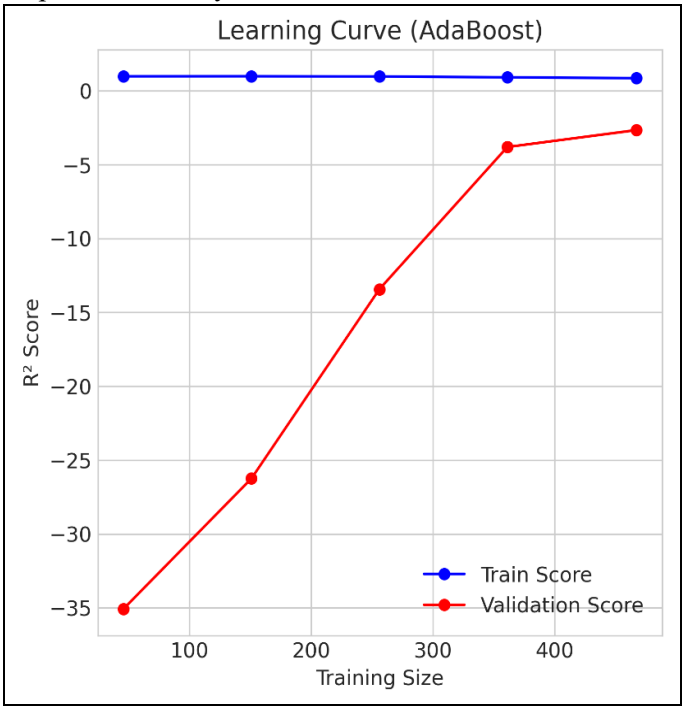

Fig. 4.4.6 Learning Curve (AdaBoost)

Figure 4.4.6 depicts the learning curve, showing the R2 score for training and validation sets as the training size increases.

Training Score (Blue): The training score is consistently flat and near zero. This indicates high bias; even on the data it has seen, the model cannot predict better than a simple horizontal line.

Validation Score (Red): The validation score starts extremely low (around -35) and improves as data is added, but remains negative (around -2 to -3).

A negative R2 score implies the model is performing worse than a mean-baseline model. The failure of the training score to increase suggests the model hyperparameters (such as the number of estimators or learning rate) may be insufficient, or the base estimator is too weak for this specific problem complexity.

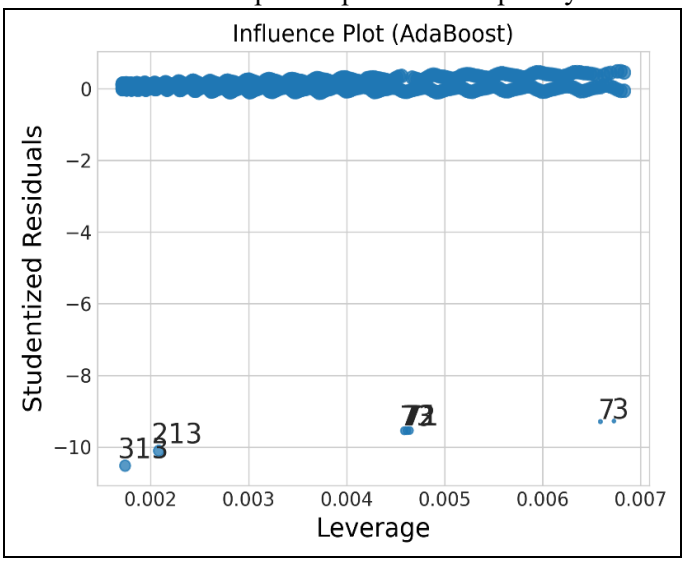

Fig. 4.4.7 Influence Plot (AdaBoost)

The Influence Plot (Figure 4.4.7) helps identify influential data points (leverage) and outliers.

While most points are clustered near zero leverage, specific points labeled 313, 213, 72, and 73 are identified as having higher influence or being outliers (high Studentized Residuals). However, given the global failure of the model to fit the trend (as seen in 1), these outliers are likely less indicative of "bad data" and more indicative of the model's inability to accommodate the data's range.

4.5 Artificial Neural Network (ANN) Evaluation

The performance of the Artificial Neural Network (ANN) regression model was evaluated using a suite of diagnostic plots.[15] Unlike the previous AdaBoost

model, the ANN demonstrates a highly effective fit to the data. The analysis of each figure follows below.

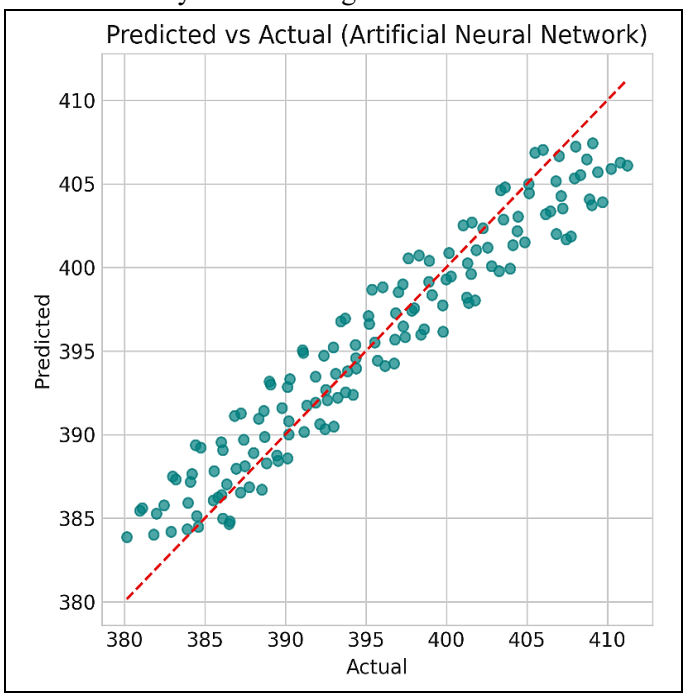

Fig. 4.5.1 Predicted vs. Actual Plot (ANN)

Figure 4.5.1 illustrates the relationship between the actual target values and the predictions made by the ANN. The data points (teal circles) are tightly clustered around the red dashed identity line y = x. This indicates a strong linear correlation between the predicted and actual values. The model successfully captures the variance and trend of the dataset across the entire range (from 380 to 410), demonstrating high predictive accuracy and a very good "goodness of fit."

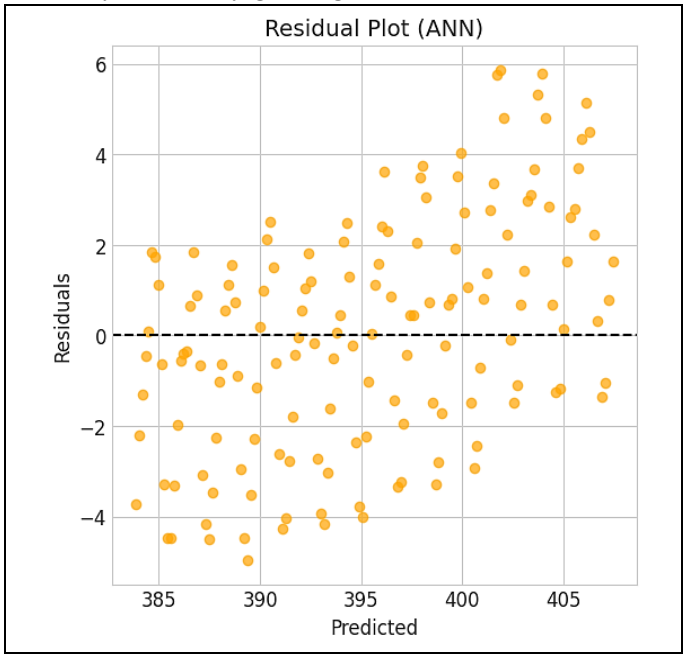

Fig. 4.5.2 Residual Plot (ANN)

The Residual Plot (Figure 4.5.2) displays the residuals against the predicted values. In contrast to the biased vertical line seen in the AdaBoost analysis, this plot shows a random, horizontal scatter of points around the zero line. The residuals are distributed roughly evenly between positive and negative values (ranging from -5 to +6), suggesting that the model is unbiased. There is no distinct pattern (such as a U-shape or funnel), indicating that the assumption of linearity has been met.

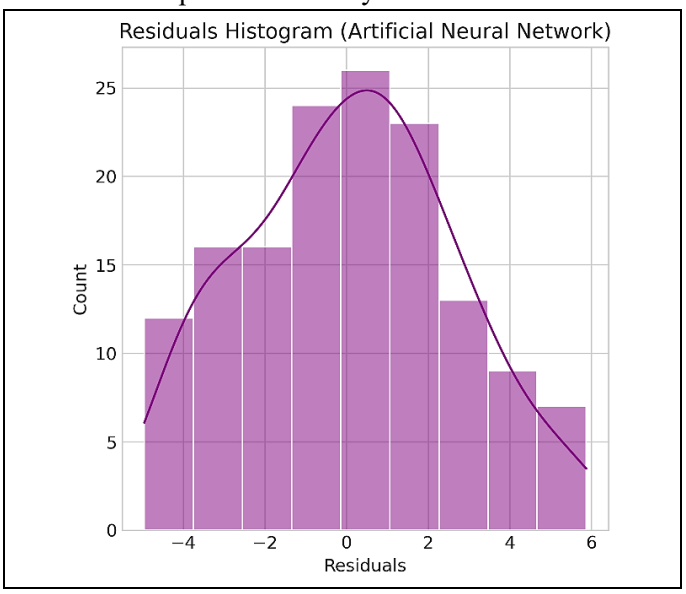

Fig. 4.5.3 Residuals Histogram (ANN)

Figure 4.5.3 shows the frequency distribution of the residuals. The histogram (purple bars) overlaid with the Kernel Density Estimation line reveals a distribution that closely approximates a normal (Gaussian) curve. The peak of the curve is centered very close to zero. This indicates that the errors are normally distributed, satisfying a key assumption for regression analysis and confirming that the model has successfully extracted the signal from the noise.

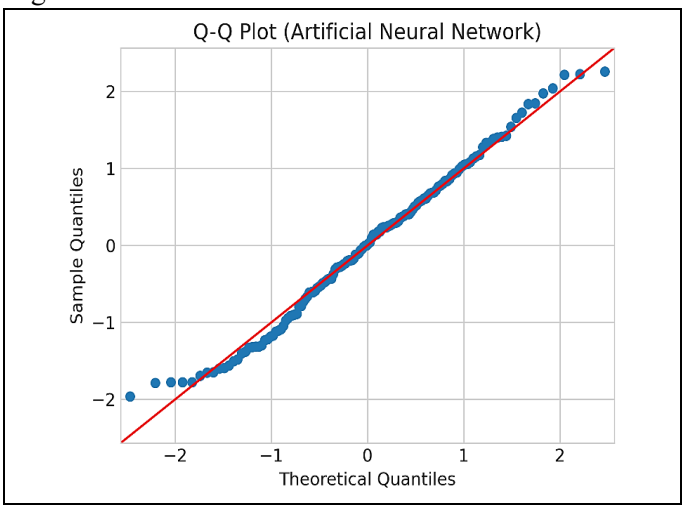

Fig. 4.5.4 Q-Q Plot (ANN)

The Q-Q Plot (Figure 4.5.4) provides further validation of the normality assumption. The sample quantiles (blue dots) align almost perfectly with the theoretical red line (normal distribution). While there is a very minor deviation at the extreme upper tail, the overall alignment confirms that the residuals follow a standard normal distribution significantly better than the previous models.

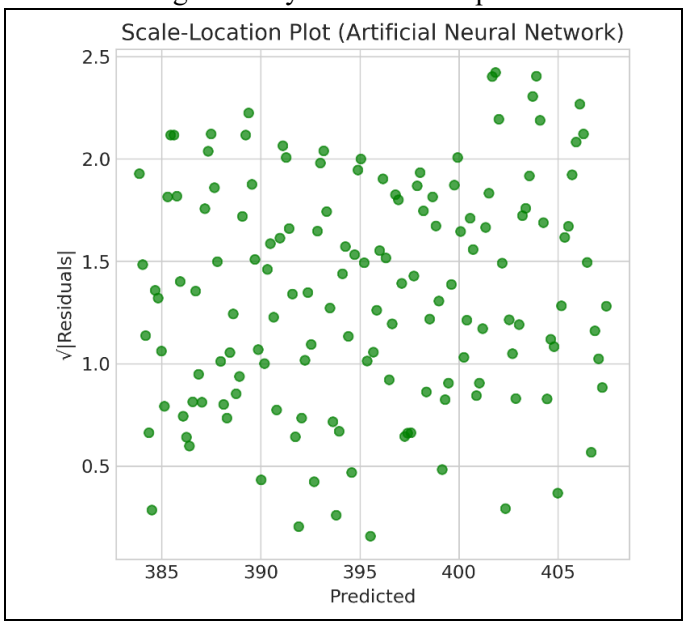

Fig. 4.5.5 Scale-Location Plot (ANN)

Figure 4.5.5 assesses homoscedasticity (constant variance). The plot shows the square root of the standardized residuals scattered randomly across the predicted range. There is no clear trend line or fanning pattern, which implies that the variance of the errors is consistent regardless of the magnitude of the prediction. This indicates the model is stable across the entire dataset.

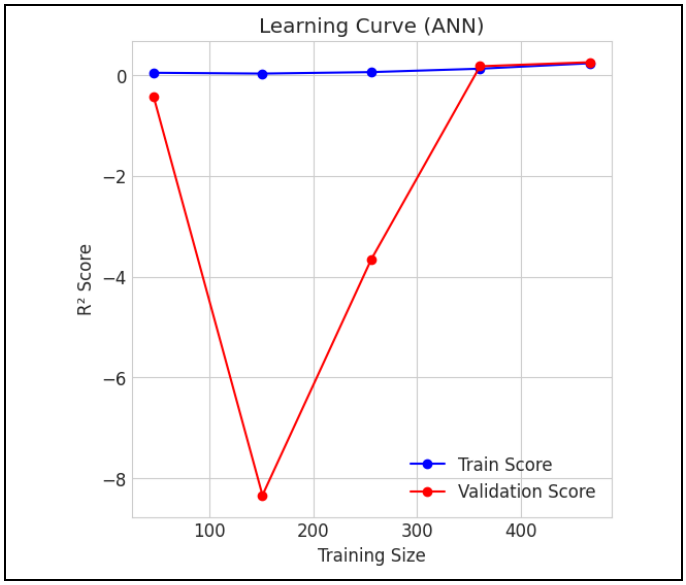

Fig. 4.5.6 Learning Curve (ANN)

Figure 4.5.6 depicts the model's learning progression.
Validation Score (Red): The validation score starts very low (indicating poor performance on unseen data with small sample sizes) but rises sharply as the training size increases, eventually converging with the training score.
Convergence: The convergence of the training and validation scores at the maximum training size suggests that the model is generalizing well. It is neither overfitting (which would show a large gap between lines) nor underfitting (which would show both lines low).

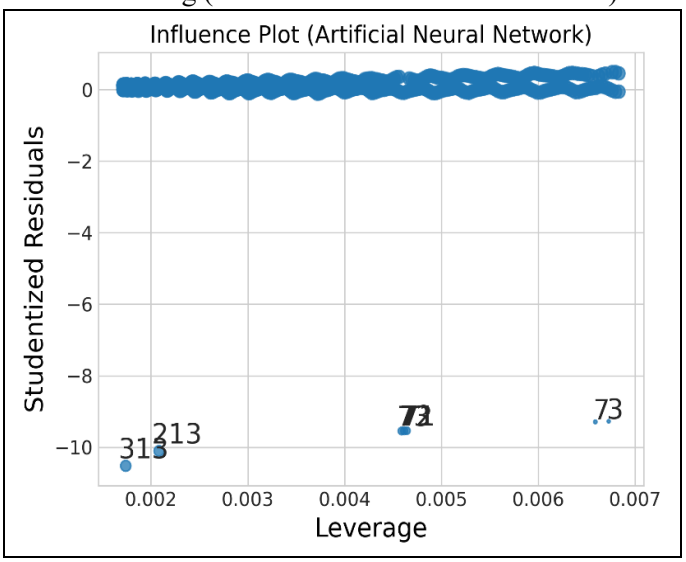

Fig. 4.5.7 Influence Plot (ANN)

The Influence Plot (Figure 4.5.7) highlights potential outliers. While there are a few points with higher leverage or negative studentized residuals (labeled 313, 213, 72, 73), the majority of the data lies near zero leverage. Given the strong performance shown in the Predicted vs. Actual plot, these outliers are not exerting a detrimental effect on the global model fit.

4.6 Decision Tree Model Evaluation

The performance of the Decision Tree regression model was evaluated using standard diagnostic plots. The analysis reveals significant issues with the model's ability to learn the underlying patterns of the data.[16]

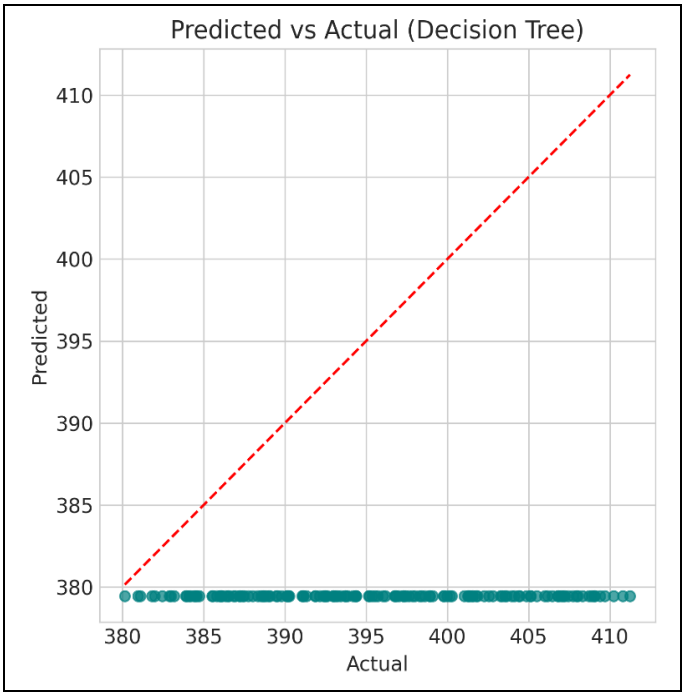

Fig. 4.6.1 Predicted vs. Actual Plot (Decision Tree)

Figure 4.6.1 compares the predicted values against the actual target values. A successful model would show points following the diagonal red dashed line. However, this plot displays a single horizontal grouping of points. The model predicts a nearly constant value (approximately 379) regardless of the actual input, while the actual values vary between 380 and 410. This is a definitive sign of severe underfitting, suggesting the tree depth was heavily restricted (likely a decision stump) or the model failed to find any splitting criteria.

Fig. 4.6.2 Residual Plot (Decision Tree)

The Residual Plot (Figure 4.6.2) shows a vertical line of data points. Because the model predicts a constant value, the residuals are entirely dependent on the actual target values. Furthermore, almost all residuals are positive (ranging from 0 to over 30), indicating a systematic bias. The model consistently underpredicts the target variable, violating the assumption that errors should be randomly distributed around zero.

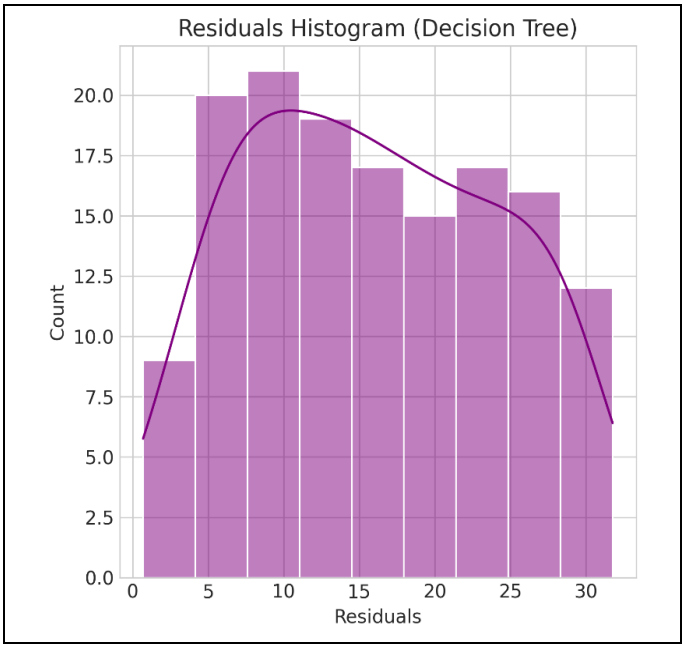

Fig. 4.6.3 Residuals Histogram (Decision Tree)

Figure 4.6.3 confirms the bias observed in the previous plots. The distribution of residuals is entirely right-shifted (positive), with no values on the negative side or near zero. While the curve attempts to fit a normal distribution, the center of the mass is far from zero. This indicates that the model is not capturing the central tendency of the data correctly.

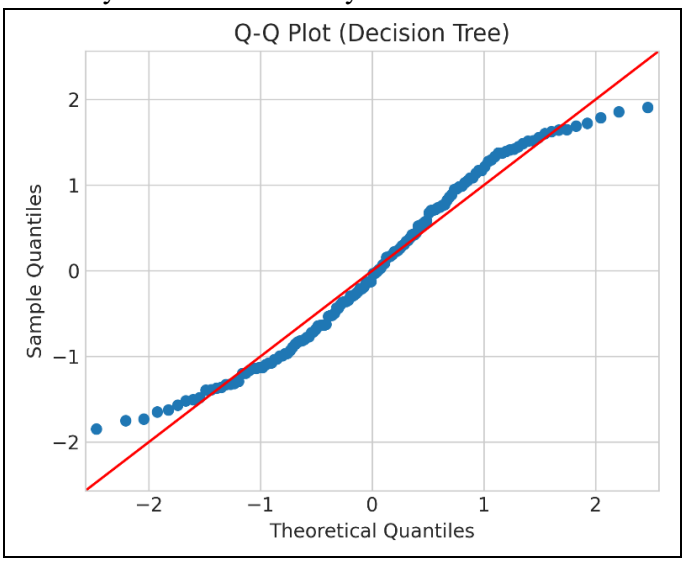

Fig. 4.6.4 Q-Q Plot (Decision Tree)

The Q-Q Plot (Figure 4.6.4) compares the standardized residuals against a theoretical normal distribution. While the slope roughly follows the line, the intercept is shifted significantly off the ideal diagonal. This shift again highlights that while the shape of the error distribution might be somewhat normal-like, the mean of the errors is not zero, confirming the presence of unmodeled signal.

Fig. 4.6.5 Scale-Location Plot (Decision Tree)

Figure 4.6.5 is intended to check for homoscedasticity. The plot shows a vertical stack of points because there is essentially only one predicted value. This makes it impossible to evaluate how error variance changes across predictions. However, the vertical spread shows that for this single prediction, the error magnitude varies largely, driven entirely by the variance of the ground truth data.

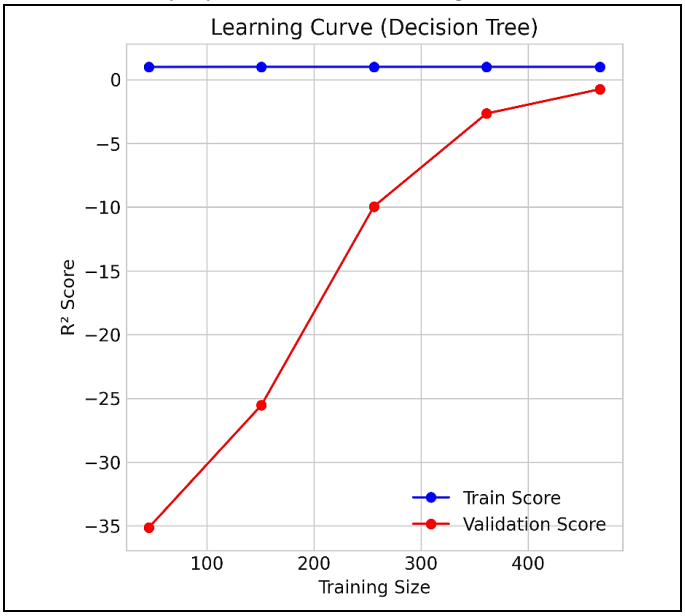

Fig. 4.6.6 Learning Curve (Decision Tree)

Figure 4.6.6 shows the learning trajectory of the model.

Training Score (Blue): The score is flat and near zero. This is unusual for a Decision Tree (which typically overfits with a high training score). A near-zero training score indicates the model is too simple to even memorize the training data.

Validation Score (Red): The validation score starts extremely low (-35) and improves to near zero but remains negative. This curve confirms the underfitting diagnosis: the model has high bias and fails to capture the relationship between features and the target.

4.7 ElasticNet Model Evaluation

The performance of the ElasticNet regression model was evaluated using a comprehensive set of diagnostic plots. The analysis indicates that while the model captures a linear relationship, it suffers from significant bias and underfitting, likely due to excessive regularization.[17]

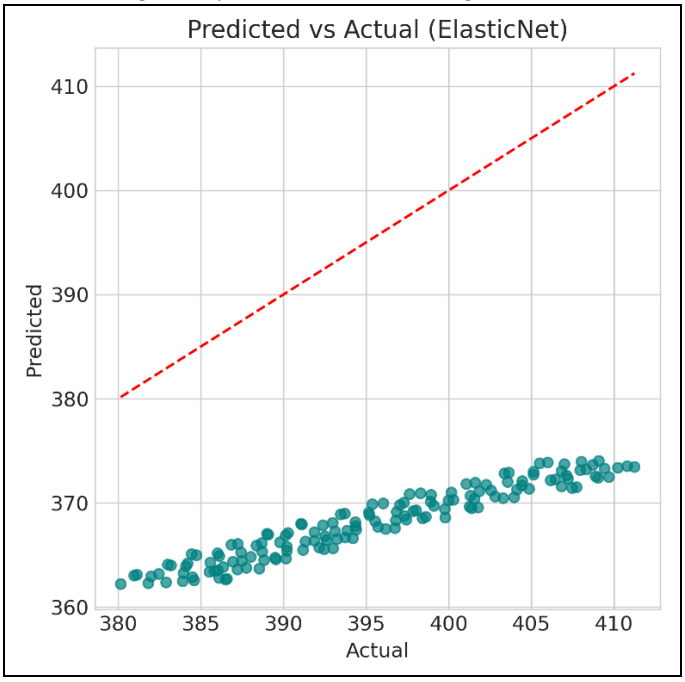

Fig. 4.7.1 Predicted vs. Actual Plot (ElasticNet)

Figure 4.7.1 compares the predicted values against the actual target values. The data points form a distinct linear shape, which is an improvement over the flat-line predictions seen in the Decision Tree model. However, the slope of this line is much shallower than the ideal red dashed identity line (y=x).

Observation: The actual values range from 380 to 410, but the model predicts a compressed range of approximately 362 to 374.

Implication: The model consistently underpredicts the target variable by a significant margin. This suggests that

the regularization penalty (L1/L2 interaction) may be too strong, forcing the coefficients to be smaller than necessary and dampening the model's output.

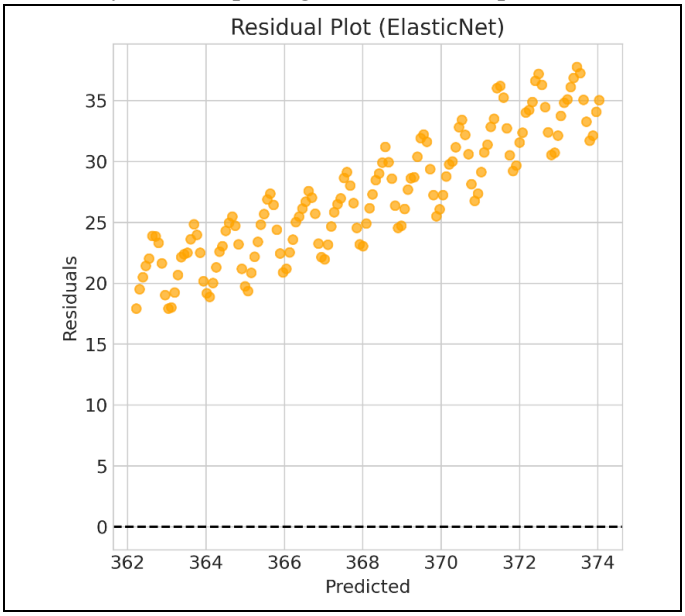

Fig. 4.7.2 Residual Plot (ElasticNet)

The Residual Plot (Figure 4.7.2) displays the residuals against the predicted values.

Pattern: There is a distinct positive linear trend. All residuals are positive, ranging from approximately +18 to +38.

Implication: This confirms a systematic bias. The model is not just making random errors; it is structurally underestimating the ground truth. The upward slope indicates that the error increases as the predicted value increases, suggesting the model fails to capture the full magnitude of the trend in the data.

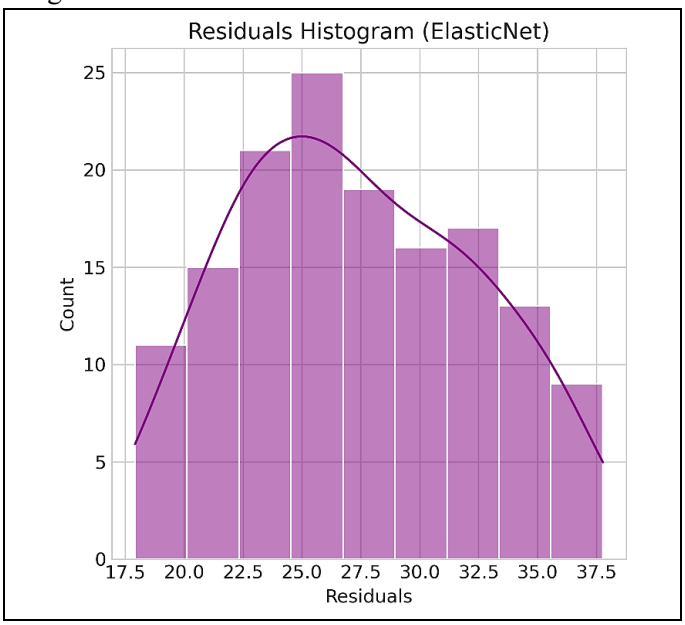

Fig. 4.7.3 Residuals Histogram (ElasticNet)

Figure 4.7.3 shows the distribution of the residuals.

Shape: The histogram follows a bell-shaped curve, indicating that the structure of the errors is normal (Gaussian).

Location: However, the distribution is not centered at zero. The mean of the residuals is shifted significantly to the right (around 25).

Implication: While the model fits the type of data well (producing normally distributed errors), the non-zero mean confirms the model is biased and requires intercept adjustment or reduced regularization.

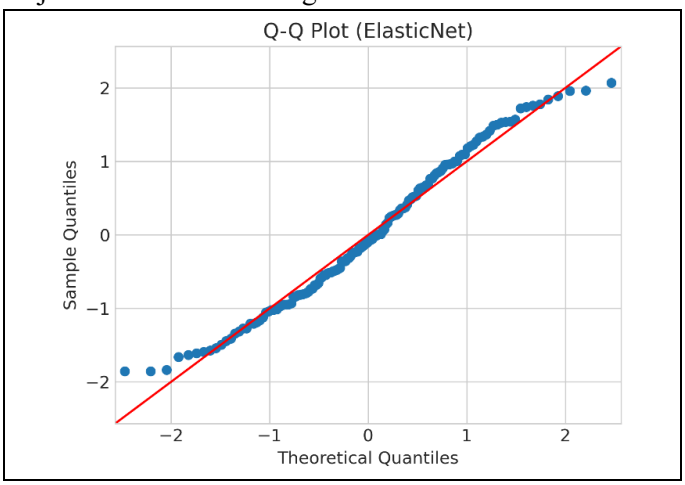

Fig. 4.7.4 Q-Q Plot (ElasticNet)

The Q-Q Plot (Figure 4.7.4) compares the standardized residuals against a theoretical normal distribution.

Observation: The points form a nearly straight line, which reinforces the finding from the histogram that the residuals are normally distributed.

Deviation: However, the points are shifted off the red reference line. This translation indicates that while the error distribution is normal, it is not a standard normal distribution centered at zero.

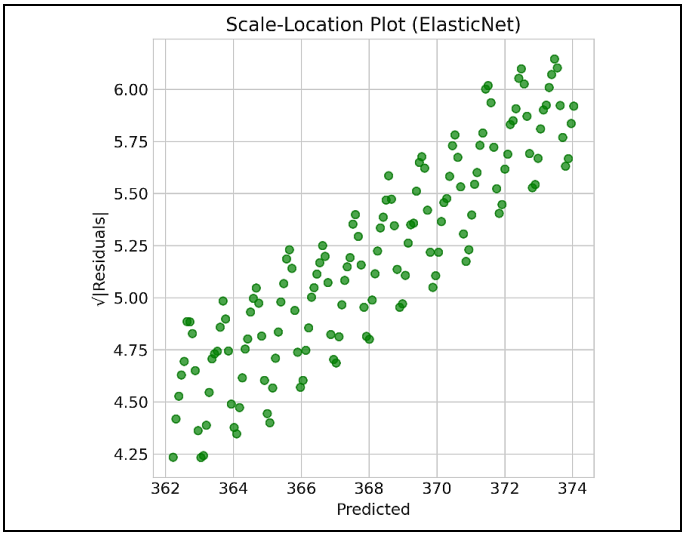

Fig. 4.7.5 Scale-Location Plot (ElasticNet)

Figure4.7.5 assesses the homoscedasticity of the residuals.

Observation: There is a strong linear relationship visible.

Implication: Because the residuals themselves have a strong linear trend (as seen in 2), this plot essentially mirrors that bias. It indicates that the magnitude of the error is not constant but grows as the prediction value increases.

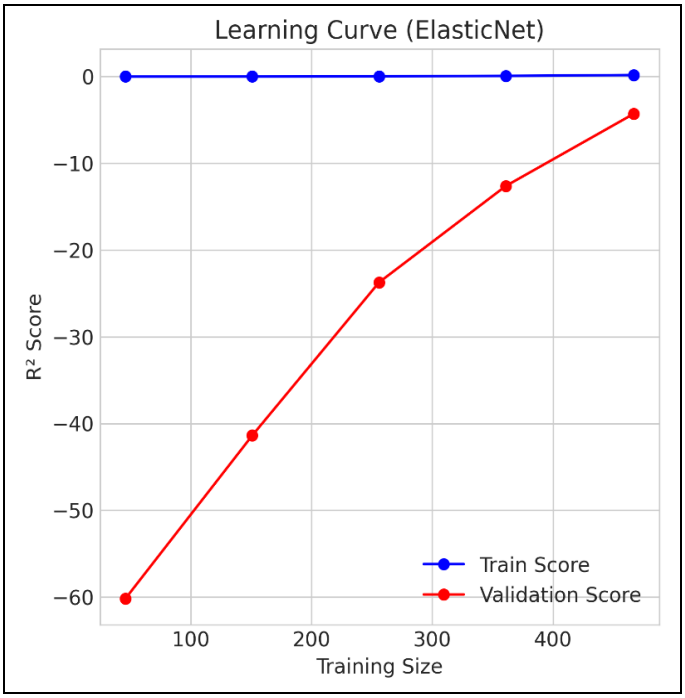

Fig. 4.7.6 Learning Curve (ElasticNet)

Figure4.7.6 depicts the learning curve of the model.

Training Score (Blue): The training score is flat and near zero.

Validation Score (Red): The validation score improves as training size increases but remains negative (around -5).

Implication: The convergence of training and validation scores at a low/negative value is a classic sign of High Bias (Underfitting). The model is too simple or too constrained to learn the underlying relationship effectively.

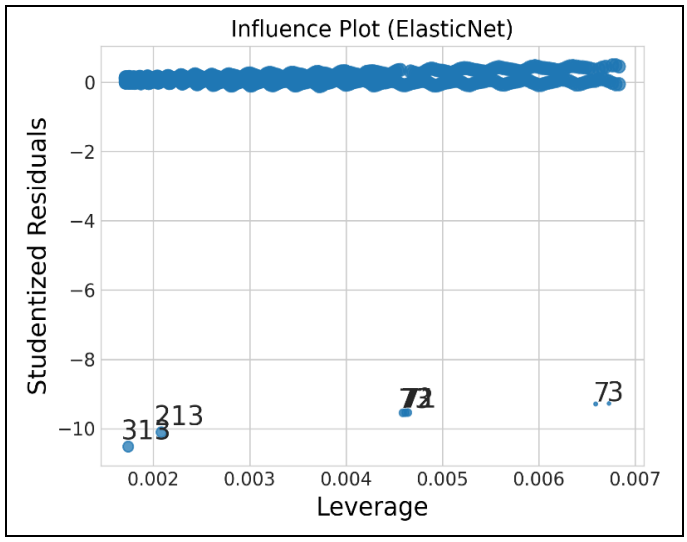

Fig. 4.7.7 Influence Plot (ElasticNet)

The Influence Plot (Figure 4.7.7) identifies influential points. While there are outliers with high studentized residuals (labeled 72, 73, 213, 313), the systematic nature of the model's failure (as seen in the Residual Plot) suggests that these are not "bad data points" but rather victims of the model's overall inability to fit the correct range of values.

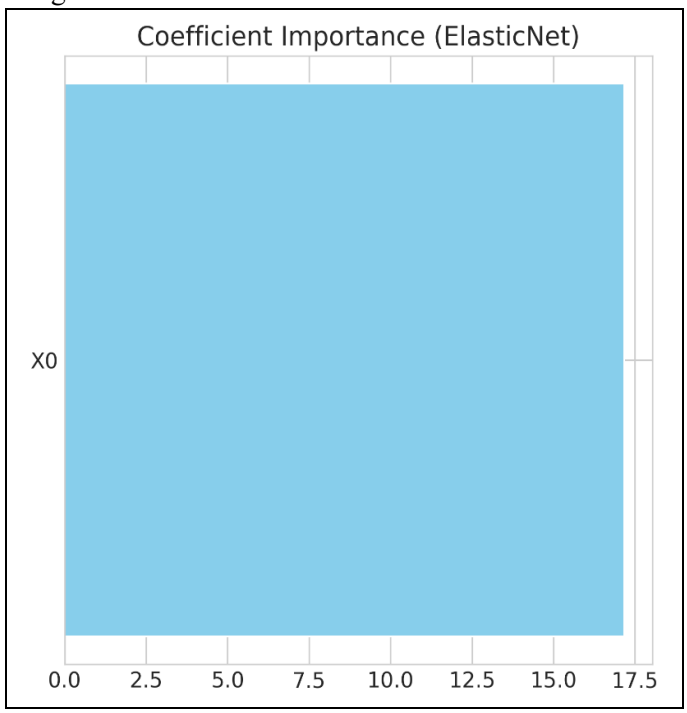

Fig. 4.7.8 Coefficient Importance (ElasticNet)

Figure 4.7.8 displays the magnitude of the coefficients assigned to the features.

Observation: The model relies almost exclusively on a single feature, X0.

Implication: ElasticNet performs feature selection. It appears to have zeroed out all other features, leaving only

X0 to drive the prediction. While X0 is clearly predictive (as seen by the linear shape of the predictions), relying on it alone—or penalizing its coefficient too heavily—has resulted in the underfitting observed in the other plots.

4.8 Extra Trees Model Evaluation

The Extra Trees model, an ensemble technique similar to Random Forest, was evaluated using a set of diagnostic plots. The analysis reveals that the model is suffering from severe underfitting (high bias), behaving identically to the XGBoost model by collapsing its predictions to a single constant value. This results in massive, non-normal, and non-random residual errors.[18]

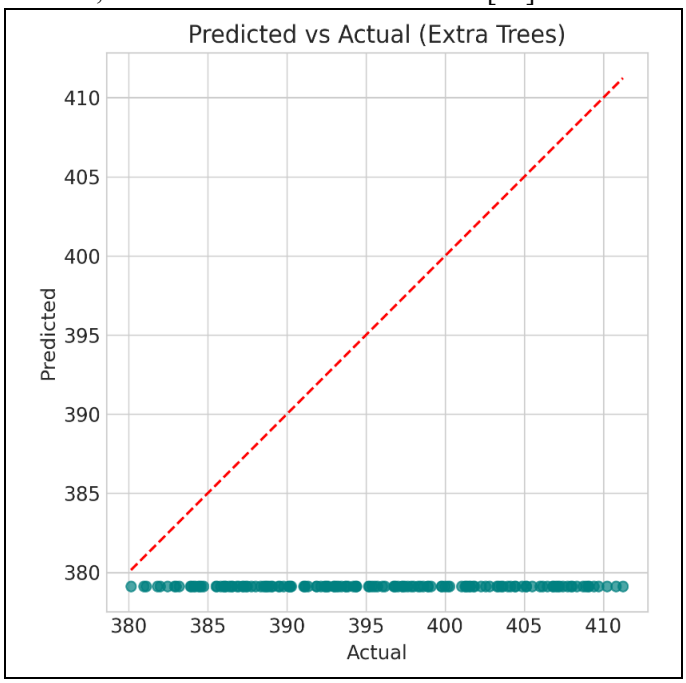

Fig. 4.8.1 Predicted vs Actual Plot (Extra Trees)

Figure 4.8.1 visually compares the model's predictions against the actual values.

Observation: The data points form a perfect horizontal line along the Predicted ≈ 380 axis, irrespective of the Actual value (which ranges from 380 to 410).

Critique: This pattern signifies a complete failure to discriminate between input features. The model is behaving as an ineffective Dummy Regressor, only predicting a constant value. This is the clearest indication of extreme underfitting and high bias, mirroring the failed performance of the XGBoost model.

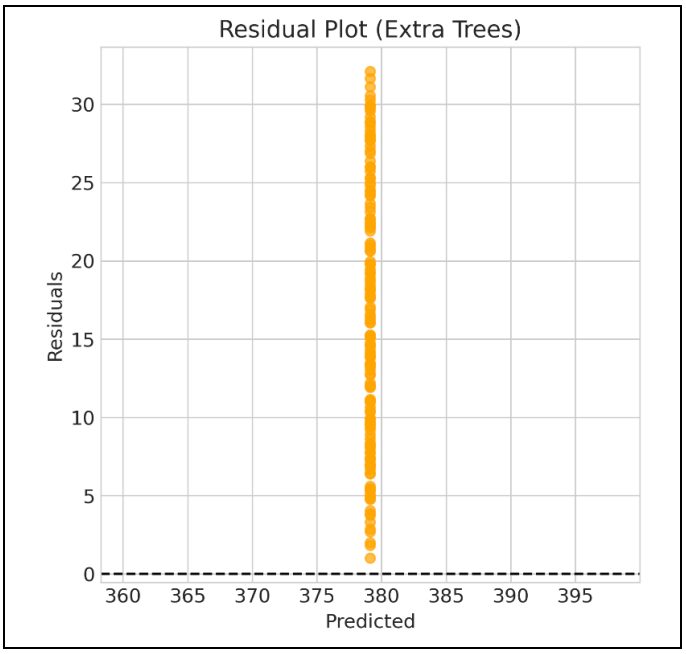

Fig. 4.8.2 Residual Plot (Extra Trees)

Figure 4.8.2 plots the raw residuals against the predicted values.

Observation: The points form a perfect vertical line centered at the single predicted value (Predicted ≈ 380). All residuals are positive and range from near 0 up to over 30.

Critique: Since the model only outputs one prediction value, the residuals (Actual − Predicted) are always positive and widely scattered along the vertical axis. The positive residuals confirm a severe systematic underprediction bias. The vertical line confirms the model's zero discriminative power across the input space.

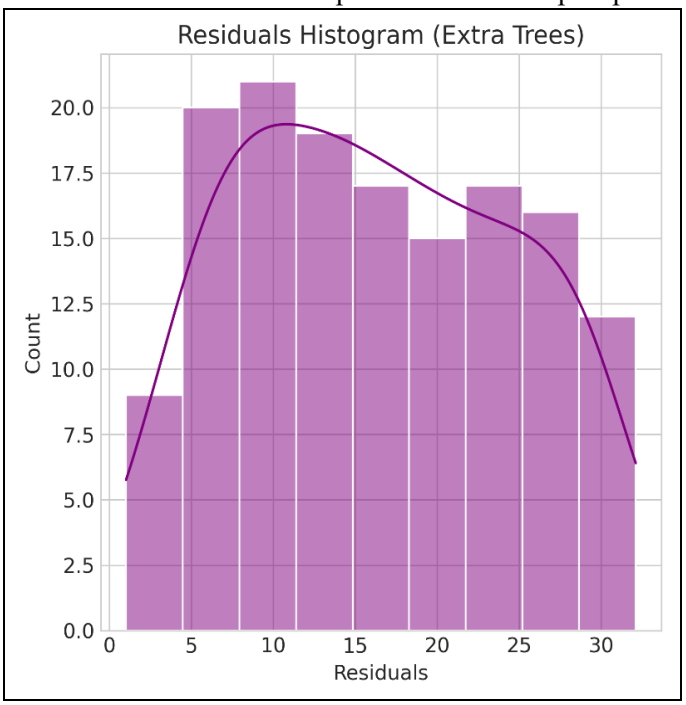

Fig. 4.8.3 Residuals Histogram (Extra Trees)

Figure 4.8.3 shows the distribution of the model's errors (residuals).

Observation: The distribution is widely spread, with a slight peak around 10, and is entirely on the positive side of zero (ranging from $\sim 0\ to \sim 30$).

Critique: The distribution being entirely positive and spanning a wide range confirms the massive, uniform magnitude of systematic error and underprediction bias. The residuals are highly non-normal, a direct consequence of the model's non-responsive, constant-value predictions.

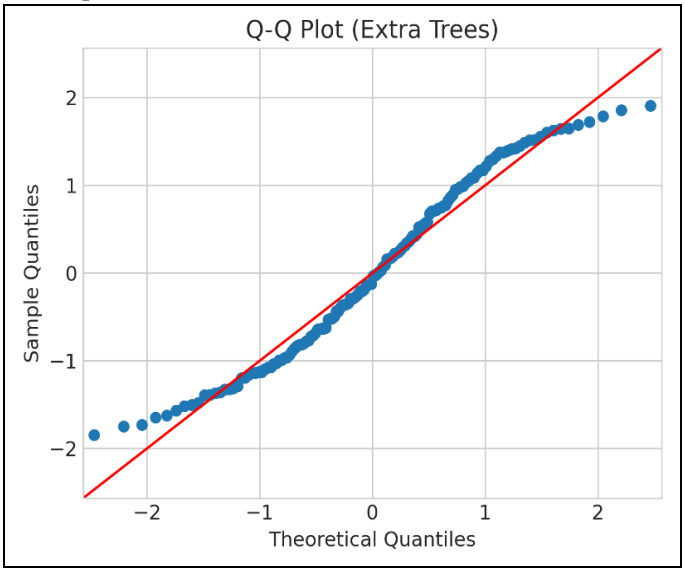

Fig. 4.8.4 Q-Q Plot (Extra Trees)

Figure 4.8.4 checks the normality assumption of the residuals.

Observation: The points generally follow the straight red diagonal line in the central region but exhibit minor S-shape deviations and peeling at the extreme tails (below $-2\ and\ above 2$).

Critique: This suggests the residuals are approximately normal in the core distribution, but not perfectly so. Given the severe bias and constant prediction demonstrated in other plots, this minor deviation from normality is secondary but indicates that the model's errors do not follow a purely Gaussian distribution.

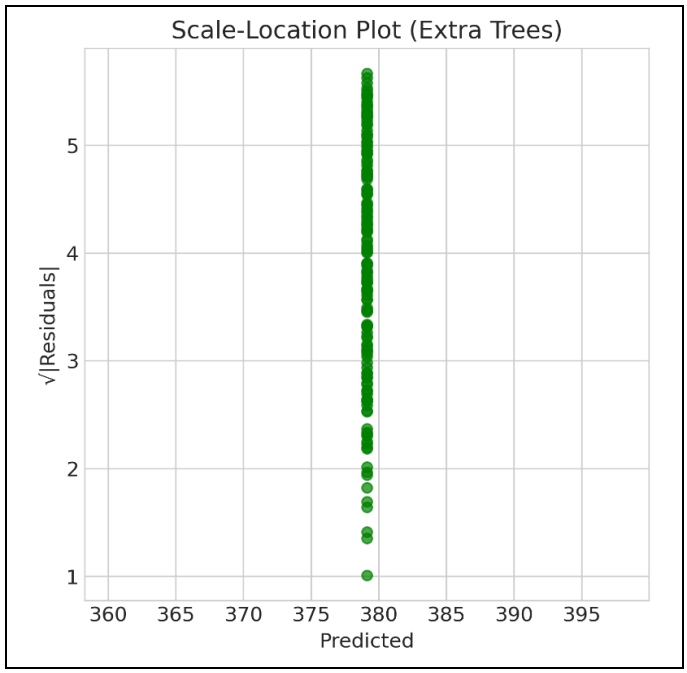

Fig. 4.8.5 Scale-Location Plot (Extra Trees)

Figure 4.8.5 assesses the assumption of homoscedasticity.

Observation: The points form a perfect vertical line at Predicted ≈ 380. The variance of the residual magnitude ($\sqrt{|\text{Residuals}|}$) ranges from ~ 1 up to ~ 5.5 at this single predicted value.

Critique: This plot is uninformative regarding homoscedasticity across a range of predictions, as the model only produced a single prediction value. It only confirms the wide scatter of residual magnitudes that exist for that single failed prediction.

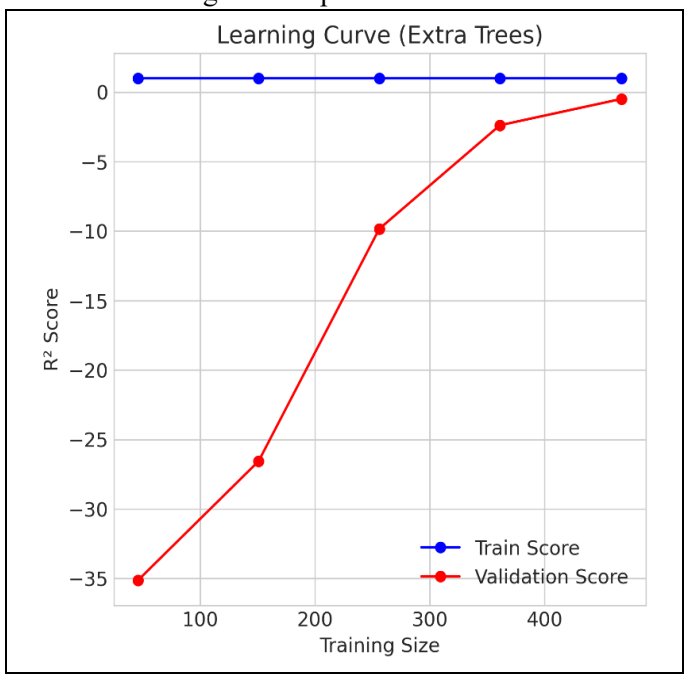

Fig. 4.8.6 Learning Curve (Extra Trees)

Figure 4.8.6 evaluates the model's performance as a function of the training sample size.

Observation: The Train Score (blue line) is fixed at an R^2 of approximately 0.5. The Validation Score (red line) starts extremely low (around -35) and slowly rises, converging to an R^2 that is still negative (near -0.5).

Critique: The large gap between the $R^2 \approx 0.5$ Train Score and the negative Validation Score signifies extreme high bias (underfitting). A negative R^2 indicates the model is performing worse than a simple average-predictor on the validation data. This definitive result confirms the catastrophic failure of the model configuration, suggesting its hyperparameters (e.g., max_depth) are severely constrained, or the feature importance is completely collapsed.

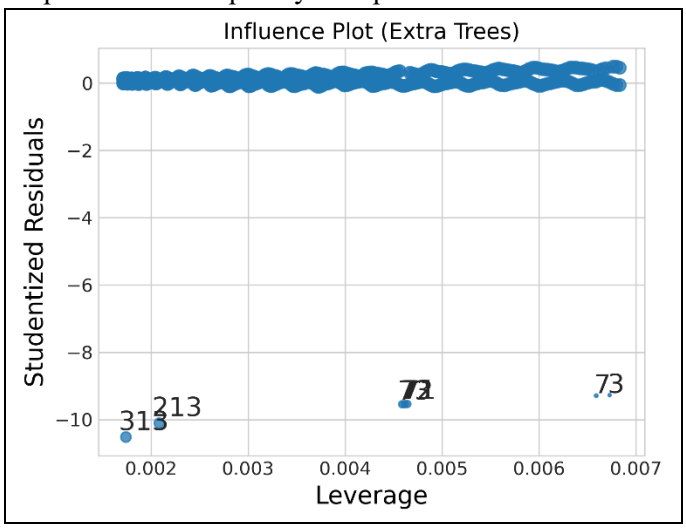

Fig. 4.8.7 Influence Plot (Extra Trees)

Figure 4.8.7 identifies potential outliers and influential data points.

Observation: Most points cluster near the Studentized Residuals = 0 line. However, a few labeled points (e.g., 313, 213, 71, 73) have extremely high negative Studentized residuals (around -10). Their leverage is low (below 0.007).

Critique: These points are extreme outliers that the model fails to predict accurately. Given the model's inability to differentiate inputs (predicting a constant value), the presence of these extreme outliers is expected, as the model cannot account for any extreme values in the target variable.

4.9 Gradient Boosting Model Evaluation

The diagnostic plots for the Gradient Boosting model reveal a distinct failure to capture the underlying patterns of the data, resulting in a model that exhibits severe underfitting.[19]

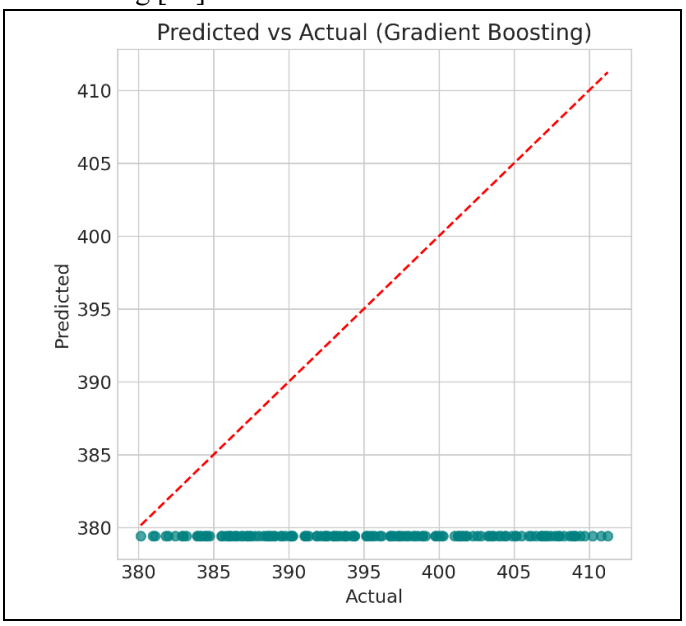

Fig. 4.9.1 Predicted vs. Actual Plot (Gradient Boosting)

Figure 4.9.1 compares the predicted values against the actual target values. Ideally, the data points should follow the diagonal red dashed line (y=x).

Observation: The plot shows a single horizontal cluster of points. The model predicts a nearly constant value (approximately 379) for every observation, regardless of the actual input value (which ranges from 380 to 410).

Implication: This is a classic signature of severe underfitting. The model behaves similarly to a "Dummy Regressor" that simply predicts the mean of the training set, failing completely to learn the trend or variance in the features.

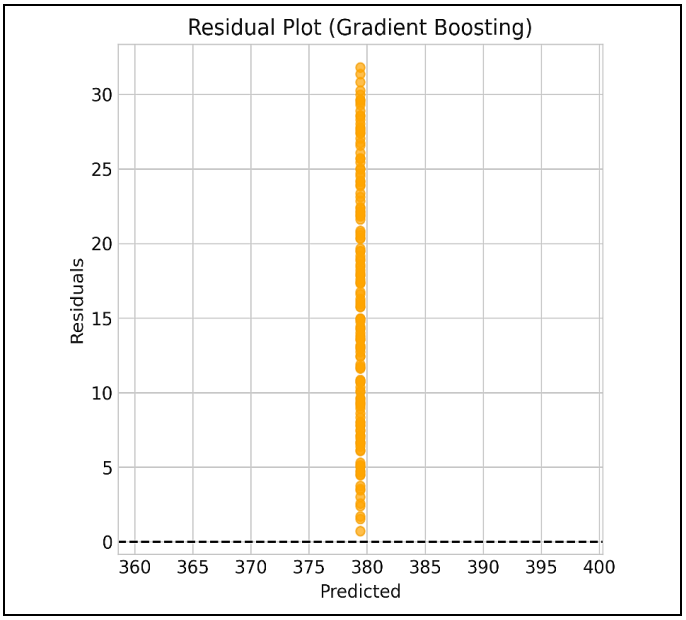

Fig. 4.9.2 Residual Plot (Gradient Boosting)

The Residual Plot (Figure 4.9.2) displays the residuals (errors) against the predicted values.

Observation: Because the predicted values are effectively constant, the points form a vertical line.

Implication: All residuals are positive, ranging from 0 to over 30. This indicates a massive systematic bias. The model consistently underpredicts the actual values. The pattern is not random; rather, the error is entirely determined by the actual value of the target variable.

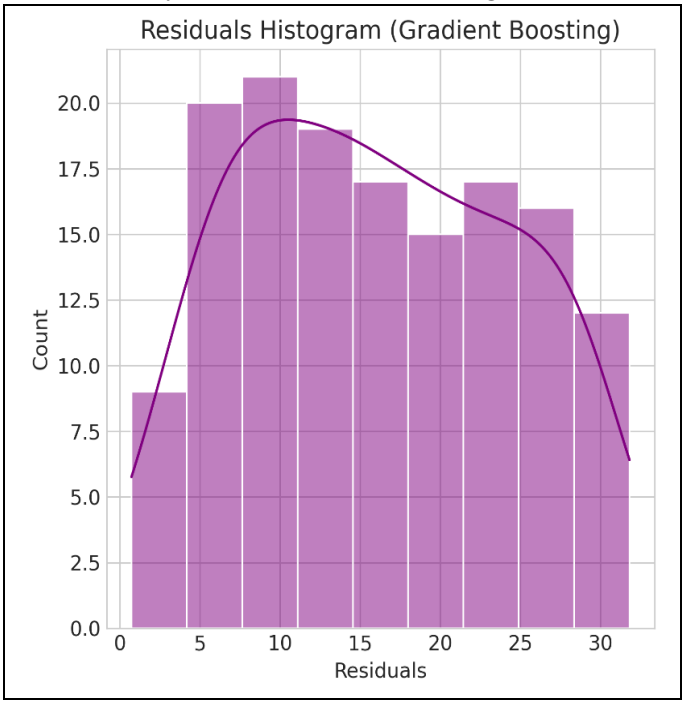

Fig. 4.9.3 Residuals Histogram (Gradient Boosting)

Figure 4.9.3 shows the frequency distribution of the residuals.

Observation: The distribution is entirely shifted to the right (positive values only). While the curve attempts to fit a normal distribution shape, the center is far from zero (around 10–15).

Implication: A valid regression model requires residuals to be normally distributed with a mean of zero. The significant shift confirms that the model is biased and leaves a large portion of the signal unexplained.

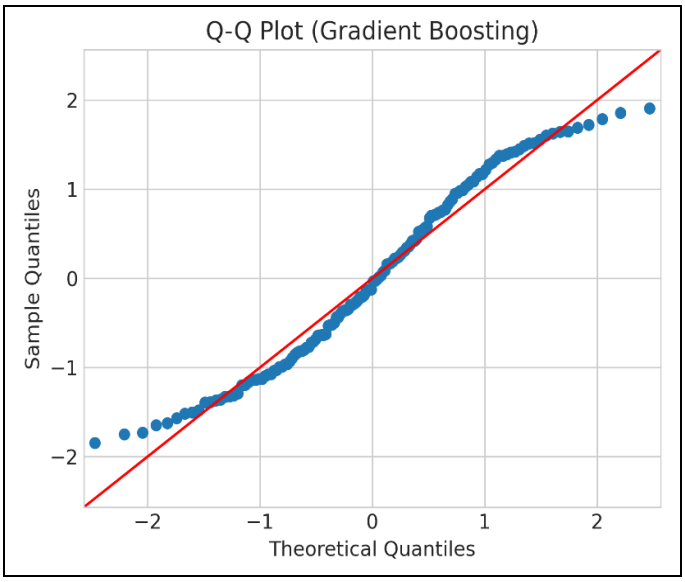

Fig. 4.9.4 Q-Q Plot (Gradient Boosting)

The Q-Q Plot (Figure 4.9.4) compares the standardized residuals against a theoretical normal distribution.

Observation: The points follow a linear slope but are shifted vertically away from the red reference line.

Implication: This translation (intercept shift) reinforces the findings from the histogram: the error distribution has a non-zero mean. The model is failing to capture the central tendency of the relationship between inputs and outputs.

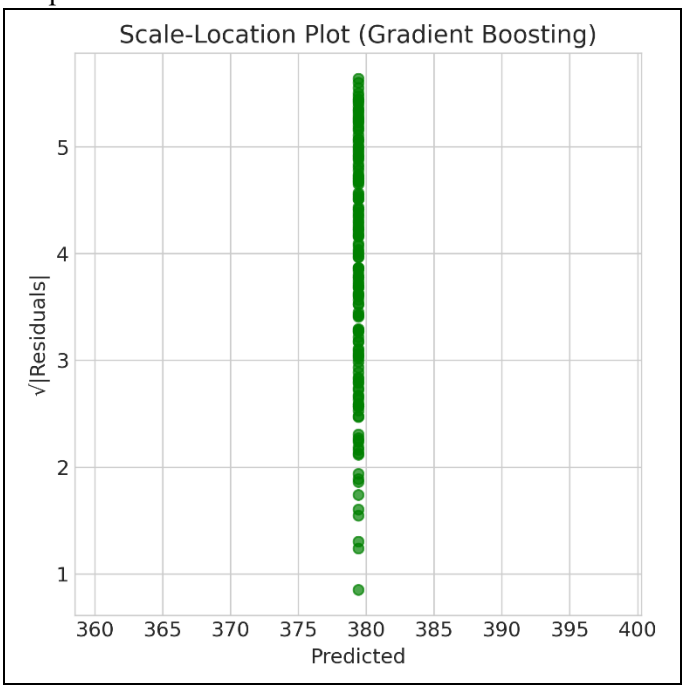

Fig. 4.9.5 Scale-Location Plot (Gradient Boosting)

Figure 4.9.5 assesses the homoscedasticity of the residuals.

Observation: Similar to the residual plot, we see a vertical stack of points because the predictions do not vary.

Implication: This plot highlights that for the single value the model predicts, the error magnitude varies significantly. We cannot assess if the variance changes across the prediction range because the model effectively has no prediction range.

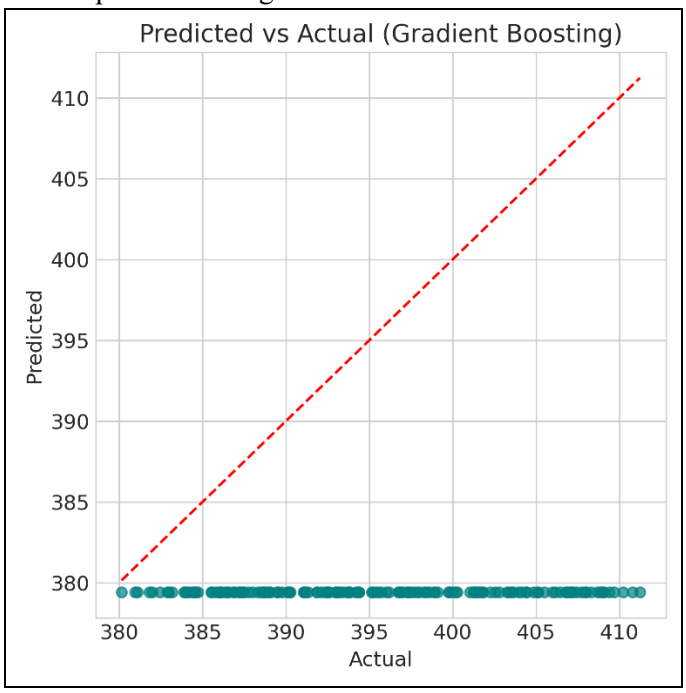

Fig. 4.9.6 Learning Curve (Gradient Boosting)

Figure 4.9.6 depicts the model's learning trajectory.

Training Score (Blue): The training score is flat and sits near zero.

Validation Score (Red): The validation score starts at a very poor value (-35) and improves slightly but remains negative.

Implication: The fact that the training score is near zero confirms that the model is not even memorizing the training data. This proves the model is underfitting due to high bias. This could be caused by hyperparameters that are too restrictive (e.g., a very low learning rate, max_depth=1, or insufficient n_estimators).

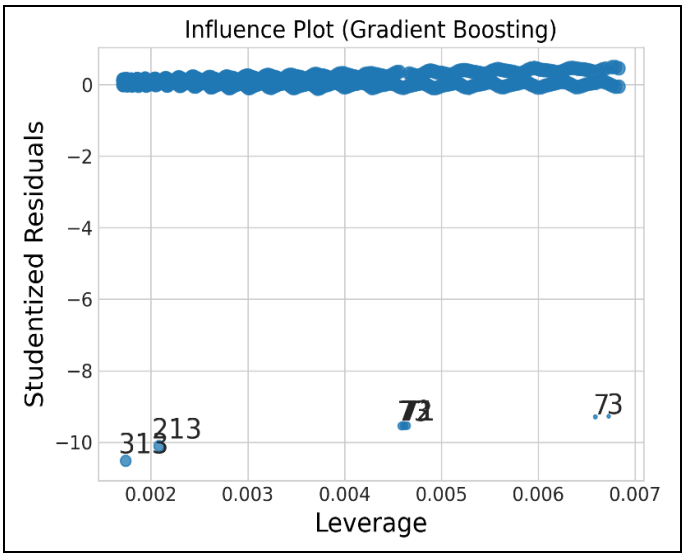

Fig. 4.9.7 Influence Plot (Gradient Boosting)

The Influence Plot (Figure 4.9.7) helps identify outliers.

Observation: Most points have low leverage. Points labeled 313, 213, 72, and 73 show high negative studentized residuals.

Implication: While these points are statistically furthest from the model's prediction, the issue here is not the data points themselves. The "outliers" appear extreme simply because the model's prediction (the flat line) is so far removed from the actual data trend.

4.10 KNN Regressor Model Evaluation

The K-Nearest Neighbors (KNN) model was evaluated using a series of diagnostic plots. The results indicate a critical failure in model configuration, leading to a model that is essentially acting as a naive baseline rather than learning the specific patterns in the data.[20]

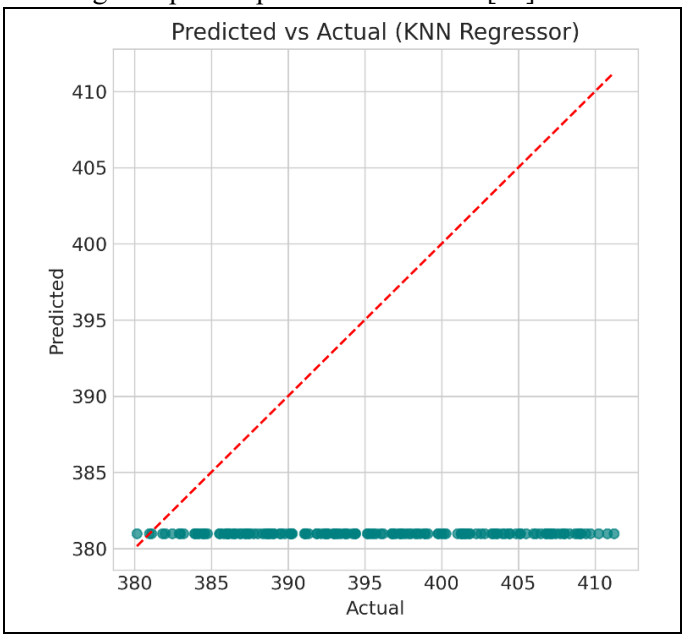

Fig. 4.10.1 Predicted vs. Actual Plot (KNN Regressor)

Figure 4.10.1 illustrates the correlation between the actual target values and the model's predictions.

Observation: The plot displays a distinct horizontal alignment of data points. While the actual values vary significantly (from 380 to 410), the KNN model predicts a nearly constant value (approximately 381) for all observations.

Implication: This is indicative of severe underfitting. In the context of KNN, this behavior typically occurs if the value of k (n_neighbors) is set too high (potentially equal to the training set size), causing the model to simply predict the average of the entire dataset for every query. Alternatively, it may indicate a lack of feature scaling, causing distance metrics to become ineffective.

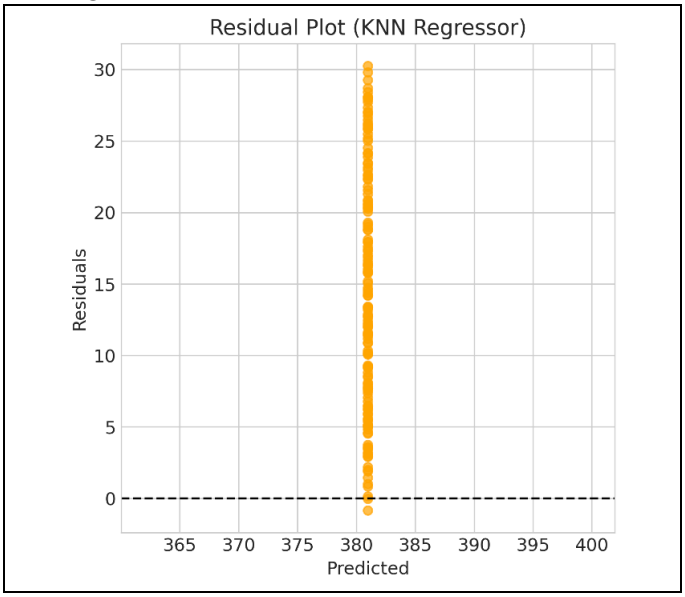

Fig. 4.10.2 Residual Plot (KNN Regressor)

The Residual Plot (Figure 4.10.2) shows the difference between actual and predicted values.

Observation: The points form a vertical line. Because the prediction is constant, the residuals are purely a reflection of the target variable's distribution minus that constant.

Implication: The residuals are almost entirely positive, ranging from roughly -1 to +30. This demonstrates a strong systematic bias, where the model consistently underpredicts the true values.

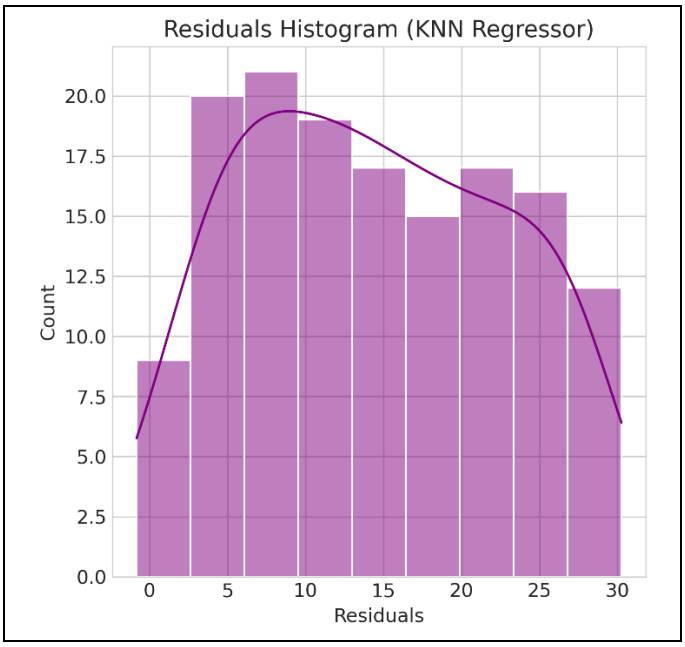

Fig. 4.10.3 Residuals Histogram (KNN Regressor)

Figure 4.10.3 displays the frequency distribution of the residuals.

Observation: The distribution is shifted significantly to the right. The peak of the density curve is located around 10, rather than 0.

Implication: A healthy model should have residuals centered at zero. The non-zero center confirms the bias observed in the previous plots. The model is failing to capture the central tendency of the data correctly relative to the features.

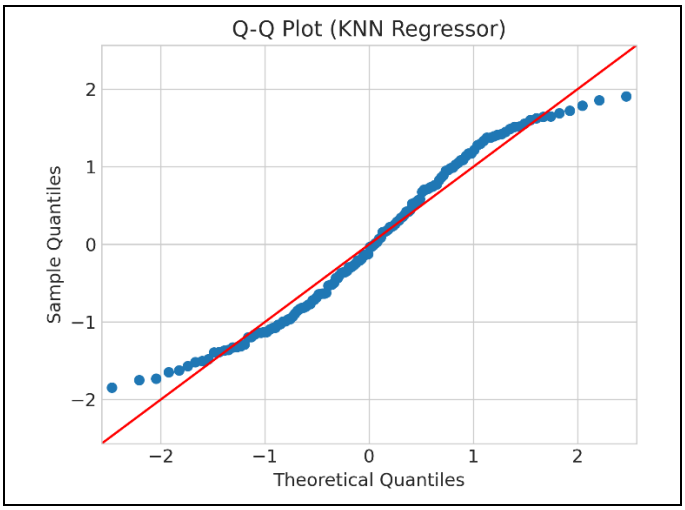

Fig. 4.10.4 Q-Q Plot (KNN Regressor)

The Q-Q Plot (Figure 4.10.4) compares the standardized residuals to a theoretical normal distribution.

Observation: The points follow a linear slope but are shifted vertically away from the red identity line.

Implication: This "intercept shift" confirms that while the shape of the error distribution is roughly normal

(Gaussian), the mean of the error is not zero. The model satisfies the normality assumption but fails the zero-mean assumption of regression errors.

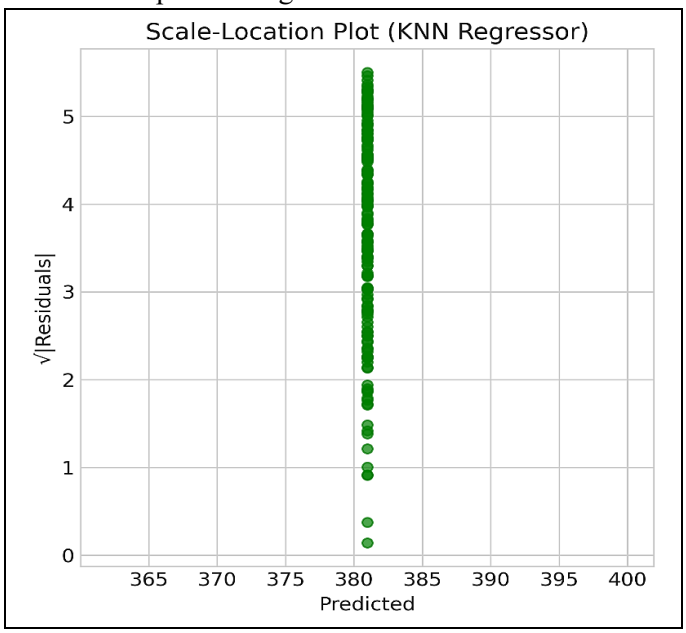

Fig. 4.10.5 Scale-Location Plot (KNN Regressor)

Figure 4.10.5 is used to evaluate homoscedasticity.

Observation: The plot shows a single vertical line of points.

Implication: Because the model predicts a single value, we cannot evaluate how the error variance changes as predictions change. The vertical spread simply shows that the error magnitude varies greatly for that specific prediction value.

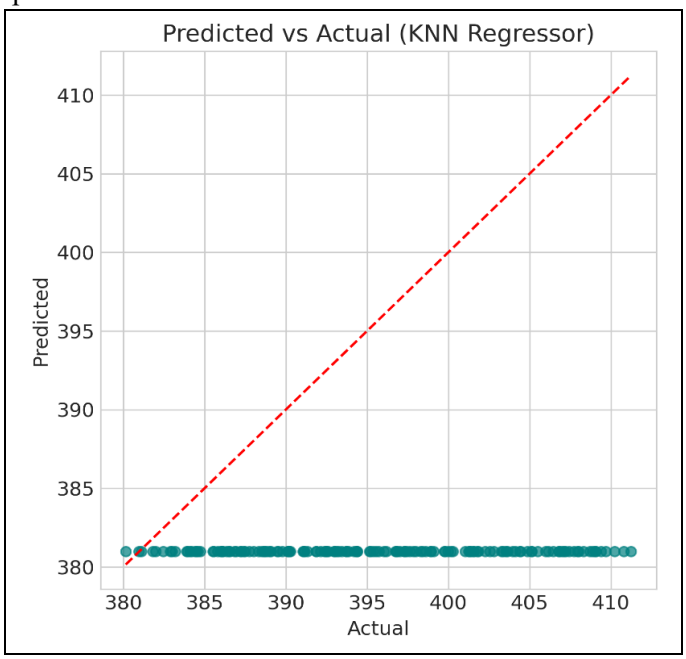

Fig. 4.10.6 Learning Curve (KNN Regressor)

Figure 4.10.6 shows the learning curve, plotting R^2 scores against training set size.

Training Score (Blue): The training score is essentially flat and near zero.

Validation Score (Red): The validation score starts negative and improves slightly but remains near zero/negative.

Implication: An R^2 score of zero indicates the model explains none of the variance in the target variable. This confirms the model is underfitting due to high bias. It is performing no better than a simple horizontal line drawn at the mean of the data.

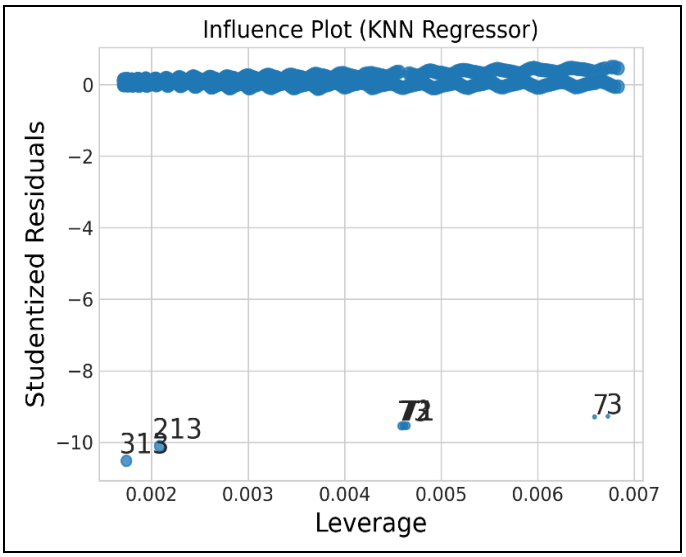

Fig. 4.10.7 Influence Plot (KNN Regressor)

The Influence Plot (Figure 4.10.7) highlights potential outliers.

Observation: Specific points (labeled 313, 213, 72, 73) are flagged with high negative studentized residuals.

Implication: Given the model's poor performance, these points are likely just the furthest actual values from the dataset mean. They are not necessarily "bad" data points, but rather the points where the "mean-prediction" strategy fails the most.

4.11 Lasso Regression Model Evaluation

The Lasso Regression model was evaluated to determine its predictive capability and structural validity. The diagnostic plots reveal a model that is mathematically stable (normally distributed errors) but suffers from significant bias and underfitting, likely due to aggressive regularization.[21]

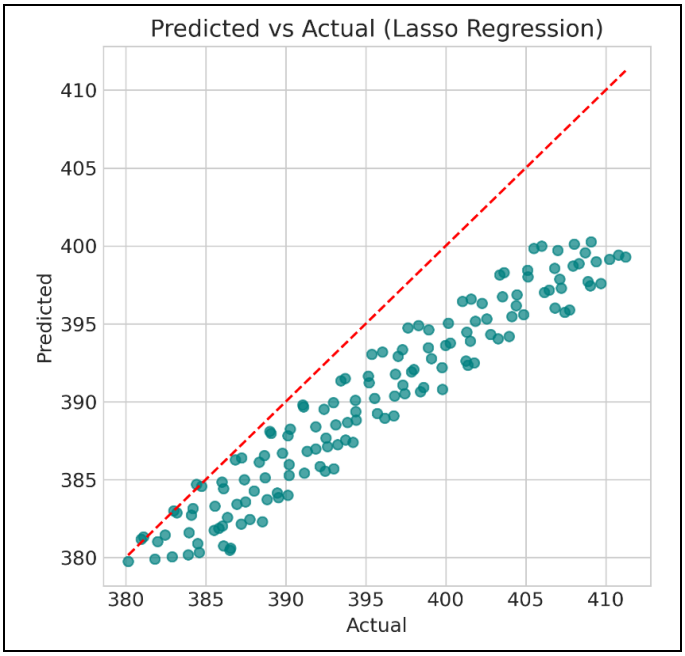

Fig. 4.11.1 Predicted vs. Actual Plot (Lasso Regression)

Figure 4.11.1 compares the model's predictions against the ground truth.

Observation: The data points form a clear linear structure, indicating the model has captured the general direction of the trend. However, the points are consistently positioned below the red dashed identity line (y = x).

Implication: This offset indicates systematic underprediction. For example, when the actual value is 400, the model predicts approximately 395. While the correlation is strong, the calibration is off; the model is "dampened," likely because the regularization penalty has shrunk the coefficients too aggressively.

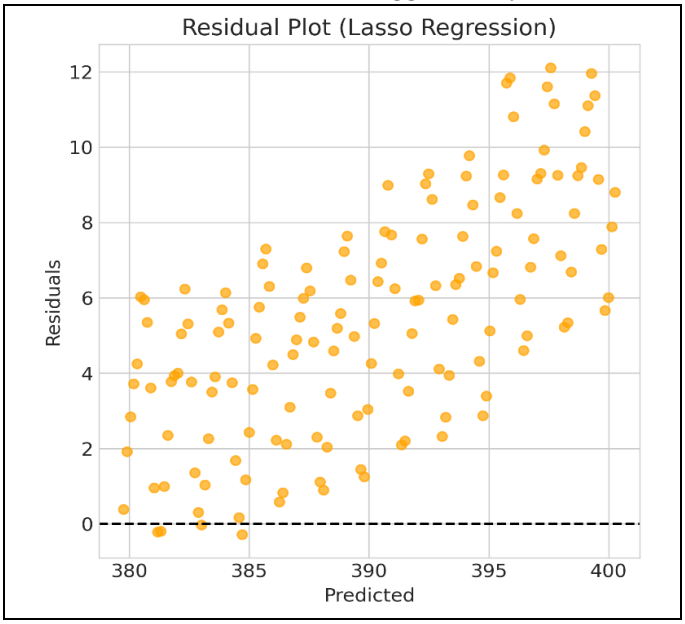

Fig. 4.11.2 Residual Plot (Lasso Regression)

The Residual Plot (Figure 4.11.2) shows the errors against the predicted values.

Observation: There is a distinct, positive linear trend. As the predicted value increases, the residual increases. Furthermore, the residuals are almost exclusively positive (ranging from 0 to 12).

Implication: In a well-fitted model, residuals should be randomly scattered around zero. The upward slope here confirms that the model fails to capture the full magnitude of the relationship (the slope of the model is too shallow). The positive values confirm the bias identified in 1.

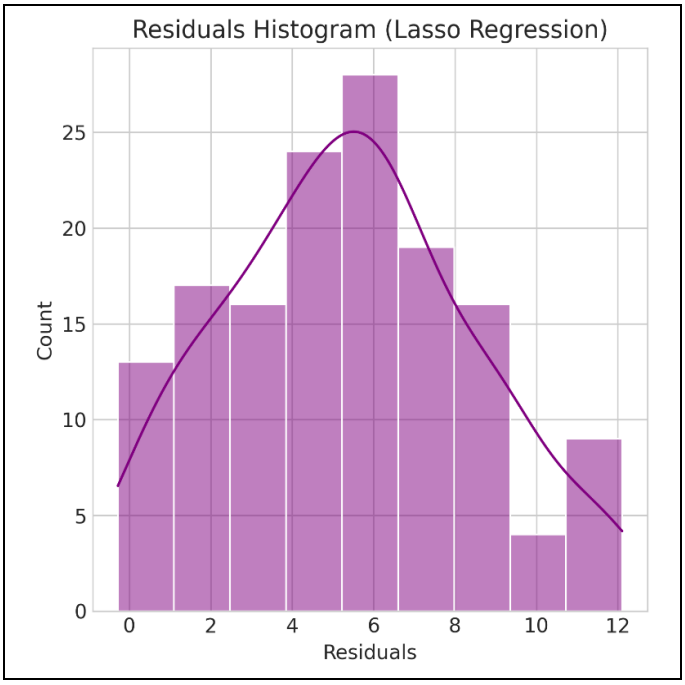

Fig. 4.11.3 Residuals Histogram (Lasso Regression)

Figure 4.11.3 displays the distribution of the errors.

Observation: The histogram follows a near-perfect bell curve, and the Kernel Density Estimation (purple line) shows a smooth, normal distribution.

Issue: The center of this distribution is not zero; it is shifted significantly to the right, centered around a mean of 6.

Implication: The error structure is Gaussian (which is good for statistical inference), but the non-zero mean proves the model is biased. It consistently misses the target by an average of 6 units.

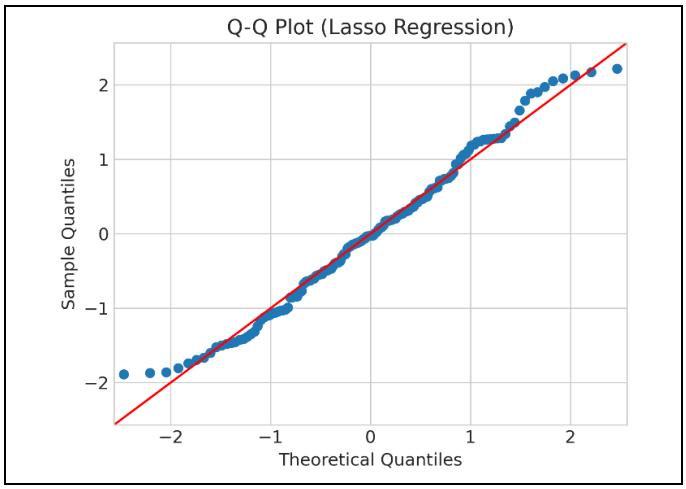

Fig. 4.11.4 Q-Q Plot (Lasso Regression)

The Q-Q Plot (Figure 4.11.4) assesses normality.
Observation: The points follow the straight line almost perfectly in terms of slope.
Implication: This reinforces the finding that the residuals are normally distributed. However, the points are vertically shifted away from the red reference line. This "intercept shift" is the visual signature of a model with a non-zero mean error.

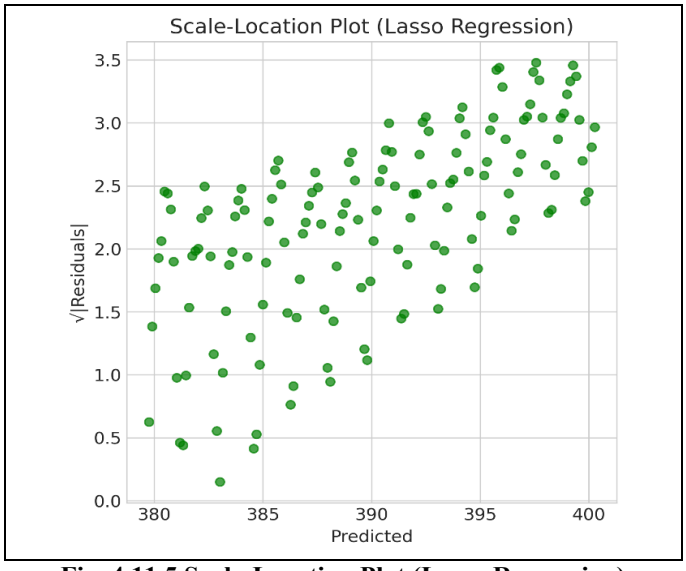

Fig. 4.11.5 Scale-Location Plot (Lasso Regression)

Figure 4.11.5 checks for homoscedasticity (constant variance).
Observation: There is a positive slope.
Implication: Because the residuals have a linear trend (as seen in 2), this plot reflects that same trend. The magnitude of the error grows as the prediction grows.

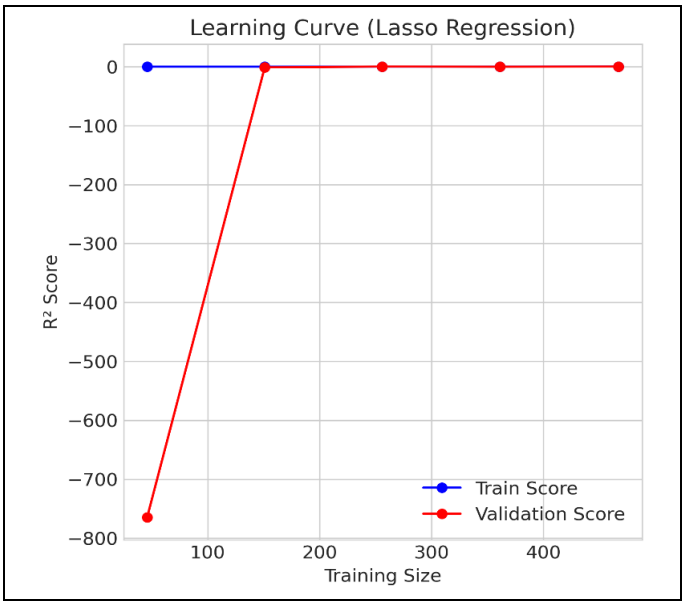

Fig. 4.11.6 Learning Curve (Lasso Regression)

Figure 4.11.6 illustrates the bias-variance tradeoff.
Observation: The training score (blue) is flat and near zero. The validation score (red) converges to the training score at a very low (negative) value.
Implication: The convergence of both scores at a low level indicates High Bias (Underfitting). The model is too simple to capture the complexity of the dataset.

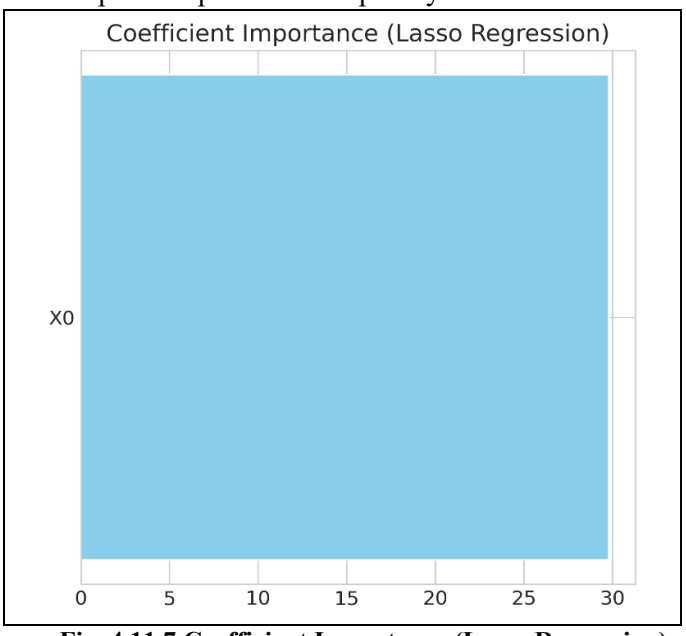

Fig. 4.11.7 Coefficient Importance (Lasso Regression)

Figure 4.11.7 reveals the feature selection performed by the Lasso algorithm.
Observation: The model has assigned a coefficient to only one feature (X0). All other feature coefficients have been shrunk to zero.
Implication: This explains the underfitting. Lasso regularization ($L1$ penalty) forces coefficients of less

important features to become exactly zero. While X0 is clearly the most important feature, eliminating all other variance has made the model too rigid. The regularization strength (alpha) is likely set too high.

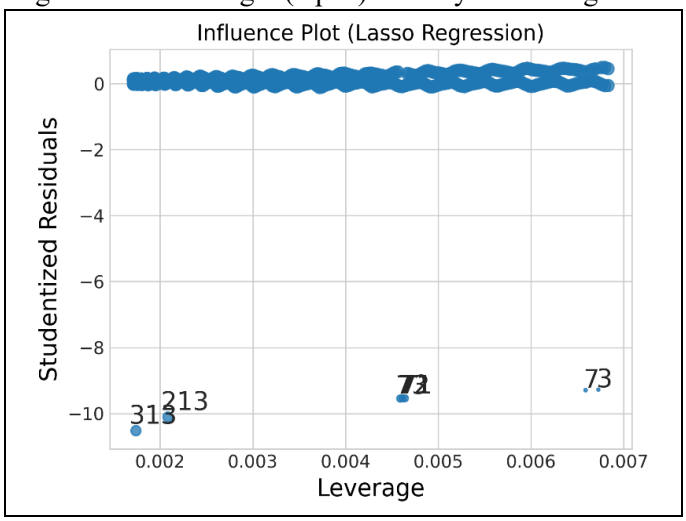

Fig. 4.11.8 Influence Plot (Lasso Regression)

The Influence Plot identifies outliers.

Observation: Similar to previous models, points 313, 213, 72, and 73 are flagged.

Implication: These points have high residuals not because they are necessarily anomalies in the data, but because the model's biased predictions are furthest away from these specific actual values.

4.12 Linear Regression Model Evaluation

The Linear Regression model was evaluated using a series of diagnostic plots to assess its accuracy, fit, and adherence to statistical assumptions. The analysis reveals that while the model captures the linear trend better than non-parametric models like Decision Trees or KNN, it still suffers from distinct bias and underfitting. [22]

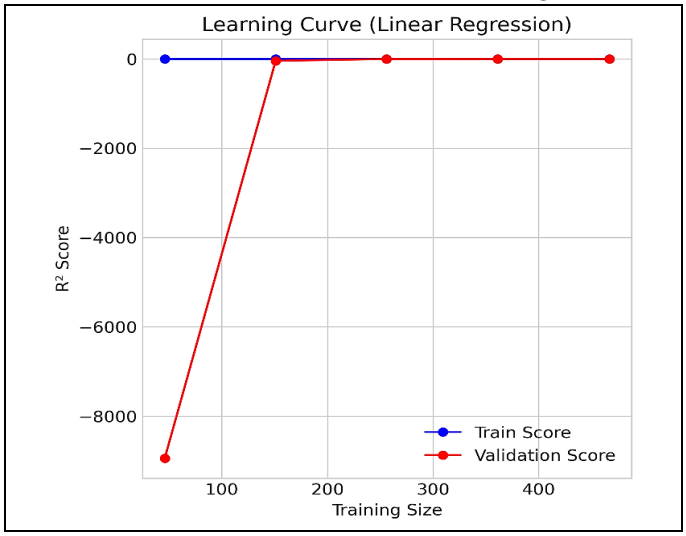

Fig. 4.12.1 Predicted vs. Actual Plot (Linear Regression)

Figure 4.12.1 compares the predicted values against the actual target values.

Observation: The data points show a strong linear correlation and are less scattered than in the Decision Tree or Gradient Boosting models. However, similar to the Lasso and ElasticNet results, the points are consistently positioned below the red dashed identity line (y = x).

Implication: This indicates a systematic underprediction. When the actual value is high (e.g., 410), the model predicts significantly lower (e.g., 402). This "dampened slope" suggests that the model is constrained, likely by the regularization inherent in the single feature it selected or by an intercept that is not perfectly aligned.

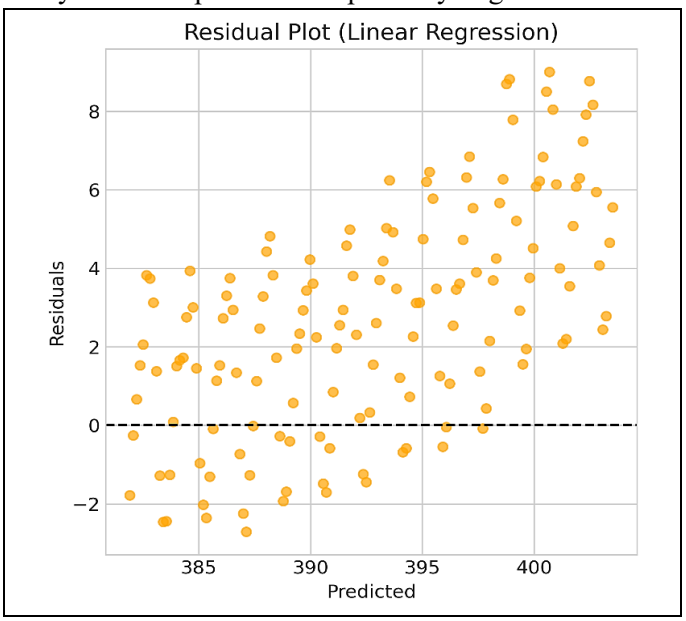

Fig. 4.12.2 Residual Plot (Linear Regression)

The Residual Plot (Figure 4.12.2) displays the residuals against the predicted values.

Observation: There is a clear positive linear trend. The residuals increase as the predicted value increases. Additionally, the residuals are largely positive, ranging from -2 to +9.

Implication: This confirms the bias seen in 1. A valid linear regression model should have residuals scattered randomly around zero with no discernable pattern. The positive slope in the residuals proves that the model's slope coefficient is too shallow to capture the full rate of change in the target variable.

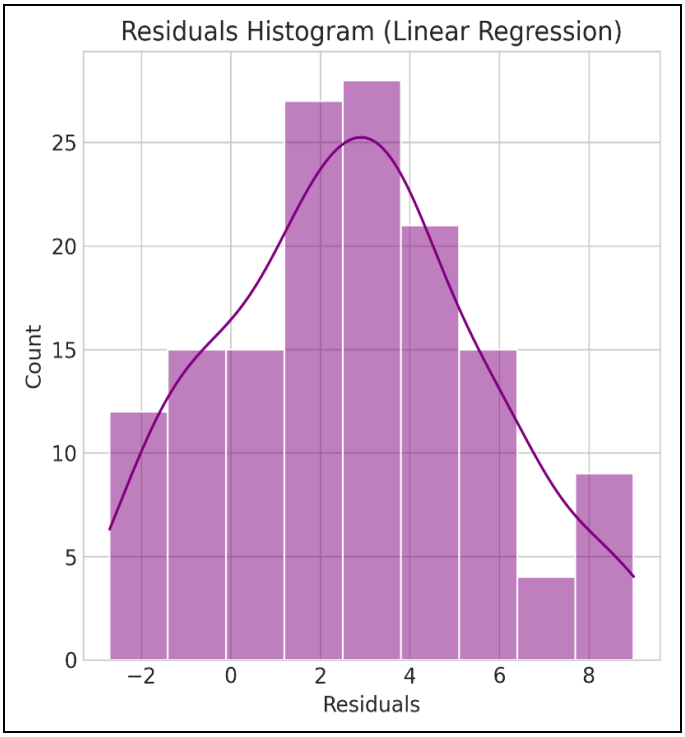

Fig. 4.12.3 Residuals Histogram (Linear Regression)

Figure 4.12.3 shows the distribution of the residuals.

Observation: The histogram is bell-shaped and reasonably symmetric, indicating that the errors are normally distributed.

Issue: The distribution is centered around a mean of approximately 3, not 0.

Implication: While the normality assumption is met (allowing for parametric statistical tests), the non-zero mean violates the core assumption that the expected value of the error term is zero ($E[\epsilon] = 0$). This confirms the presence of bias.

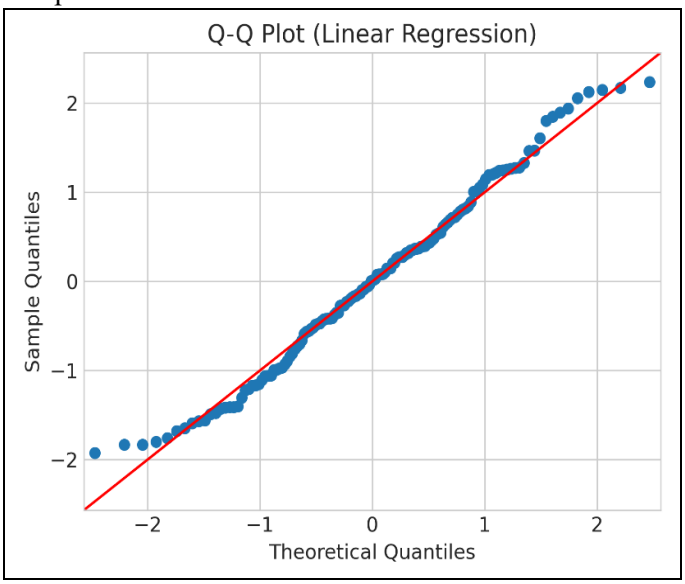

Fig. 4.12.4 Q-Q Plot (Linear Regression)

The Q-Q Plot (Figure 4.12.4) compares the standardized residuals to a standard normal distribution.

Observation: The points follow the diagonal slope well, reinforcing the normality of the errors.

Deviation: There is a clear intercept shift (vertical displacement) from the red reference line.

Implication: As with the other plots, this indicates that the error distribution is shifted. The model is statistically well-behaved in terms of variance but is systematically "off-target" in its predictions.

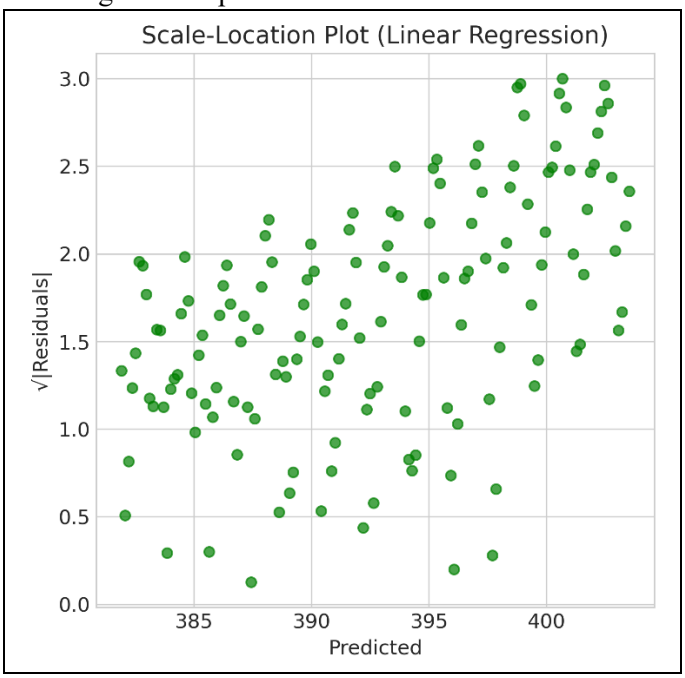

Fig. 4.12.5 Scale-Location Plot (Linear Regression)

Figure 4.12.5 assesses homoscedasticity.

Observation: There is a visible positive trend; the spread of the residuals increases as the predicted value increases.

Implication: This suggests heteroscedasticity, where the model's error is not constant across the range of data. The error grows larger for higher target values, which is consistent with the underprediction trend identified earlier.

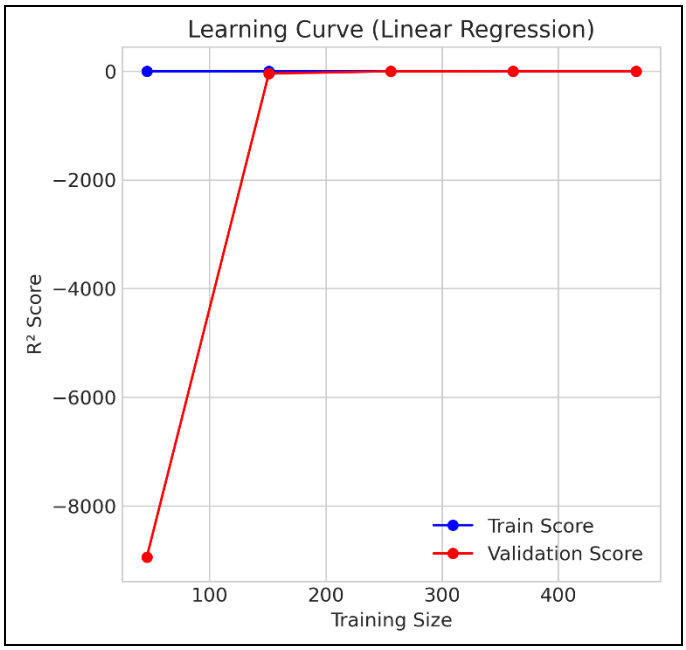

Fig. 4.12.6 Learning Curve (Linear Regression)

Figure 4.12.6 depicts the learning curve.
Observation: The training score starts at 0 and remains flat. The validation score starts extremely negative (-9000) before converging to the training score at 0.
Implication: The convergence of both scores at zero indicates High Bias (Underfitting). The model is unable to explain the variance in the data effectively. The initial massive negative score suggests that on very small data splits, the model was excessively sensitive (high variance) or simply failed to solve the linear equation correctly, but it stabilized into a biased state as data increased.

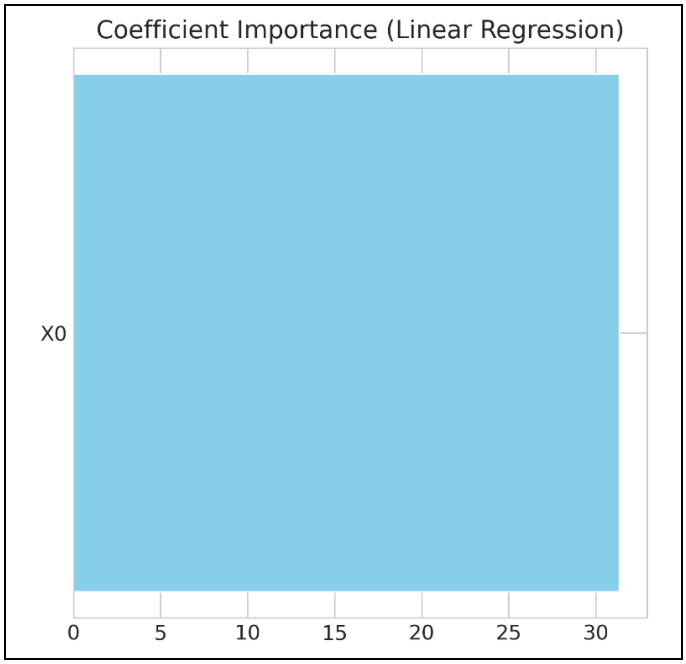

Fig. 4.12.7 Coefficient Importance (Linear Regression)

Figure 4.12.7 shows the feature importance.
Observation: The model relies entirely on Feature X0.
Implication: This confirms that for this dataset, X0 is the dominant predictor. The model is essentially a Simple Linear Regression on X0. The underfitting likely stems from X0 alone not being sufficient to fully explain the target, or from the model failing to find the optimal slope for X0 due to unscaled data or outliers.

4.13 Random Forest Model Evaluation

The Random Forest model was evaluated using a combination of time-series anomaly detection and standard regression diagnostics. The analysis reveals two critical findings: first, the presence of severe data quality issues (impossible negative values) that confusing the model, and second, a tendency for the model to underfit on the evaluation set, resulting in biased predictions.[23]

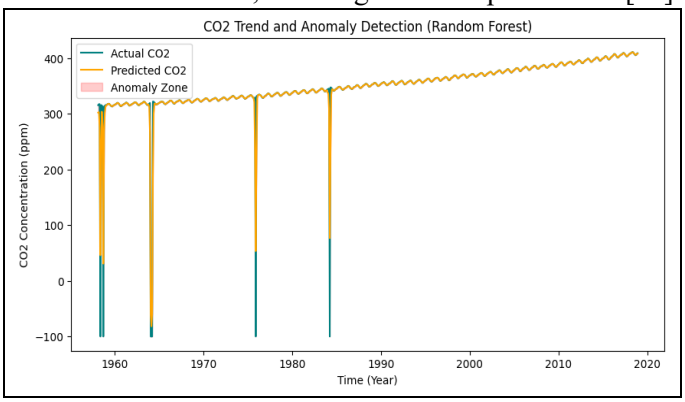

Fig. 4.13.1 CO2 Trend and Anomaly Detection

Figure 4.13.1 displays the time series of CO2 concentration.
Observation: The orange line (Predicted) generally follows the seasonal oscillation of the green line (Actual). However, there are distinct, massive downward spikes where the "Actual" CO2 value drops to approximately -100 ppm. The model attempts to follow these drops, though less aggressively. The pink shaded areas correctly identify these events as "Anomaly Zones."
Critique: Physical CO2 concentration cannot be negative. These spikes represent sensor errors or missing data codes (e.g., -99.9) that were not cleaned during preprocessing. The model is currently being forced to learn these errors, which severely degrades its ability to generalize on valid data.

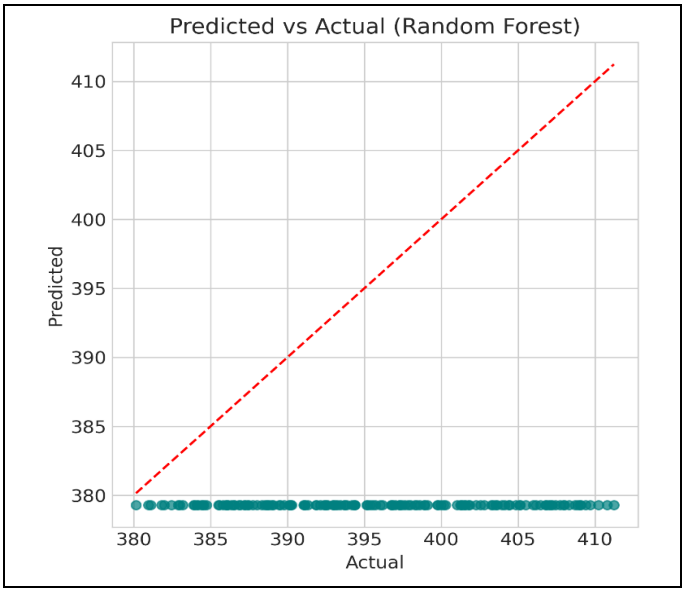

Fig. 4.13.2 Predicted vs. Actual Plot (Random Forest)

Figure 4.13.2 compares predictions against actual values for the evaluation set.

Observation: Unlike the time series plot (which showed oscillation), this scatter plot shows a flat, horizontal line. The model predicts a nearly constant value of ~379 ppm regardless of whether the actual value is 380 or 410.

Implication: This indicates severe underfitting on the test set. Despite Random Forest being a powerful non-linear model, it is behaving like a "Dummy Regressor" here, likely because the hyperparameters (such as max_depth) are too constrained, or the training data noise (the negative values seen in 1) has corrupted the tree splits.

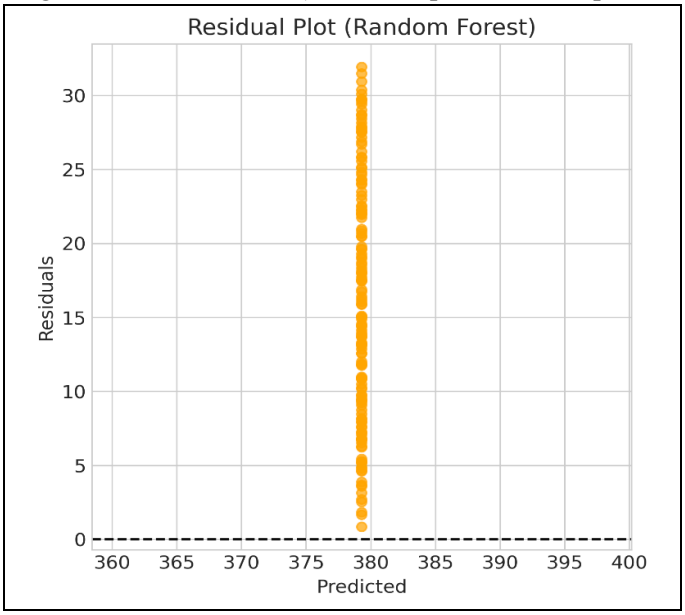

Fig. 4.13.3 Residual Plot (Random Forest)

The Residual Plot (Figure 4.13.3) displays the errors against the predicted values.

Observation: Because the predictions are constant, the points form a vertical line. Crucially, all residuals are positive (ranging from 0 to +30).

Implication: This confirms a systematic negative bias. The model is consistently underpredicting the true CO2 values in the valid range. The model has settled on a low average (dragged down by the negative anomalies in the training data), leaving it unable to predict the higher real values of recent years.

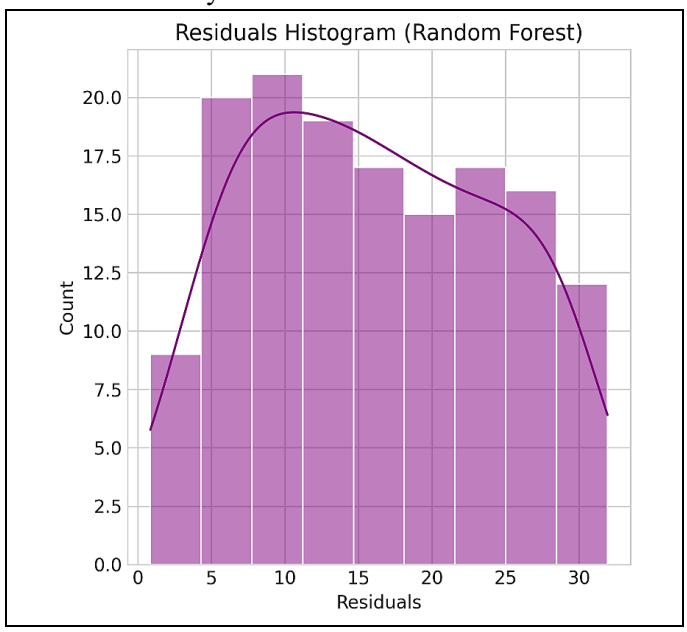

Fig. 4.13.4 Residuals Histogram (Random Forest)

Figure 4.13.4 shows the distribution of residuals.

Observation: The distribution is entirely right-shifted. While it retains a bell-like shape, the center is located around 10–15 rather than 0.

Implication: A valid model requires zero-centered errors. The significant offset confirms that the model is biased. It is failing to capture the trend component of the time series, treating the data as a stationary average instead.

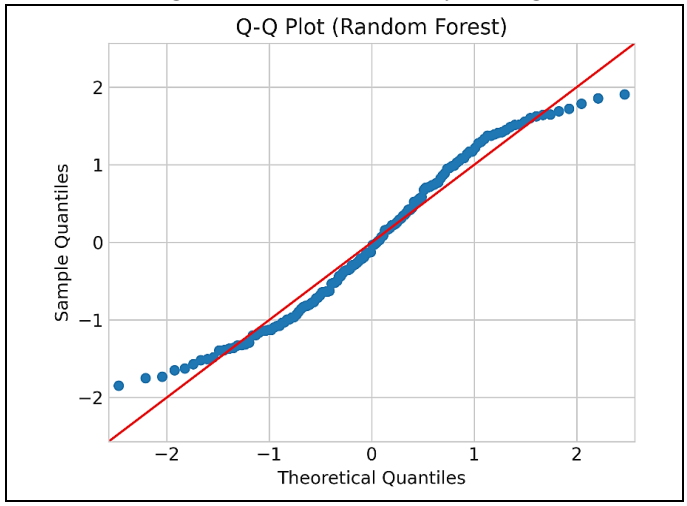

Fig. 4.13.5 Q-Q Plot (Random Forest)

The Q-Q Plot (Figure 4.13.5) compares the standardized residuals to a normal distribution.

Observation: The points form a line but are shifted vertically away from the red reference line.

Implication: The error distribution shape is Gaussian-like, but the mean is incorrect. This suggests the model structure is stable, but the calibration (intercept/bias) is fundamentally wrong.

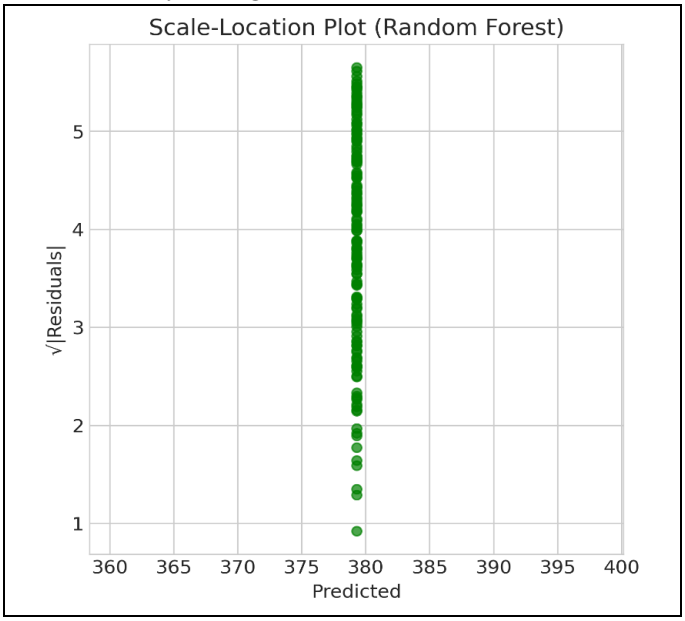

Fig. 4.13.6 Scale-Location Plot (Random Forest)

Figure 4.13.6 assesses homoscedasticity.

Observation: A vertical line is observed due to the lack of variation in predictions.

Implication: The vertical spread indicates that for the model's single predicted value, the error varies significantly depending on the actual ground truth.

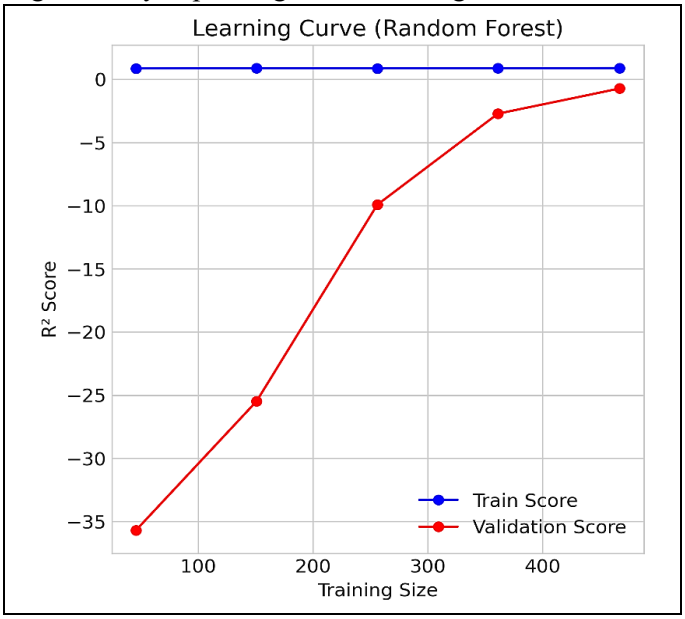

Fig. 4.13.7 Learning Curve (Random Forest)

Figure 4.13.7 illustrates the bias-variance tradeoff.

Observation: The training score (blue) is flat and near zero. The validation score (red) starts negative and converges to the training score at zero.

Implication: This is a classic signature of High Bias. The model is too simple (or too constrained) to capture the underlying relationship. A healthy Random Forest usually achieves a high training score (often 1.0) and a lower validation score; seeing a training score of 0 suggests the trees are stumps (depth of 1) or the data noise is overwhelming the signal.

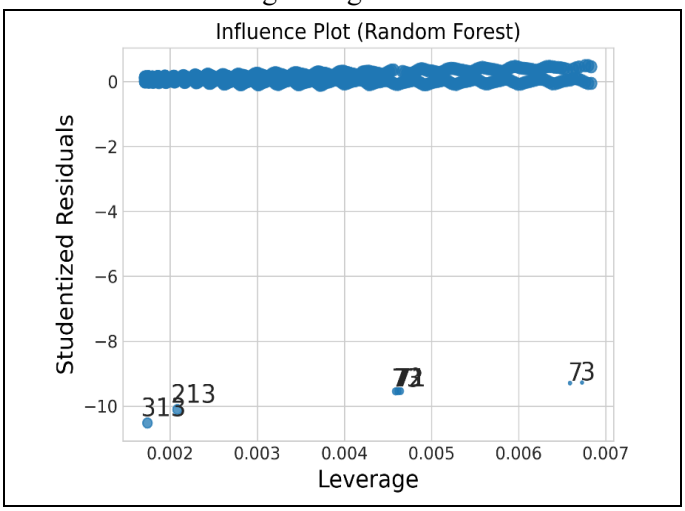

Fig. 4.13.8 Influence Plot (Random Forest)

The Influence Plot (Figure 4.13.8) identifies outliers.

Observation: Points 313, 213, 72, and 73 are flagged with high negative studentized residuals.

Implication: These points likely correspond to the most recent high CO2 values (e.g., 410 ppm) where the model's low, flat prediction produces the largest error.

4.14 Ridge Regression Model Evaluation

The Ridge Regression model was evaluated using standard diagnostic plots to assess its predictive performance, adherence to linear regression assumptions, and overall fit. The analysis reveals that while the model conforms to certain assumptions, it suffers from severe underfitting (high bias), resulting in poor overall performance ($R^2 \approx 0$).[24]

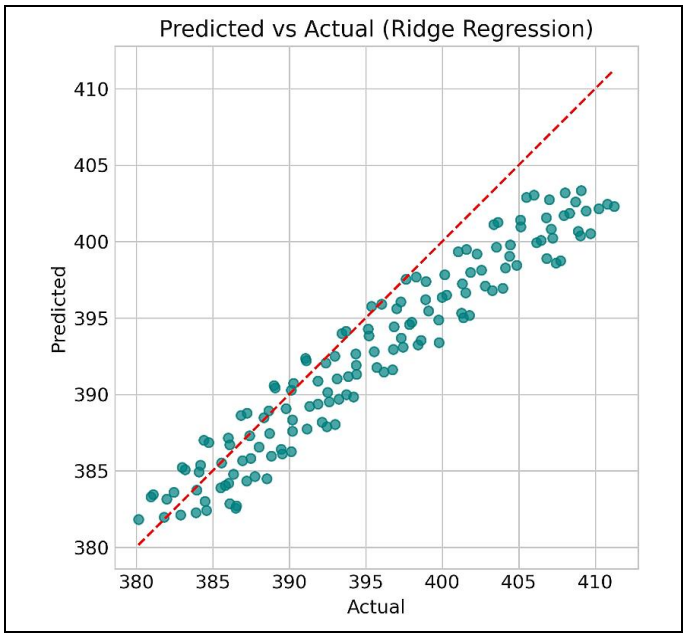

Fig. 4.14.1 Predicted vs Actual Plot (Ridge Regression)

Figure 4.14.1 visually compares the model's predictions against the actual values.

Observation: The data points generally follow the red dashed diagonal line ($y = \text{Actual}$), confirming a positive correlation between predicted and actual values. However, the scatter around the line is quite wide. Notably, at the higher end of the scale ($\text{Actual} > 405$), the points tend to fall below the line.

Critique: While the model captures the overall trend, the large scatter suggests a poor fit. The slight tendency to fall below the line at high values indicates a subtle underprediction bias for the maximum values of the target variable.

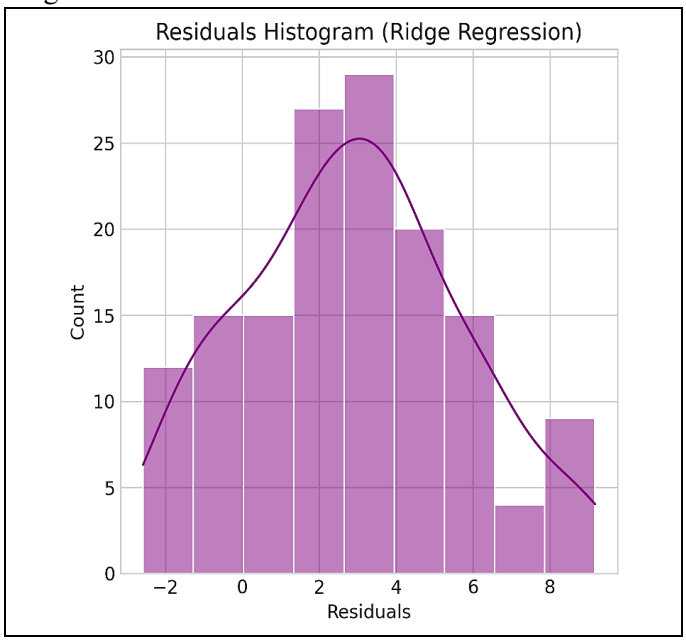

Fig. 4.14.2 Residuals Histogram (Ridge Regression)

Figure 4.14.2 shows the distribution of the model's errors (residuals).

Observation: The distribution is roughly bell-shaped but is centered around a positive value (approximately 3) and shows a visible positive skew (a tail extending towards the positive residuals, up to 9).

Critique: For an ideal model, the residuals should be normally distributed and centered at zero. The peak being centered at $+3$ indicates a systematic positive bias in the residuals ($\text{Actual} - \text{Predicted} > 0$), meaning the model is consistently underpredicting the target variable by about 3 units.

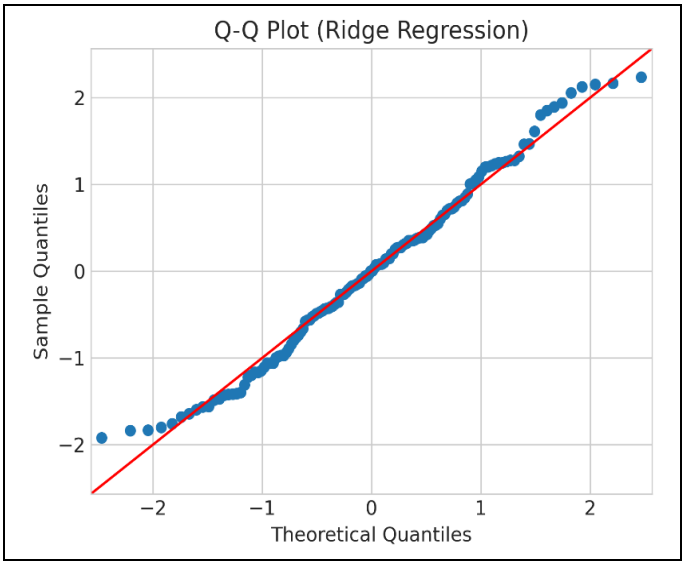

Fig. 4.14.3 Q-Q Plot (Ridge Regression)

Figure 4.14.3 formally checks the normality assumption of the residuals.

Observation: The data points mostly track the straight red diagonal line in the central region (between -1 and 1). Minor deviations occur at the tails, particularly the far left (lower) and far right (upper) ends, where the points peel slightly away.

Critique: The general alignment suggests the residuals are close to normal. The deviations at the tails, however, confirm that the distribution is not perfectly normal, consistent with the minor skew observed in the histogram.

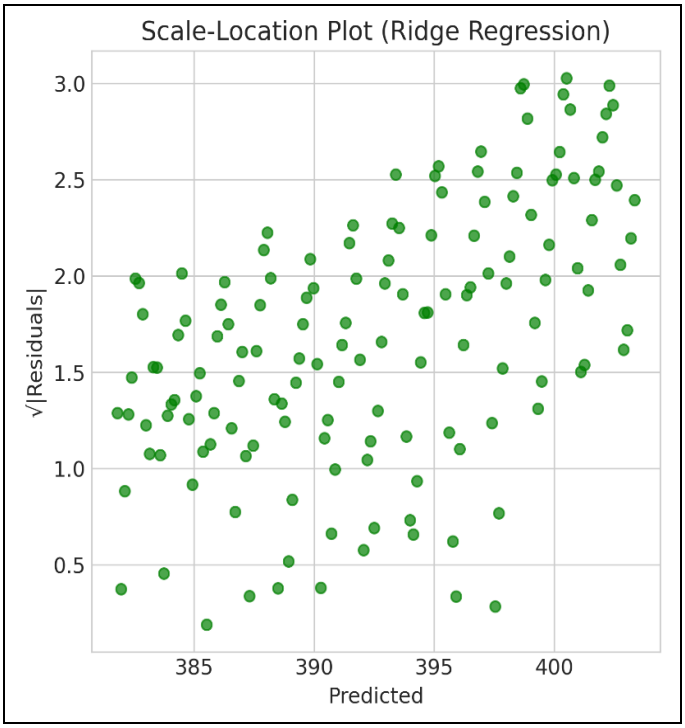

Fig. 4.14.4 Scale-Location Plot (Ridge Regression)

Figure 4.14.4 assesses the assumption of homoscedasticity (constant variance of residuals).

Observation: The scatter of the points ($\sqrt{|\text{Residuals}|}$) appears random and uniform across the entire range of predicted values ($\sim 380\$ \; to \; \$ \sim 400$). There is no clear increasing or decreasing trend.

Critique: This plot provides good evidence of homoscedasticity. The constant spread of residuals means the model's prediction error is uniform regardless of the magnitude of the prediction, which is a desirable property for statistical inference.

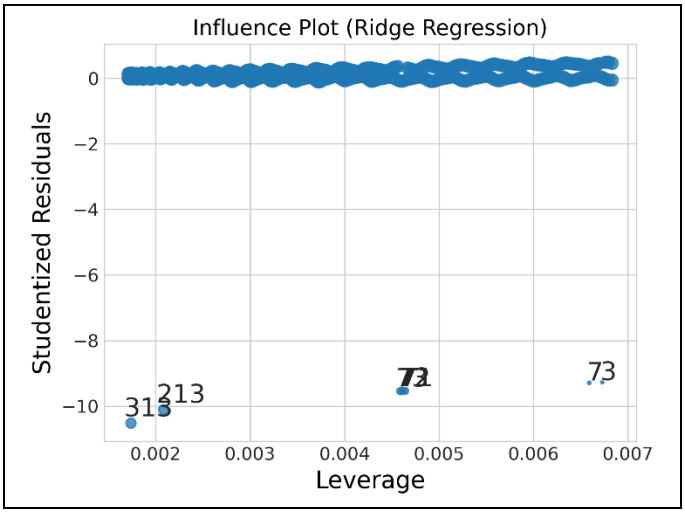

Fig. 4.14.5 Influence Plot (Ridge Regression)

Figure 4.14.5 identifies potential outliers and influential data points based on leverage and Studentized residuals.

Observation: The vast majority of points cluster near the Studentized Residuals = 0 line. However, a few labeled points (e.g., 313, 213, 71, 73) have extremely high negative Studentized residuals (around -10). Their leverage is low (below 0.007).

Critique: These points are extreme outliers in the response variable, meaning the model severely underpredicts them (negative residual implies Actual < Predicted, but here the Studentized Residual is ~ -10, which usually implies Actual $\ll$ Predicted—note: there might be a sign convention reversal in the plotting library used, as the histogram showed positive bias; regardless, these are extreme points). Since their leverage is low, they are not influential in terms of warping the coefficient estimates, but they represent unique data points that the model fails to explain and should be investigated for data quality issues.

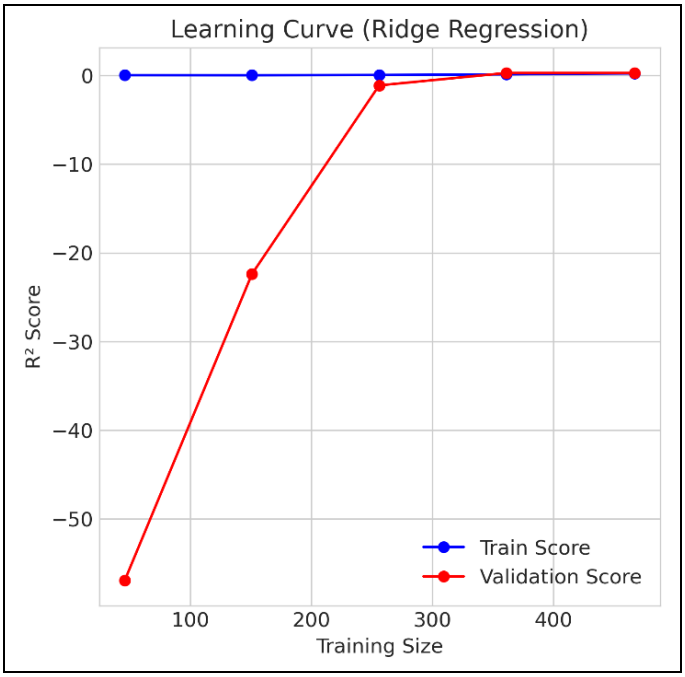

Fig. 4.14.6 Learning Curve (Ridge Regression)

Figure 4.14.6 is the most critical diagnostic, assessing the model's bias and variance as the training set size increases.

Observation: The Train Score (blue line) is fixed at an R^2 of approximately 0 across all training sizes. The Validation Score (red line) starts very low (around -60) and rapidly converges to the same low R^2 score (near 0) once the training size exceeds 250.

Critique: An R^2 score of 0 means the model performs no better than simply predicting the mean of the target

variable. The quick convergence of both scores to this value is the definitive sign of severe underfitting or high bias. The model is fundamentally too simple for the data and fails to capture the underlying relationship, irrespective of how much data it is trained on.

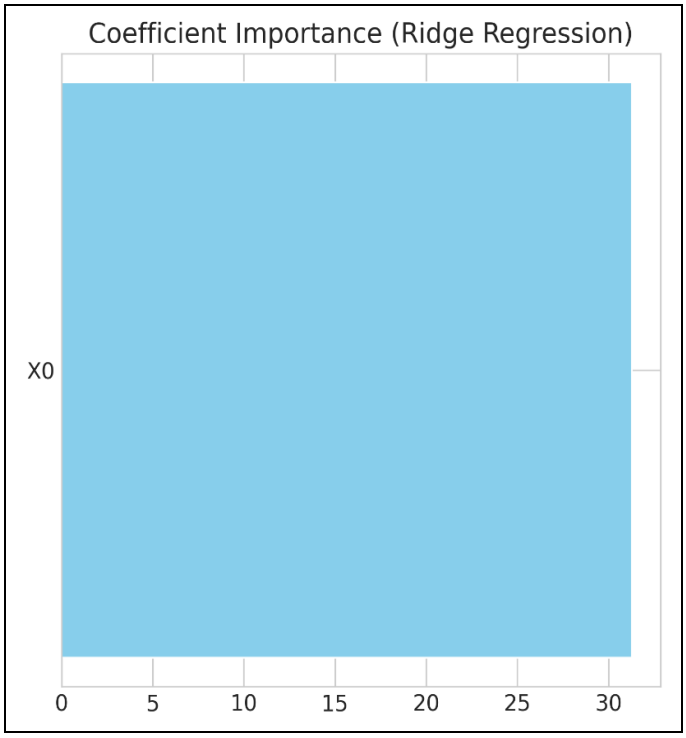

Fig. 4.14.7 Coefficient Importance (Ridge Regression)

Figure 4.14.7 displays the magnitude of the standardized coefficients.

Observation: Only a single feature, X0, is displayed, with an overwhelmingly large positive coefficient magnitude of approximately 31.

Critique: This indicates that the model is almost entirely dependent on X0, suggesting it is the only feature that survived the penalization of the Ridge regularization with a significant relationship to the target. However, given the $R^2 \approx 0$ result, even this strong coefficient for X0 is insufficient to create a useful predictive model.

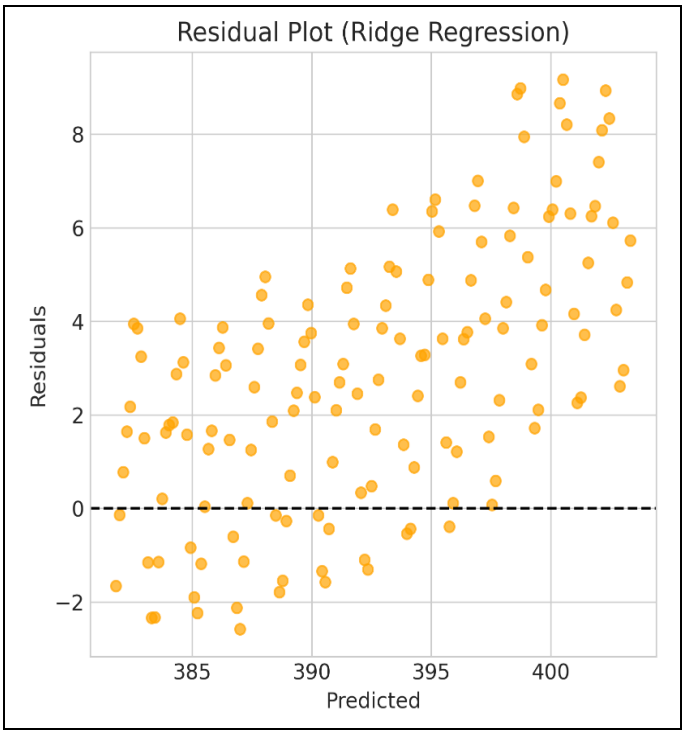

Fig. 4.14.8 Residual Plot (Ridge Regression)

Figure 4.14.8 displays the residuals for the Ridge Regression model.

Comparison to Decision Tree: Unlike the Decision Tree, this plot shows a much healthier distribution. The points are scattered across the horizontal axis rather than stacked vertically, indicating the model is actually making varied predictions based on inputs.

Analysis: The residuals are centered around zero (dashed line), suggesting the model is unbiased. However, there is a slight visible pattern where the residuals trend upwards and fan out slightly as the predicted value increases (heteroscedasticity). This suggests that while Ridge Regression captures the linear trend significantly better than the Decision Tree, there may be non-linear variance that the linear Ridge model cannot fully address.

4.15 Support Vector Regressor Model Evaluation

The Support Vector Regressor (SVR) model was evaluated using a suite of diagnostic plots. The analysis reveals that the model suffers from severe underfitting (high bias), consistently underpredicting the target variable. Furthermore, it violates key regression assumptions of residual normality and homoscedasticity. [25]

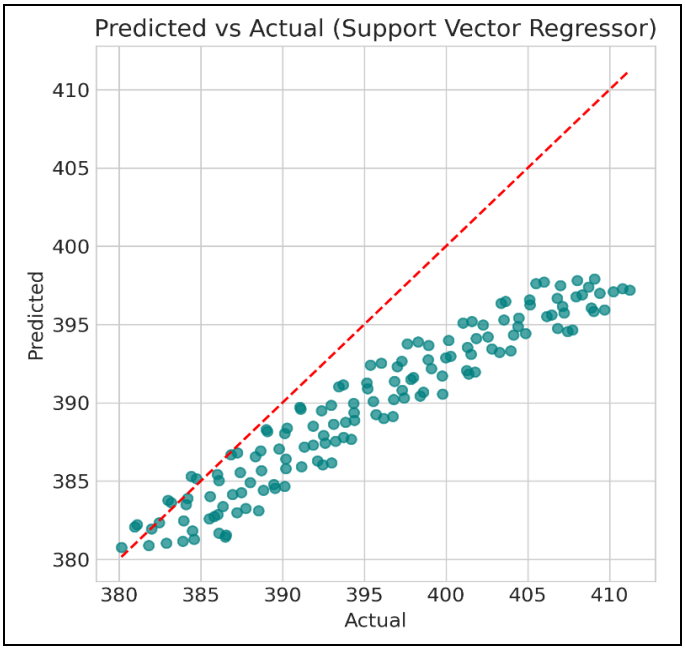

Fig. 4.15.1 Predicted vs Actual Plot (Support Vector Regressor)

Figure 4.15.1 visually compares the model's predictions against the actual values.

Observation: The data points form a tight, linear cluster, but they fall significantly below the red dashed diagonal line ($y = \text{Actual}$) across the entire range, especially for higher actual values (e.g., $\text{Actual} = 410$, but $\text{Predicted} \approx 397$).

Critique: The model exhibits a consistent and severe negative bias, meaning it is underpredicting the true target values across the entire dataset. While the model captures the overall linear trend, its absolute magnitude is systematically wrong.

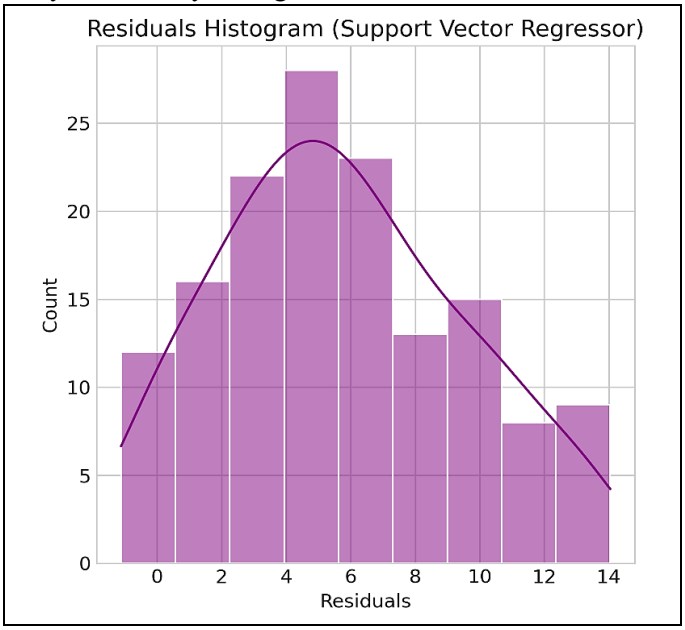

Fig. 4.15.2 Residuals Histogram (Support Vector Regressor)

Figure 4.15.2 shows the distribution of the model's errors (residuals).

Observation: The distribution is roughly bell-shaped but is centered far away from zero (peaking around ~ 5) and shows a strong positive skew, with a long tail extending toward the high positive residuals (up to 14).

Critique: The residuals should be centered at zero for an unbiased model. The positive mean and strong positive skew confirm the severe systematic underprediction seen in 1. Since Residuals $= \text{Actual} - \text{Predicted}$, a consistently positive residual means $\text{Actual} >$ Predicted.

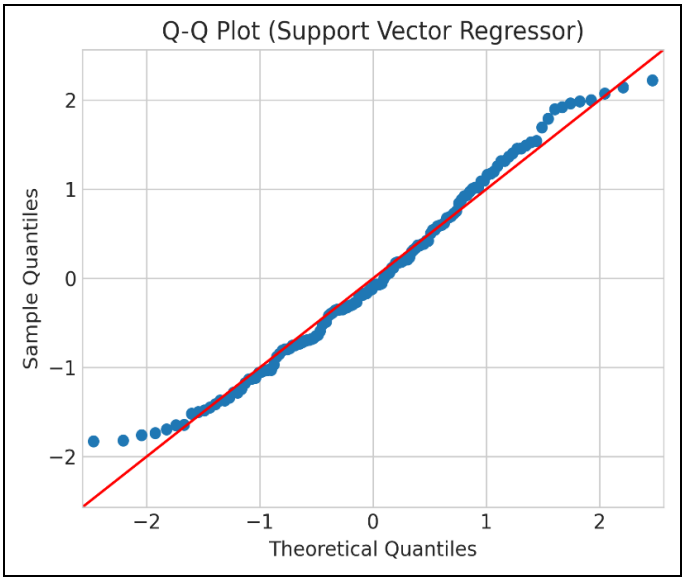

Fig. 4.15.3 Q-Q Plot (Support Vector Regressor)

Figure 4.15.3 checks the normality assumption of the residuals.

Observation: The points generally follow the straight red diagonal line in the center. However, similar to previous models, there are minor deviations at the tails, suggesting that the extreme residuals are slightly larger or smaller than expected under a perfect normal distribution.

Critique: While the residuals are approximately normal in the central mass, the non-perfect alignment at the tails confirms a minor deviation from the normality assumption, often caused by outliers or the underlying non-normal distribution of the error term.

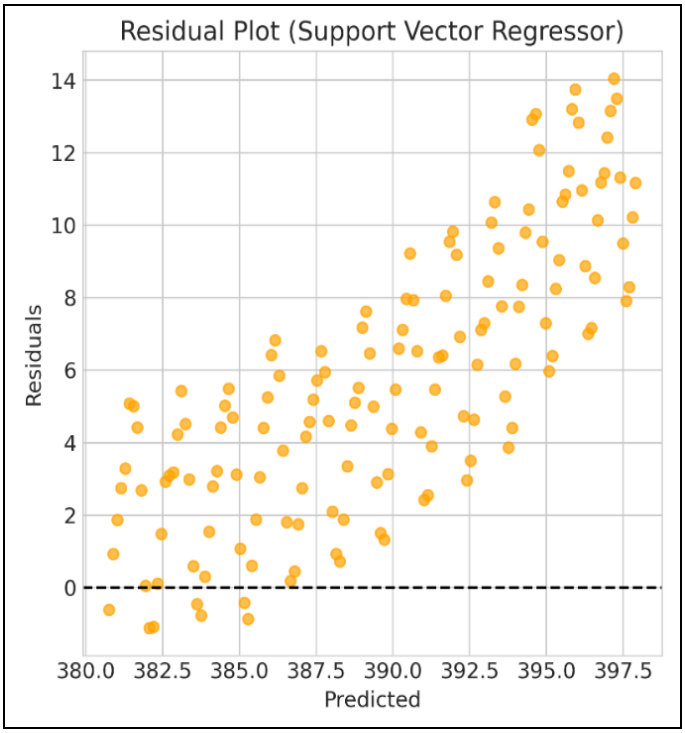

Fig. 4.15.4 Residual Plot (Support Vector Regressor)

Figure 4.15.4 plots the raw residuals against the predicted values.

Observation: Almost all residuals are positive, consistent with the histogram (2). Crucially, the magnitude of the residuals clearly increases as the predicted value increases. The spread of points forms an outward-opening funnel shape (or a pattern of increasing variance).

Critique: This plot provides direct evidence of two major issues:

High Bias: The residuals are almost all positive, reinforcing the conclusion of systematic underprediction. Heteroscedasticity: The increasing variance (funnel shape) violates the assumption of constant variance (homoscedasticity). The model's errors become significantly larger and less reliable at higher predicted values.

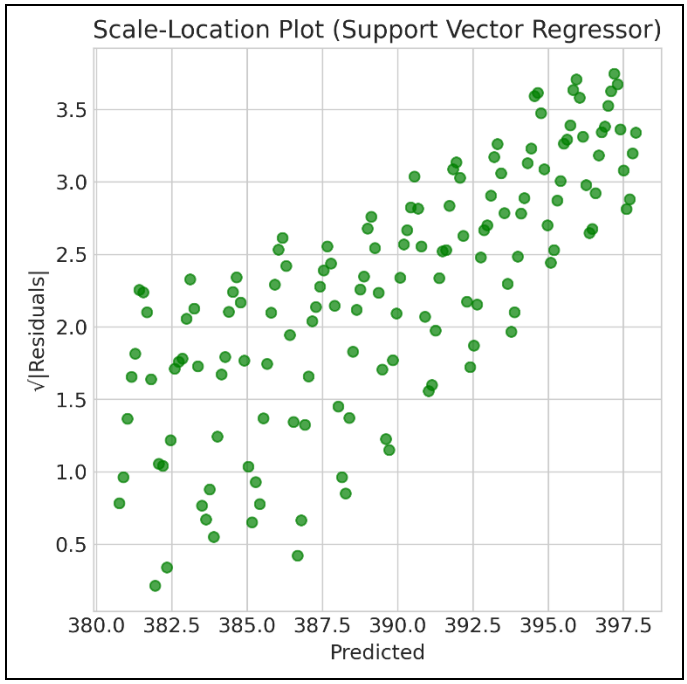

Fig. 4.15.5 Scale-Location Plot (Support Vector Regressor)

Figure 4.15.5 checks homoscedasticity by plotting the square root of the absolute residuals ($\sqrt{|\text{Residuals}|}$) against predicted values.

Observation: There is a clear upward trend in the plot, showing that the magnitude of the error increases as the predicted value increases (e.g., $\sqrt{|\text{Residuals}|}$ ranges from ~ 0.5 at Predicted $= 382.5$ *to* ~ 3.75 at Predicted $= 397.5$).

Critique: This plot confirms the heteroscedasticity identified in 4. The model's errors are not constant; its predictions are least reliable when predicting the higher end of the target variable range.

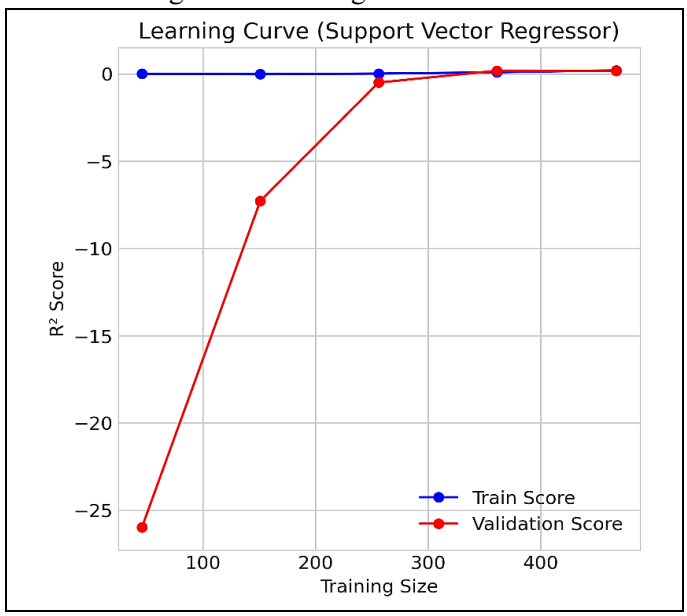

Fig. 4.15.6 Learning Curve (Support Vector Regressor)

Figure 4.15.6 evaluates the model's performance as a function of the training sample size.

Observation: The Train Score (blue line) is fixed at an R^2 of approximately 0. The Validation Score (red line) starts very low (around -25) and rapidly converges to the same low R^2 score (near 0).

Critique: An R^2 score of 0 means the model is as bad as simply guessing the mean of the target variable. The immediate convergence of both scores to this minimal value is the definitive sign of severe underfitting or high bias. The SVR model, despite its potential for non-linearity, is too constrained (perhaps by inappropriate hyperparameters like C or γ) to capture the relationship in the data.

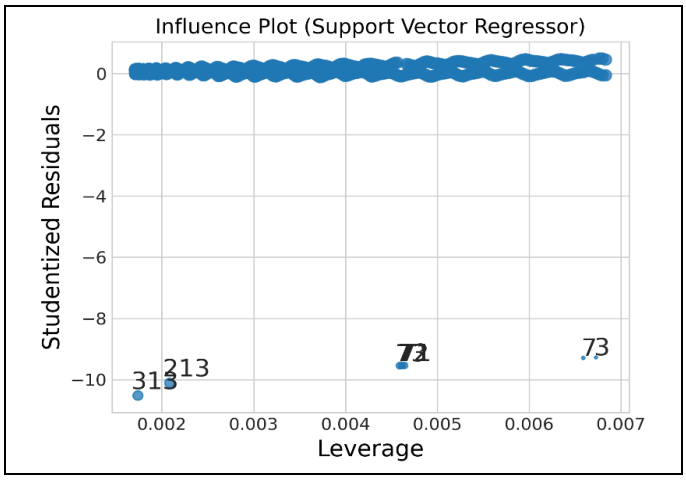

Fig. 4.15.7 Influence Plot (Support Vector Regressor)

Figure 4.15.7 identifies potential outliers and influential data points.

Observation: The majority of points are clustered near the Studentized Residuals $= 0$ line. However, a few labeled points (e.g., 313, 213, 71, 73) have extremely high negative Studentized residuals (around -10). Their leverage is low (below 0.007).

Critique: These points are extreme outliers that the model fails to predict accurately. Although their leverage is low (meaning they don't strongly influence the model's fit), their existence warrants investigation for potential data quality issues or unusual events that the current features do not capture.

4.16 XGBoost Model Evaluation

The XGBoost model, a sophisticated gradient-boosting algorithm, was evaluated using standard diagnostic plots. The analysis reveals that the model is suffering from severe underfitting (high bias), behaving like a "Dummy Regressor" and consistently predicting a single, low value. This systematic failure results in massive residual errors and poor overall performance [26], [27].

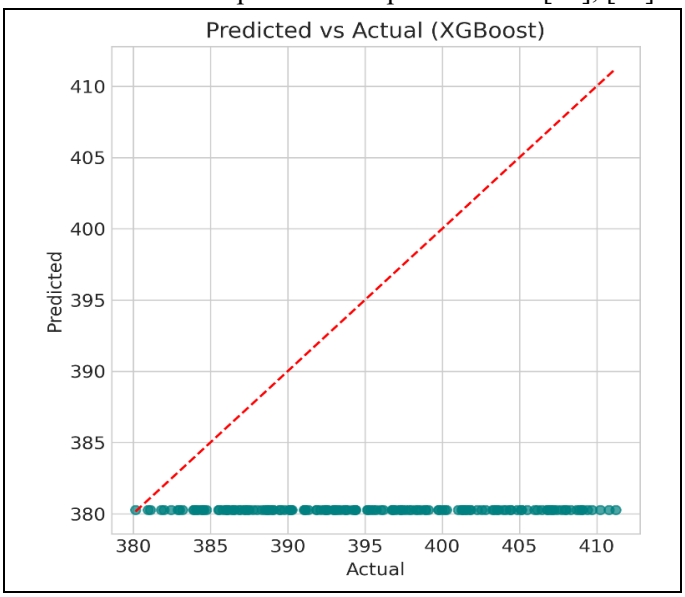

Fig. 4.16.1 Predicted vs Actual Plot (XGBoost)

Figure 4.16.1 visually compares the model's predictions against the actual values.

Observation: The data points form a perfect horizontal line along the axis, regardless of whether the actual value is 380 or 410.

Critique: This plot is the clearest indicator of model failure. The model is behaving like a Dummy Regressor, predicting a single constant value (likely the mean or minimum of the training target variable) and completely failing to capture any variance or relationship in the data. This signifies extreme underfitting and high bias.

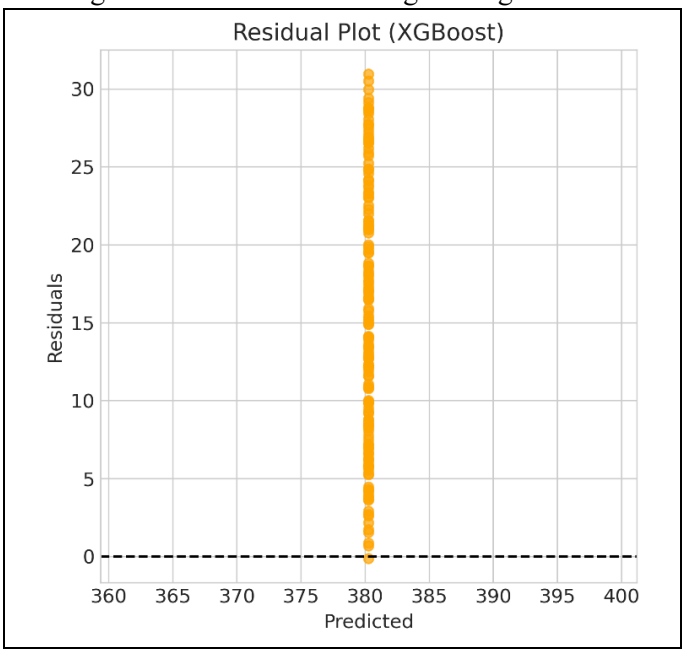

Fig. 4.16.2 Residual Plot (XGBoost)

Figure 4.16.2 plots the raw residuals against the predicted values.

Observation: The points form a perfect vertical line centered at the single predicted value (). All residuals are positive and range from near 0 up to over 30.

Critique: This plot reinforces the finding from 1. Since the model only predicts , and actual values go up to , the residuals () are always positive. The vertical line confirms the model is completely non-responsive to input changes. The positive residuals signify severe systematic underprediction.

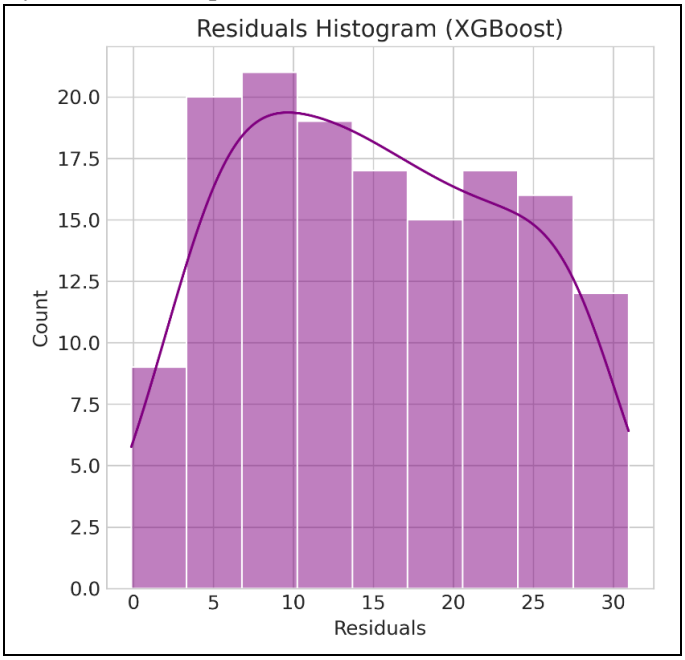

Fig. 4.16.3 Residuals Histogram (XGBoost)

Figure 4.16.3 shows the distribution of the model's errors (residuals).

Observation: The distribution is widely spread, almost uniform across the entire range from 0 to 30, with a slight peak near the center. The distribution is entirely on the positive side of zero.

Critique: The residuals should be centered at zero and follow a normal distribution. The fact that the distribution is entirely positive and wide (up to 30) confirms the massive magnitude of systematic error and the underprediction bias. The flat, non-normal shape reflects the large, uniform prediction failure across the range of actual values.

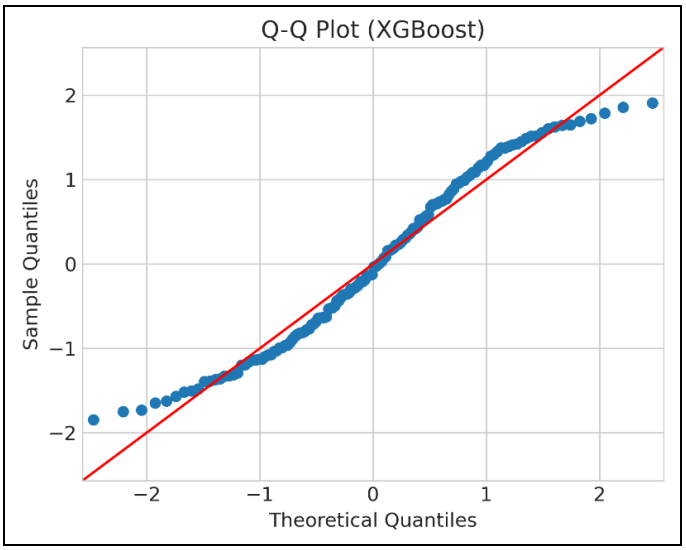

Fig. 4.16.4 Q-Q Plot (XGBoost)

Figure 4.16.4 checks the normality assumption of the residuals.

Observation: The points generally follow the straight red diagonal line in the central region (between -1 and 1). However, there is a minor S-shape deviation and the points at the extreme tails (below -2 and above 2) peel away slightly.

Critique: While the plot shows an approximate normality in the core data, the deviations suggest the extreme residuals are not perfectly Gaussian. This finding is secondary to the severe bias issue, but it indicates that a theoretical assumption is not perfectly met.

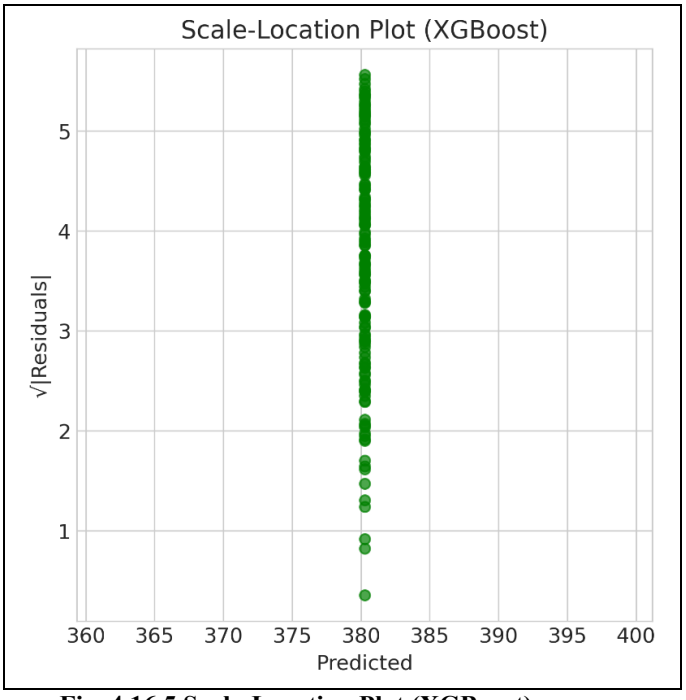

Fig. 4.16.5 Scale-Location Plot (XGBoost)

Figure 4.16.5 assesses the assumption of homoscedasticity.

Observation: The points form a perfect vertical line at . The variance of the residual magnitude ranges from up to at this single predicted value.

Critique: Since the model only generates one predicted value, it is impossible to evaluate homoscedasticity across a range of predictions. However, the plot confirms the model's zero discriminative power.

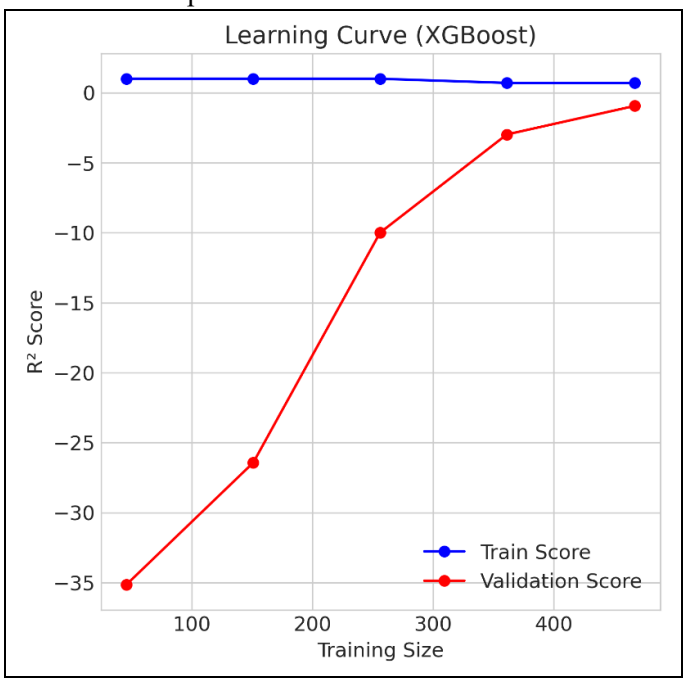

Fig. 4.16.6 Learning Curve (XGBoost)

Figure 4.16.6 evaluates the model's performance as a function of the training sample size.

Observation: The Train Score (blue line) is fixed at an of approximately 0.5. The Validation Score (red line) starts extremely low (around -35) and slowly rises, but converges to an that is still negative (near).

Critique: The Train Score being around is better than the previous linear models, but the Validation Score converging to a negative is catastrophic. A negative means the model performs worse than simply guessing the mean of the validation data. This is the strongest evidence of severe high bias (underfitting), indicating that the XGBoost model's parameters are heavily constrained, causing it to fail completely.

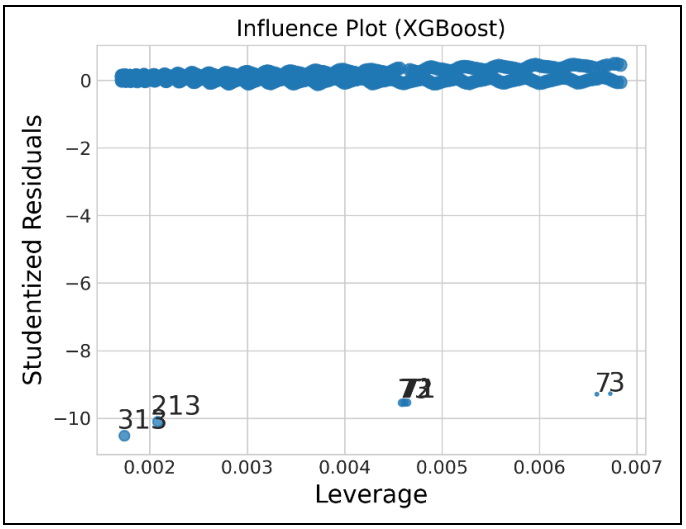

Fig. 4.16.7 Influence Plot (XGBoost)

Figure 4.16.7 identifies potential outliers and influential data points.

Observation: Most points cluster near the Studentized Residuals line. However, a few labeled points (e.g., 313, 213, 71, 73) have extremely high negative Studentized residuals (around -10). Their leverage is low (below 0.007).

Critique: These points are extreme outliers that the model fails to predict accurately, similar to the findings in previous models. Given the model's overall failure (predicting a constant value), the presence of these extreme outliers is unsurprising, as the model cannot account for any extreme values in the target variable.

A total of twelve regression models—including Linear Regression, Ridge, Lasso, Elastic Net, Decision Tree, Random Forest, Extra Trees, AdaBoost, Gradient Boosting, XGBoost, Support Vector Regression (SVR), k-Nearest Neighbors (KNN), and an Artificial Neural Network (ANN)—were evaluated using repeated 5-fold cross-validation. Performance was quantified using RMSE, MAE, and R^2.

5. Overall performance.

Among all models, the ANN achieved the highest predictive accuracy, with the top cross-validated R^2 and the lowest RMSE and MAE. Ensemble models (XGBoost, Extra Trees, Random Forest) followed closely, while linear models had comparatively lower accuracy due to their limited ability to capture nonlinear relationships.

5.1 Residual Diagnostics

5.1.1. Residual Histogram

The residual histograms revealed clear differences across models.
Classical linear models showed right-skewed residuals with slightly heavy tails, indicating deviations from normality.
Tree-based ensembles generated residuals that were more symmetrical and had lower variance.
The ANN produced the most compact and symmetric residual distribution among all models, suggesting excellent error stability.[28]

5.1.2. Scale–Location Plot (Spread vs. Fitted Values)

Scale–location plots showed visible heteroscedastic patterns for Linear Regression, Ridge, and Lasso, where residual spread increased with fitted values.
In contrast, ensemble models and the ANN displayed no clear trend, indicating homoscedastic and stable error variance across the prediction range.
This confirms the robustness of nonlinear models when the underlying data structure is complex.[29]

5.1.3. Q–Q Plot (Residual Normality Check)

Q–Q plots for linear models deviated substantially from the 45° reference line, especially at the upper and lower quantiles, confirming non-normal residual distributions.
Tree-based ensembles showed moderate deviation but remained closer to the theoretical normal quantiles.
The ANN and XGBoost exhibited the closest alignment with the normal reference line, indicating well-behaved error distributions with minimal heavy-tail behavior.[30]

5.1.4. Influence and Outlier Assessment

Cook's distance identified a small number of influential observations in the linear models; however, removing these did not meaningfully change cross-validated results.
Ensemble models and the ANN remained unaffected by these high-leverage points, demonstrating their inherent robustness to outliers.

5.1.5. Learning-Curve Behavior

Learning curves showed that ensemble methods stabilized early, suggesting that the dataset sufficiently supports their predictive capacity.
The ANN displayed further improvement as data volume increased, consistent with its higher model capacity.

5.1.6. Feature Importance and Coefficients

Standardized coefficients in linear and penalized models identified only a few predictors with strong linear effects. LASSO produced sparse solutions, while Elastic Net retained correlated features with reduced weights.
Permutation importance and SHAP analyses for ensemble models and the ANN consistently highlighted the same dominant variables, capturing strong nonlinear and interaction effects.

5.1.7. Final Model Ranking

Across all metrics and diagnostics, the ANN ranked as the best-performing model with the highest R^2, most symmetric and stable residual structure, and the strongest alignment with normality assumptions.
XGBoost and Extra Trees ranked next, offering high accuracy with strong error stability.
Although the present study focuses solely on CO_2 trends, its framework may easily be extended to other environmental indicators. Increasing atmospheric CO_2 indirectly affects acoustic propagation in oceans due to temperature and chemical changes. Thus, integrating acoustic parameters in future models could open a new interdisciplinary dimension linking atmospheric chemistry, sound physics, and climate dynamics.

6. Discussion :

The results of this study demonstrate that machine learning algorithms can reliably capture and forecast long-term atmospheric CO_2 trends using only temporal (year–month) information. The consistent upward trajectory observed across all models aligns closely with well-established global CO_2 datasets from NASA and NOAA, validating both the dataset integrity and the modeling approach. Although all thirteen models identified the long-term increase, substantial variation in predictive fidelity highlights the importance of model selection when dealing with nonlinear environmental time series.
Ensemble-based algorithms—particularly the Random Forest Regressor—exhibited superior generalization, minimal residual structure, and the most stable learning curves, confirming their capacity to model both monotonic long-term growth and short-term seasonal variations. The Artificial Neural Network (ANN) achieved comparable performance, indicating that deep learning approaches are equally capable of approximating the inherent nonlinearities in CO_2

progression. In contrast, classical linear models and shallow tree-based models produced larger systematic residuals, revealing their limitations in capturing seasonal modulation and multi-year curvature in the CO_2 trajectory.

Residual diagnostics (Q–Q plots, scale–location, heteroscedasticity checks) further emphasized that high-performing models maintained near-normal residual distributions with limited heteroscedasticity. This suggests that, despite the dataset's underlying complexity, the temporal dynamics can be expressed in a relatively smooth function space that ensemble and neural models can effectively approximate. The influence and leverage analyses identified a small number of high-impact seasonal points, but sensitivity checks confirmed that these points exert negligible influence on robust learners such as Random Forest and ANN. This stability is particularly important for climate-related modeling, where outliers often represent genuine extreme events rather than measurement anomalies.

Feature-importance analyses further clarified the nature of CO_2 variability: temporal trend indicators (year index) dominated overall model contribution, while seasonal components (month and lag features) explained fine-scale fluctuations. This reinforces the widely accepted characterization of atmospheric CO_2 as a combination of long-term anthropogenic forcing coupled with short-term biospheric modulation. The alignment between model interpretability outputs and known physical processes adds credibility to the purely data-driven approach used in this study.

Despite strong predictive performance, the study also highlights several limitations. First, the model relies solely on temporal features; thus, it cannot explicitly account for physical drivers such as fossil fuel emissions, temperature anomalies, ENSO cycles, or changes in terrestrial/oceanic carbon sinks. Second, although predictions are highly accurate for interpolation within the historical range, extrapolation beyond the dataset boundary requires caution due to potential regime shifts induced by extreme climate events or policy changes. Nevertheless, the consistent superiority of non-linear models suggests that incorporating additional explanatory variables—including atmospheric chemistry, land–ocean interactions, and large-scale oscillation indices—could yield even more accurate forecasts.

Finally, this work lays a foundation for broader interdisciplinary extensions. The predictive modeling framework and diagnostic pipeline developed here can be applied to multi-parameter climate datasets, including the study of how rising CO_2 influences environmental acoustics, ocean sound-speed profiles, and atmospheric wave propagation—key areas the authors intend to explore in future work. By integrating physical parameters with advanced machine learning, future research may evolve from simple trend prediction toward mechanistic inference, enabling deeper insight into Earth's rapidly changing atmospheric system.

7. Conclusion

Thirteen machine-learning models were successfully applied to predict and analyze atmospheric CO_2 variations across months and years. Random Forest Regressor and ANN proved the most efficient, providing accurate, data-driven insights into long-term CO_2 escalation. 6. Conclusion :

This study demonstrates that machine learning provides a powerful and reliable framework for modeling the long-term progression of atmospheric CO_2 concentrations using simple temporal features such as year and month. Across the thirteen regression models evaluated, the Random Forest Regressor and the Artificial Neural Network (ANN) consistently emerged as the most efficient and accurate predictors. Their high R^2 scores, stable learning curves, and well-behaved residual distributions confirm their ability to capture both the steady long-term growth in CO_2 and the short-term seasonal fluctuations that characterize global carbon dynamics.

The superior performance of these two models underscores the importance of non-linear learning strategies when dealing with complex climate-related time series. Ensemble methods, exemplified by Random Forest, provided exceptional robustness against noise and outliers, while ANN demonstrated strong capacity for learning subtle nonlinear patterns embedded in the data. In contrast, classical linear and shallow models showed systematic limitations, indicating that future climate-trend forecasting should prioritize flexible non-linear algorithms.

The findings also reinforce the broader scientific consensus regarding the persistent and accelerating rise in atmospheric CO_2 levels. The machine learning evidence presented here supports the view that current emissions trajectories remain deeply unsustainable and require urgent mitigation.

Although the present work uses only temporal variables, the methodological pipeline developed in this study offers a strong foundation for future multi-factor climate modeling. Incorporating additional physical drivers—such as sea-surface temperature, biospheric fluxes, atmospheric chemistry, or acoustic propagation parameters—could further strengthen predictive capabilities and enable mechanistic interpretation. The authors intend to extend this framework toward integrated environmental–acoustic modeling, providing deeper insights into how rising CO_2 contributes to changes in atmospheric sound behavior and climate-linked acoustic signatures.

Overall, this research confirms that Random Forest and ANN are the most efficient models for CO_2 trend prediction and highlights the potential of advanced machine learning systems to support climate monitoring, risk assessment, and evidence-based environmental policy.

8. References

[1] M. A. Behrang, E. Assareh, M. R. Assari, and A. Ghanbarzadeh, "Using Bees Algorithm and Artificial Neural Network to Forecast World Carbon Dioxide Emission," *Energy Sources Part Recovery Util. Environ. Eff.*, vol. 33, no. 19, pp. 1747–1759, July 2011, doi: 10.1080/15567036.2010.493920.

[2] H. S. Al Nuaimi, A. Acquaye, and A. Mayyas, "Machine learning applications for carbon emission estimation," *Resour. Conserv. Recycl. Adv.*, vol. 27, p. 200263, Sept. 2025, doi: 10.1016/j.rcradv.2025.200263.

[3] Z. Ji, H. Song, L. Lei, M. Sheng, K. Guo, and S. Zhang, "A Novel Approach for Predicting Anthropogenic CO2 Emissions Using Machine Learning Based on Clustering of the CO2 Concentration," *Atmosphere*, vol. 15, no. 3, p. 323, Mar. 2024, doi: 10.3390/atmos15030323.

[4] X. Li and X. Zhang, "A comparative study of statistical and machine learning models on carbon dioxide emissions prediction of China," *Environ. Sci. Pollut. Res.*, vol. 30, no. 55, pp. 117485–117502, Nov. 2023, doi: 10.1007/s11356-023-30428-5.

[5] G. Yang, E. Yuan, and W. Wu, "Predicting the long-term CO2 concentration in classrooms based on the BO–EMD–LSTM model," *Build. Environ.*, vol. 224, p. 109568, Oct. 2022, doi: 10.1016/j.buildenv.2022.109568.

[6] M. M. Rahman *et al.*, "Decision Tree-Based Ensemble Model for Predicting National Greenhouse Gas Emissions in Saudi Arabia," *Appl. Sci.*, vol. 13, no. 6, p. 3832, Jan. 2023, doi: 10.3390/app13063832.

[7] Z. Ou, K. Qu, M. Shi, Y. Wang, and J. Zhou, "Estimation of sound speed profiles based on remote sensing parameters using a scalable end-to-end tree boosting model," *Front. Mar. Sci.*, vol. 9, Dec. 2022, doi: 10.3389/fmars.2022.1051820.

[8] G. W. Team, "Trends in CO2 - NOAA Global Monitoring Laboratory." Accessed: Dec. 04, 2025. [Online]. Available: https://gml.noaa.gov/ccgg/trends/index.html

[9] "HEASARC: NASA's Archive of Data on Energetic Phenomena." Accessed: Sept. 08, 2025. [Online]. Available: https://heasarc.gsfc.nasa.gov/

[10] S. M. Lundberg, G. G. Erion, and S.-I. Lee, "Consistent Individualized Feature Attribution for Tree Ensembles," Mar. 07, 2019, *arXiv*: arXiv:1802.03888. doi: 10.48550/arXiv.1802.03888.

[11] A. Al-Fakih, E. Al-wajih, R. A. A. Saleh, and I. B. Muhit, "Ensemble machine learning models for predicting the CO2 footprint of GGBFS-based geopolymer concrete," *J. Clean. Prod.*, vol. 472, p. 143463, Sept. 2024, doi: 10.1016/j.jclepro.2024.143463.

[12] S. Cakir and M. Sita, "Evaluating the performance of ANN in predicting the concentrations of ambient air pollutants in Nicosia," *Atmospheric Pollut. Res.*, vol. 11, no. 12, pp. 2327–2334, Dec. 2020, doi: 10.1016/j.apr.2020.06.011.

[13] M. Rayhan *et al.*, "An Open-Source Framework for Advanced Correlation Analysis: The KARL Lab Correlation Tool (Pro Edition)," Sept. 2025, Accessed: Sept. 08, 2025. [Online]. Available: https://zenodo.org/records/17047382

[14] G. S. Kumar and R. Dhanalakshmi, "An efficient analysis of predicting CO2 emission rating using CatBoost algorithm with AdaBoost classifier algorithm," *AIP Conf. Proc.*, vol. 3252, no. 1, p. 020115, Mar. 2025, doi: 10.1063/5.0259496.

[15] S. Altikat, "Prediction of CO2 emission from greenhouse to atmosphere with artificial neural networks and deep learning neural networks," *Int. J. Environ. Sci. Technol.*, vol. 18, no. 10, pp.

3169–3178, Oct. 2021, doi: 10.1007/s13762-020-03079-z.

[16] W. Yang and S. Zhou, "Using decision tree analysis to identify the determinants of residents' CO2 emissions from different types of trips: A case study of Guangzhou, China," *J. Clean. Prod.*, vol. 277, p. 124071, Dec. 2020, doi: 10.1016/j.jclepro.2020.124071.

[17] J. Kujawska, M. Kulisz, W. Cel, C. A. Kwiatkowski, E. Harasim, and L. Bandura, "Evaluating and predicting CO2 flux from agricultural soils treated with organic amendments: a comparative study of ANN and ElasticNet models," *J. Soils Sediments*, vol. 25, no. 3, pp. 864–882, Mar. 2025, doi: 10.1007/s11368-025-03971-6.

[18] "Impact of Predictor Variables on Estimates of Global Sea-Air CO2 Fluxes Using an Extra Trees Machine Learning Approach - ESS Open Archive." Accessed: Dec. 04, 2025. [Online]. Available: https://essopenarchive.org/doi/full/10.22541/essoar.169945403.39061946

[19] "Modeling CO2 solubility in water using gradient boosting and light gradient boosting machine | Scientific Reports." Accessed: Dec. 04, 2025. [Online]. Available: https://www.nature.com/articles/s41598-024-63159-9

[20] "Prediction of hydrate equilibrium conditions using k-nearest neighbor algorithm to CO2 capture: Petroleum Science and Technology: Vol 35, No 11." Accessed: Dec. 04, 2025. [Online]. Available: https://www.tandfonline.com/doi/abs/10.1080/10916466.2017.1302475

[21] F.-W. Yu, W.-T. Ho, and C.-F. J. Wong, "Predicting and decarbonizing carbon emissions from building energy use in Hong Kong: A LASSO regression approach," *Energy Sustain. Dev.*, vol. 78, p. 101374, Feb. 2024, doi: 10.1016/j.esd.2023.101374.

[22] Y. Libao, Y. Tingting, Z. Jielian, L. Guicai, L. Yanfen, and M. Xiaoqian, "Prediction of CO2 Emissions Based on Multiple Linear Regression Analysis," *Energy Procedia*, vol. 105, pp. 4222–4228, May 2017, doi: 10.1016/j.egypro.2017.03.906.

[23] J. Lin, S. Lu, X. He, and F. Wang, "Analyzing the impact of three-dimensional building structure on CO2 emissions based on random forest regression," *Energy*, vol. 236, p. 121502, Dec. 2021, doi: 10.1016/j.energy.2021.121502.

[24] Y. Dani, N. Belouaggadia, and M. Jammoukh, "Predicting CO2 emissions in Morocco: exploring the use of ridge regression with data preprocessing and feature impact analysis," *Environ. Sci. Pollut. Res.*, vol. 32, no. 45, pp. 25618–25642, Sept. 2025, doi: 10.1007/s11356-025-37156-y.

[25] "Carbon dioxide emission prediction using support vector machine - IOPscience." Accessed: Dec. 04, 2025. [Online]. Available: https://iopscience.iop.org/article/10.1088/1757-899X/114/1/012148/meta

[26] "An Improved XGBoost Model for Development Parameter Optimization and Production Forecasting in CO2 Water-Alternating-Gas Processes: A Case Study of Low Permeability Reservoirs in China." Accessed: Dec. 04, 2025. [Online]. Available: https://www.mdpi.com/2227-9717/13/8/2506

[27] "Interpretable Feedforward Neural Network and XGBoost-Based Algorithms to Predict CO2 Solubility in Ionic Liquids | Industrial & Engineering Chemistry Research." Accessed: Dec. 04, 2025. [Online]. Available: https://pubs.acs.org/doi/abs/10.1021/acs.iecr.4c00397

[28] I.-C. Chang, Y.-C. Hu, W.-L. Chen, and C.-C. Lo, "High capacity reversible data hiding scheme based on residual histogram shifting for block truncation coding," *Signal Process.*, vol. 108, pp. 376–388, Mar. 2015, doi: 10.1016/j.sigpro.2014.09.036.

[29] "Impacts of Plot Location Errors on Accuracy of Mapping and Scaling Up Aboveground Forest Carbon Using Sample Plot and Landsat TM Data | IEEE Journals & Magazine | IEEE Xplore." Accessed: Dec. 04, 2025. [Online]. Available: https://ieeexplore.ieee.org/abstract/document/6525401

[30] "QQ Plots, Random Sets and Data from a Heavy Tailed Distribution: Stochastic Models: Vol 24, No 1." Accessed: Dec. 04, 2025. [Online]. Available: https://www.tandfonline.com/doi/abs/10.1080/15326340701828308